Engineering Journal

American Institute of Steel Construction

First Quarter 2008 Volume 45, No. 1

www.aisc.org

ENGINEERING JOURNAL

AMERICAN INSTITUTE OF STEEL CONSTRUCTION

Dedicated to the development and improvement of steel construction, through the interchange of ideas, experiences and data.

ENGINEERING JOURNAL (ISSN 0013-8029) is published quarterly. Subscriptions: Members: one subscription, $20 per year, included in dues; Additional Member Subscriptions: $15 per year. Non-Members U.S., Canada, and Mexico: $40 per year, $110 for three years, single copy $15. International Members and Non-Members: $90 per year; $250 for three years; single copy $25. Published by the American Institute of Steel Construction at One East Wacker Drive, Suite 700, Chicago, IL 60601.

Periodicals postage paid at Chicago, IL and additional mailing offices. **Postmaster:** Send address changes to ENGINEERING JOURNAL in care of the American Institute of Steel Construction, One East Wacker Drive, Suite 700, Chicago, IL 60601.

MESSAGE FROM THE EDITOR:

As you may have noticed, since the completion of the 2005 AISC *Specification for Structural Steel Buildings* and publication of the 13th Ed. AISC *Steel Construction Manual*, we have had issues of the *Engineering Journal* containing articles providing background and discussion of topics contained in those AISC documents. This quarter there is one additional article that will provide background and insight into the provisions for composite columns and beam-columns in Chapter I of the 2005 AISC Specification. This article entitled, "Limit State Response of Composite Columns and Beam-Columns, Part II: Application of Design Provisions for the 2005 AISC Specification" is a sequel to Part I published in the 4th Q 2007 issue. As before, we have identified this article with the header, 2005 Spec/Manual Reference.

Cynthia J. Duncan
Editor

Acknowledgment

All AISC *Engineering Journal* articles are peer reviewed prior to publication for accuracy, content, and style. AISC thanks the following engineers for their voluntary review assistance to the *Engineering Journal* Review Board throughout 2007.

Farid Alfawakhiri
American Iron and Steel Institute

Barry L. Barger
Southern Iron Works, Inc.

Michael Barker
University of Wyoming

Jeffrey W. Berman
University of Washington

Omer W. Blodgett
The Lincoln Electric Company

Michael Brennan
LD Astorino

Roger L. Brockenbrough
R.L. Brockenbrough & Associates, Inc.

Michel Bruneau
University of Buffalo

Michael P. Culmo
CME Associates, Inc.

Robert Driver
University of Alberta

Carol J. Drucker
Drucker Zajdel Structural Engineers, Inc.

Donald O. Dusenberry
Simpson Gumpertz & Heger, Inc. Consulting Engineers

W. Samuel Easterling
Virginia Polytechnic Institute & State University

Bruce R. Ellingwood
Georgia Institute of Technology

Sherif El-Tawil
University of Michigan

Don Engler
BDS Steel Detailers, Inc.

Mohammed M. Ettouney
Weidlinger Associates Inc. Consulting Engineers

John W. Fisher
Lehigh University

Theodore V. Galambos
University of Minnesota

Maria Garlock
Princeton University

Louis F. Geschwindner
American Institute of Steel Construction

Subhash C. Goel
University of Michigan

John L. Gross
National Institute of Standards and Technology

Michael A. Grubb
Bridge Software Development International, Ltd.

Jerome F. Hajjar
University of Illinois at Urbana-Champaign

Ronald O. Hamburger
Simpson Gumpertz & Heger Inc. Consulting Engineers

Linda M. Hanagan
Pennsylvania State University

Allen J. Harrold
Butler Manufacturing Company

Richard A. Henige
LeMessurier Consultants, Inc.

Steve Herth
Contech Bridge Solutions, Inc.

W. Steven Hofmeister
The Thornton-Tomasetti Group, Inc.

John D. Hooper
Magnusson Klemencic Associates

Ahmad M. Itani
University of Nevada

Nestor Iwankiw
Hughes Associates

Matthew A. Johann
Ove Arup & Partners

Richard C. Kaehler
Computerized Structural Design, S.C.

Lawrence A. Kloiber
LeJeune Steel

Dean Krause
Consultant

Theodor Krauthammer
University of Florida

Geoffrey L. Kulak
University of Alberta

Keith Landwehr
Schuff Steel Company

Michael E. Lederle
Opus Architects & Engineers, Inc.

Judy Liu
Purdue University

LeRoy A. Lutz
Computerized Structural Design, S.C.

James O. Malley
Degenkolb Engineers

William McGuire
Cornell University

David L. McKenzie
S.P. International, Inc.

Ronald Meng
Lynchburg Steel Company, LLC

James A. Milke
University of Maryland

Heath E. Mitchell
PCS Structural Solutions

Michael G. Moffitt
National Steel Bridge Alliance

Larry Muir
Cives Steel Company

Thomas M. Murray
Virginia Polytechnic Institute & State University

R. Shankar Nair
Teng & Associates, Inc.

Clarkson W. Pinkham
S.B. Barnes Associates

Clinton O. Rex
Stanley D. Lindsey & Associates

Kimberly Robinson
Star Seismic

Charles W. Roeder
University of Washington

C. Mark Saunders
Rutherford & Chekene Consulting Engineers

Stephen P. Schneider
Kramer Gehlen & Associates Inc.

Benjamin Schafer
Johns Hopkins University

Robert E. Shaw
Steel Structures Technology Center, Inc.

Donald R. Sherman
University of Wisconsin, Milwaukee

James A. Swanson
University of Cincinnati

William A. Thornton
Cives Engineering Corporation

Raymond H.R. Tide
Wiss Janney Elstner Associates, Inc.

Emile W.J. Troup
Consultant

Chia-Ming Uang
University of California, San Diego

Elmar Upitis
Upitis & Associates, Inc.

Asif Usmani
University of Edinburgh

Brian Uy
University of Western Sydney

Jules Van de Pas
Computerized Structural Design, S.C.

Amit H. Varma
Purdue University

Robert D. Weber
R.D. Weber & Associates, Inc.

Michael A. West
Computerized Structural Design, S.C.

Donald W. White
Georgia Institute of Technology

Ronald Ziemian
Bucknell University

Block Shear Equations Revisited…Again

HOWARD I. EPSTEIN and LANCE J. ALEKSIEWICZ

Shortly after block shear was first identified as a possible failure mode for coped beam connections, design equations to account for it were incorporated into allowable stress design (ASD) provisions. These equations never changed, partly due to ASD not being updated since 1989. However, load and resistance factor design (LRFD) treatment of block shear changed with each new Specification. Over the years, it was suggested that the effect of eccentricity was missing from block shear equations. On the surface it appears that the effect of eccentricity on the block shear strength of connections, as suggested by previous investigators, has now been incorporated into the latest unified Specification. For many connections, however, nothing has changed. It is the conclusion of this paper that additional important cases need to be shown in Commentary Figure C-J4.2 of the 2005 AISC *Specification for Structural Steel Buildings* (AISC, 2005), hereafter referred to as the AISC *Specification,* for which block shear equations now incorporate a new factor to account for connection eccentricity. In particular, as a minimum, angles connected by only one leg or tees connected by their flanges should also be included with other connections for which block shear capacities are now reduced.

BACKGROUND: CODE TREATMENT UNTIL 2005

In 1978, destructive tests on coped beams with bolted web connections were performed with some exhibiting what has become known as block shear as the failure mode (Birkemoe and Gilmor, 1978). They proposed a design equation in which the ultimate shear strength is applied to the net shear area and ultimate tensile strength to the net tension area. Block shear occurs when the web, for this case, develops its ultimate strength along the perimeter bolt holes and a "block" of this web begins to fracture. Figure 1a shows this block shear path for a coped beam. The equation that Birkemoe and Gilmor proposed was:

Howard I. Epstein is professor, department of civil and environmental engineering, University of Connecticut, Storrs, CT.

Lance J. Aleksiewicz is structural engineer, Odeh Engineers, Inc., North Providence, RI.

$$P_{bs} = \left(0.3A_{nv} + 0.5A_{nt}\right)F_u \quad (1)$$

where

F_u = ultimate strength of the material
A_{nv} = net shear area
A_{nt} = net tensile area

Over time, this concept has become more broadly applied to many other connection applications. This equation (with the symbols A_v and A_t used for net shear and tension areas, respectively) was first incorporated into allowable stress design (ASD) in the 1978 AISC *Specification* (AISC, 1978). The 1989 AISC Specification (AISC, 1989), the last revision of ASD, included the same provisions for block shear.

The block shear equations in the load and resistance factor design (LRFD) specifications have changed with each edition. Both the first edition (AISC, 1986a) and the second edition (AISC, 1993) contain two equations for the determination of the block shear rupture design strength, ϕR_n, given by

$$\phi R_n = \phi[0.6F_y A_{gv} + F_u A_{nt}] \quad (2a)$$

and

$$\phi R_n = \phi[0.6F_u A_{nv} + F_y A_{gt}] \quad (2b)$$

where, in addition to the symbols in Equation 1,

ϕ = 0.75
F_y = specified minimum yield strength
A_{gv} = gross area subject to shear
A_{gt} = gross area subject to tension

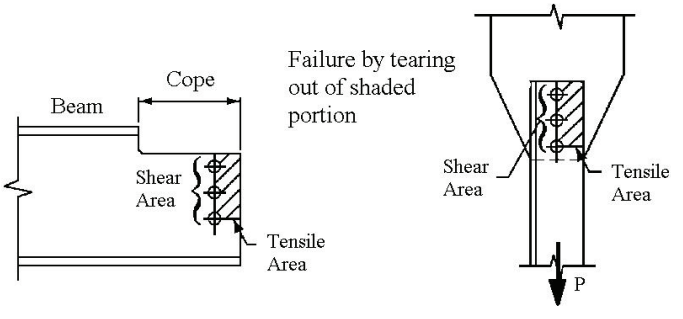

(a) Coped Beam (b) Tension Connection

Fig. 1. Block shear failure paths (AISC, 2005).

Equation 2a represents block shear strength determined by rupture on the net tensile section combined with shear yielding on the gross section on the shear plane(s). Equation 2b represents block shear strength determined by rupture on the net shear area(s) combined with yielding on the gross tensile area. These equations are based on the work of Ricles and Yura (1983) as well as that of Hardash and Bjorhovde (1985). Except for slight differences in notation, these equations did not change from the first to the second edition of the AISC LRFD *Specification*, but, for some connections, which equation governed did change.

In the first edition of the LRFD *Specification* (AISC, 1986a), these equations were found only in Chapter J of the Commentary where it stated that "the controlling equation is one that produces the *larger* force." The Commentary went on to explain that since block shear is a fracture or tearing phenomenon and not a yielding limit state, the proper formula is the one in which the fracture term is larger than the yield term. For ductile steels where F_u is considerably larger than F_y, this may be true for both equations. For steels having F_y as an appreciable portion of F_u, this may not be true for either equation. The Commentary went on to state that "where it is not obvious which failure plane fractures, it is easier just to use the larger of the two formulas." In fact, the tables in the first edition of the LRFD Manual (AISC, 1986b) stated that the equation to be used is the one producing the larger block shear strength.

The block shear equations in the second edition of the AISC LRFD *Specification* (AISC, 1993) were found in Chapter J of the Specification, as opposed to the Commentary. While the formulas were the same, the change in the second edition was contained in a check of the relative fracture strengths, F_uA_{nt}, as compared to $0.6F_uA_{nv}$, or since F_u is common to both terms, A_{nt} compared to $0.6A_{nv}$. The Specification then stated that when $F_uA_{nt} \geq 0.6F_uA_{nv}$, use Equation 2a and when $F_uA_{nt} < 0.6F_uA_{nv}$, use Equation 2b. The Commentary stated that "the proper equation to use is the one with the larger rupture term."

In both the first and second LRFD editions, the Commentary gave two extreme examples showing which of the two limiting states (shear yield/tension fracture or shear fracture/tension yield) was appropriate. One of the examples had a tension area much larger than the shear area while the other example reversed these areas. The later interpretation of using the limiting state with the larger rupture term was certainly justified on the basis of these examples. The same could not easily be said of the earlier treatment.

The first edition LRFD *Specification* specified to always use the larger strength found from Equation 2a or 2b, while the second edition either led the designer to the same equation or possibly to the equation that yields the smaller design strength. The effect was that, for some connection geometries, the second edition produced more conservative results (Epstein, 1996a).

The third edition of the AISC LRFD *Specification* (AISC, 1999) used the following equations for the determination of the block shear rupture design strength, ϕR_n:

$$\phi R_n = \phi[0.6F_yA_{gv} + F_uA_{nt}] \leq \phi[0.6F_uA_{nv} + F_uA_{nt}]$$

when $$F_uA_{nt} \geq 0.6F_uA_{nv} \quad (3a)$$

and

$$\phi R_n = \phi[0.6F_uA_{nv} + F_yA_{gt}] \leq \phi[0.6F_uA_{nv} + F_uA_{nt}]$$

when $$0.6F_uA_{nv} > F_uA_{nt} \quad (3b)$$

In Equation 3a, the term $0.6F_yA_{gv}$ shall not be taken greater than $0.6F_uA_{nv}$, and in Equation 3b, the term F_yA_{gt} shall not be taken greater than F_uA_{nt}. These two provisions didn't exist in the second edition LRFD. Equation 3a is the equivalent of using yielding of the shear plane and rupture of the tension plane. The additional provision, however, requires that the yield strength of the gross shear area be less than the ultimate strength of the net shear area. Conversely, Equation 3b implies rupture of the shear plane and yielding of the tension plane. Similar to Equation 3a, however, the third edition limited the yield strength of the gross tension area to less than or equal to the ultimate strength of the net tension area.

BACKGROUND: COPED BEAMS VERSUS ANGLE TENSION MEMBERS

"The block shear failure mode is not limited to the coped ends of beams." This statement first appeared in the first edition of the LRFD *Specification* (AISC, 1986a) and then, subsequently, in the 1989 ASD *Specification* (AISC, 1989). The examples shown in the Commentary included tension connections for angles as well as gusset plates (see Figure 1b). Prior to their inclusion, some argued that structural engineers should have recognized block shear as a possible failure mode for angles, despite the fact that many textbook examples did not consider block shear for angles in tension, even when it clearly was the governing failure mode.

It was some angles found in the wreckage of the Hartford Civic Center roof, which had failed in block shear, that served as the impetus to investigate block shear in angles. Initial finite element investigations (Epstein and Thacker, 1991) were able to accurately determine block shear as the failure mode for these Civic Center angles. That study also investigated various similar geometries. Most importantly, the study also showed that there probably should be a substantial difference in the way in which block shear is treated for coped beams (where the load is applied to the connection in the plane of the web, which is also the block shear path)

versus angles (where the load is applied eccentric to the failure plane). The first edition LRFD *Specification* (AISC, 1986a) included block shear equations in the Commentary (pages 186–188) where angles were shown.

Extensive tests of angles to determine effects of connection geometries and eccentricities were conducted at the University of Connecticut (Adidam, 1990; Epstein, 1992). The tested specimens were back-to-back angles with two rows of bolts in one leg of each angle. Among the specimens, the connection geometry was varied by using staggered and unstaggered bolt patterns, and alternating the position of the lead bolt in the staggered bolt patterns from the inside gage line to the outside gage line. It was concluded that the AISC ASD and LRFD *Specifications* provided inadequate safety factors for the block shear failure of angles. To alleviate this problem, it was suggested that the shear lag factor, U, be included in the tension terms of the code equations for block shear capacity.

The U factor, in essence the efficiency of the connection, is used to reduce the net area of angles in tension because not all of the tension area is effective in carrying the load. As the length of the outstanding leg increases, the eccentricity increases, and U decreases. The study of angles showed that as the outstanding leg increased in size, the capacity of the angle in net tension and the block shear capacity was reduced. These conclusions were also verified using nonlinear finite element models (Epstein and Chamarajanagar, 1996). The results justified applying the correction factor, U, to the block shear design equations. Another study investigated the efficiency of angles in tension rolled from high strength steel (Gross, 1994). Gross contended that the block shear equations for ASD and LRFD were not sufficient for high strength steel.

While the LRFD equations for block shear changed with each new edition, the changes did little to address the underlying problem of the eccentricity of the load to the plane in which block shear occurs. Over the years, several researchers have suggested modifications of the block shear equations to account for the reduction in capacity with increasing eccentricity. As was suggested previously (Adidam, 1990; Epstein, 1992), the simple empirical incorporation of the "shear lag" factor, U, into the tension path for block shear is probably all that is needed. For ASD, the resulting equation would be

$$P_{bs} = \left(0.3A_{nv} + 0.5UA_{nt}\right)F_u \tag{4}$$

where

$$U = 1 - \bar{x}/l \tag{5}$$

where

$\bar{x}$ = connection eccentricity
l = connection length

For LRFD, U could similarly be a factor for each tension area. Even for the simple case of pure tension fracture, not block shear, of a member with eccentricity, such as an angle, U is used to calculate an *effective* net area. Another way of treating the behavior is to think of it as combined tension and bending. Using AISC interaction equations, an equivalent reduction factor can be found (Epstein and D'Aiuto, 2002). Block shear is usually initiated with tension fracture. At the point where this occurs, the tension stresses, resulting from the load eccentricity, are more than the average load divided by the net area. Incorporating U into the block shear equations produces far more satisfactory results, not only for angles, but for flange connected tee sections as well (Epstein and Stamberg, 2002).

Before proceeding further, it should be pointed out that there has been disagreement with the idea that the block shear equations need modification to account for eccentricity. Grondin (2005) wrote that, "Although angles in tension represent a different case since both in-plane and out-of-plane eccentricities are present, the writer believes that these eccentricities are sufficiently small and the ductility of steel sufficiently large to minimize the effect of these eccentricities on the block shear capacity of angles in tension." Another study (Kulak and Grondin, 2001) concluded that, "Further research is required to investigate the effect of out-of-plane eccentricity on block shear failure." However, no change was recommended in the approach for angles, in part, because 12 of the 15 block shear failures previously documented (Epstein, 1992) involved connections with staggered gage lines. Stagger, however, was shown not to have an appreciable effect on capacity.

BACKGROUND: TEES AND OTHER SECTIONS

A limited number of tests on tee sections in tension produced surprising results (Epstein, 1996b). The tees were connected through the flange and the stem was the outstanding element. A previously undocumented *alternate* failure path in block shear was discovered during the testing (see Figure 2). This led to a full investigation of structural tees in tension. Finite element analyses were then performed, and they supported this new block shear failure mode of structural tees in tension (Epstein and McGinnis, 2000). The results compared very well with previous tests in replicating the newly discovered alternate block shear failure path. It was found that the moments caused by the eccentricity were not equal to the axial load multiplied by the eccentricity. The reactions at the first and last bolts along a line of bolts created an opposing moment, which reduced the moment caused by the eccentricity. Again, it was concluded that the shear lag factor, U, should be incorporated in the tension terms of the block shear equations.

A series of tests on 50 structural tees in tension were performed (Epstein and Stamberg, 2002). The specimens were bolted through the flange, with the stem outstanding, and had varying eccentricities and connection lengths. The geometries of the specimens were chosen such that a progression from net section failure to block shear failure would occur. The tests exhibited behavior that matched what was indicated by finite element models. As connection lengths decreased or eccentricities increased, or both, the efficiencies of the connections decreased. The previously obtained theoretical results (Epstein and D'Aiuto, 2002) for these tests were compared to the values calculated using the then current (second edition) *Specification*. Even though the theory was originally based on block shear in tees, it was found to agree with the net tension failure results as well. In addition to incorporating a reduction factor in block shear equations, it was also suggested that, as a simplified design approach, a reduced lower bound for the shear lag factor, U, may be appropriate for net section failures.

THE 2005 SPECIFICATION TREATMENT

The shear lag coefficients have been significantly reduced in the 2005 AISC *Specification for Structural Steel Buildings*, which combines ASD and LRFD into one document (AISC, 2005). Block shear design capacity is given by the basic equation for tension rupture-shear yield as

$$\phi R_n = \phi[0.6F_y A_{gv} + U_{bs} F_u A_{nt}] \quad (6)$$

In Equation 6, the term $0.6F_yA_{gv}$ shall not be taken greater than $0.6F_uA_{nv}$, which represents the rupture-rupture limit state. This, in essence, is Equation 3a with the exception of U_{bs}. U_{bs} is a new term that was added to the block shear design equation to account for the effect of eccentricity on the block shear capacity of a connection. This equation is certainly similar to what was proposed previously (Epstein, 1992). Note that shear rupture-tension yield is no longer considered. Many past research studies noted that block shear failures usually initiated with a tension fracture.

The definition and limits for the variable, U_{bs}, went through revisions during the development of the 2005 *Specification*. In an earlier treatment, the following equation was used to calculate U_{bs}:

$$U_{bs} = 1, \text{ if } e/l \le 1/3 \quad (7a)$$

or

$$U_{bs} = 1 - e/l, \text{ if } e/l > 1/3 \quad (7b)$$

where

e = eccentricity of the force tending to cause block shear rupture in the plane of the connection faying surface

l = length of the block subject to block shear rupture

The variable e is equivalent to $\bar{x}$ in Equation 5. Note that, however, l is not the same as in the Equation 5. The difference is that the term l in Equations 7a and 7b is equal to the length of the block subject to block shear and in the equation for U it is equal to the length of the connection. Therefore, for the same connection, U_{bs} will be larger than U because the length of the block subject to block shear will be greater than the length of the connection for standard connections.

In a subsequent treatment (which became the one adopted in the 2005 *Specification*) it was stated that U_{bs} is equal to 1.0 when the tension stress is uniform, and equal to 0.5 when the tension stress is nonuniform. This U_{bs} does not vary according to any parameter of a connection, such as connection length or eccentricity. This definition certainly simplifies calculations.

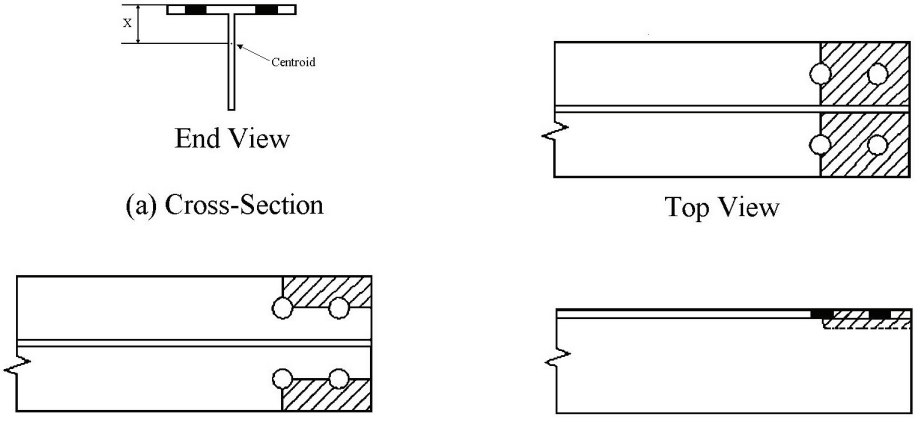

Fig. 2. Block shear failure path for tee sections.

THE EFFECT OF THE BLOCK SHEAR REVISIONS ON DESIGN CAPACITIES

In this section, the data from previous research on angles at the University of Connecticut (Epstein, 1992) will be used to examine the effect of the latest revision on block shear capacities (Equation 6). The majority (35) of the 38 geometries tested in the 1992 study showed block shear failures and only those are used herein for the comparisons. Since, with the 2005 *Specification*, ASD and LRFD treatments have coalesced, only LRFD will be presented in the following (Aleksiewicz, 2004).

Table 1 shows the material properties and geometries of the single angle specimens that were tested in the 1992 investigation (Epstein, 1992). In this table, specimen numbers are the same as used in 1992 and material properties of yield and ultimate were as measured. The bolt patterns refer to the number of bolts in the two gage lines and whether or not they were staggered (+ or – denotes stagger and which gage line had the lead bolt). For more specific details of the specimens, the reader is referred to the original paper (Epstein, 1992).

Also presented in Table 1 are the capacities, as calculated from the third edition of the LRFD *Specification* (LRFD, 1999), as well as those from the latest *Specification* (AISC, 2005). Equation 6, from the 2005 *Specification*, uses U_{bs} either equal to 1.0 (for uniform tensile stresses) or 0.5 (for nonuniform tensile stresses). Therefore, U_{bs} is determined by the type of connection, not the specific parameters of a connection such as connection length (l) or the amount of eccentricity (e or $\bar{x}$). Tension members not connected through all of their elements develop nonuniform tensile stresses due to shear lag. Also, eccentricity causes bending which creates nonuniform tensile stresses. Any connection that has either of these characteristics (angles have both) should, therefore, use the value of 0.5 for U_{bs}. The capacities for the 2005 *Specification* in Table 1 include 0.5 for U_{bs}.

Figure 3 shows the relationship between PF (professional factor, which is the ratio of the failure load determined by destructive testing divided by the corresponding design capacity based on measured material and geometric properties) versus $1 - e/l$ for the 1999 and 2005 *Specifications* for the data in Table 1. Least square "trend lines" (straight line fits of the data) are used for comparison. The 1999 data is similar to that of previous *Specifications* in that many Professional Factors are below 1.0 and as the eccentricity increased or the connection length decreased, the trend for Professional Factors decreased.

If the earlier treatment for U_{bs} in Equation 7 were used, there would be no difference in results from 1999 except for specimens #1, 3, 5, and 6, shown in Table 1, because only these had values of $1 - e/l < 0.67$. In Figure 3, because the factor $U_{bs} = 0.5$ has been applied to all block shear tension areas for the 2005 data, clearly all professional factors (PF) shown are increased when compared to the 1999 data. The trend line for 2005 clearly shows a marked improvement.

So, it appeared that the approach settled upon for block shear had been satisfactorily addressed. However, in the 2005 *Specification* Commentary Section J4.3 on block shear (see Figure 4), it becomes readily evident that there is no change for angles because "angle ends" are shown in the category of $U_{bs} = 1.0$ (Figure 4a).

It is not apparent if there is a change for tees, which also, as previously noted, have capacities (net tension and block

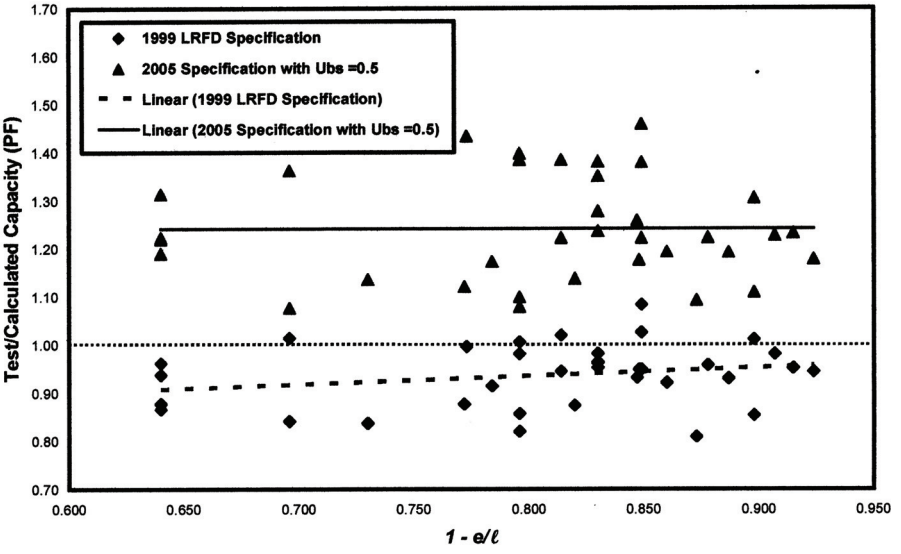

Fig. 3. 1998 LRFD vs. 2005 (with U_{bs} *= 0.5) block shear treatment for tested angles.*

Table 1. Geometry, Material Properties and Block Shear Capacities										
#	Member	Bolt Pattern	F_y ksi	F_u ksi	$1 - e/l$	P_{test} kips	1999 LRFD		2005 LRFD	
							kips	PF	kips	PF
1	6x6x5/16	2/2+	51.9	73.9	0.640	182.5	157.9	0.87	111.8	1.22
2	6x6x5/16	2/2-	51.4	77.0	0.730	204.2	182.8	0.84	134.8	1.14
3	6x6x5/16	2/2	51.0	75.5	0.640	188.7	150.8	0.94	107.7	1.31
4	6x6x5/16	2/3-	53.0	77.2	0.820	242.7	208.1	0.87	160.0	1.14
5	6x6x5/16	3/2+	49.3	73.6	0.640	204.9	175.1	0.88	129.1	1.19
6	6x6x5/16	2/3	51.4	75.0	0.640	259.7	202.4	0.96	159.6	1.22
7	6x6x5/16	3/3	51.6	74.8	0.784	237.1	194.3	0.92	151.6	1.17
9	6x4x5/16	2/2+	51.0	72.4	0.796	202.7	154.9	0.98	109.7	1.39
10	6x4x5/16	2/2-	46.8	68.2	0.847	203.9	164.1	0.93	121.5	1.26
11	6x4x5/16	2/2	50.3	71.0	0.796	194.2	144.8	1.01	104.2	1.40
12	6x4x5/16	2/3-	55.5	80.0	0.898	247.1	216.9	0.85	167.0	1.11
13	6x4x5/16	3/2+	50.5	70.2	0.796	189.1	172.8	0.82	129.0	1.10
14	6x4x5/16	2/3	49.4	68.9	0.796	219.8	192.2	0.86	152.8	1.08
15	6x4x5/16	3/3	46.5	64.9	0.878	218.6	171.1	0.96	134.0	1.22
17	6x3½x5/16	2/2+	48.3	74.5	0.830	198.2	154.1	0.96	107.6	1.38
18	6x3½x5/16	2/2-	52.5	76.6	0.873	198.8	184.2	0.81	136.4	1.09
19	6x3½x5/16	2/2	52.1	78.2	0.830	199.3	155.3	0.96	110.6	1.35
20	6x3½x5/16	2/3-	50.3	68.5	0.915	238.5	187.8	0.95	145.1	1.23
21	6x3½x5/16	3/2+	49.5	69.4	0.830	216.1	170.1	0.95	126.8	1.28
22	6x3½x5/16	2/3	48.0	69.1	0.830	250.6	191.4	0.98	151.9	1.24
23	6x3½x5/16	3/3	45.6	69.3	0.898	236.5	175.4	1.01	135.8	1.31
25	5x5x5/16	2/2+	44.3	62.0	0.696	154.1	114.0	1.01	84.8	1.36
26	5x5x5/16	2/2-	44.6	61.5	0.772	155.8	133.2	0.88	104.2	1.12
27	5x5x5/16	2/3-	45.1	63.2	0.848	194.9	153.9	0.95	124.2	1.18
28	5x5x5/16	3/2+	50.4	70.1	0.696	169.6	151.1	0.84	118.1	1.08
29	5x3½x5/16	2/2+	47.9	71.6	0.814	174.1	128.0	1.02	94.3	1.38
30	5x3½x5/16	2/2-	45.0	67.8	0.860	171.8	139.8	0.92	107.9	1.19
31	5x3½x5/16	2/3-	45.2	68.2	0.907	208.8	159.6	0.98	127.5	1.23
32	5x3½x5/16	3/2+	48.8	72.6	0.814	189.9	150.7	0.94	116.5	1.22
33	5x3x5/16	2/2+	42.5	59.4	0.849	149.4	109.2	1.03	81.2	1.38
34	5x3x5/16	2/2-	43.1	61.0	0.887	161.5	130.2	0.93	101.5	1.19
35	5x3x5/16	2/3-	42.5	62.6	0.924	187.2	148.6	0.94	119.1	1.18
36	5x3x5/16	3/2+	42.2	61.1	0.849	163.0	128.7	0.95	100.0	1.22
37	5x3x5/16	1/2-	46.1	65.4	0.849	173.3	119.9	1.08	89.1	1.46
38	5x3x5/16	2/1+	44.1	61.8	0.773	126.8	95.4	1.00	66.3	1.43

shear) that are significantly reduced when only the flange is connected. Further, since W shapes connected only by the flanges are usually treated as half tees, one would assume that their block shear strength would also be compromised. It is not clear what value of U_{bs} should be used for this case.

A User Note in Section J4.3 of the 2005 *Specification* states that, "The cases where U_{bs} must be taken equal to 0.5 are illustrated in the Commentary"(Figure 4 herein). So, are only coped beam connections having significant in-plane eccentricities affected by the new treatment for block shear?

There is a recent study of the treatment of block shear equations that are presented in various design standards (Driver, Grondin and Kulak, 2006). In this study, several standards were compared for many tests of gusset plates, angles, tees and coped beams. It was concluded that, except for gusset plates, there should be a reduction factor (comparable to U_{bs}) applied to the tension term of the block shear equation. (It was also proposed to modify the shear term with a combination of yield and ultimate stresses).

In particular, for coped beams, Driver et al. (2006) proposed a reduction factor of 0.9 for the tension term in coped beams where there is one row of bolts (as shown in Figure 4a wherein U_{bs} is 1.0). For coped beams with two rows of bolts (as shown in Figure 4b wherein U_{bs} is 0.5), they proposed 0.3. In reality, the factor used for the single row coped beam connection is not that critical since the tension term is only a fraction of the shear term. For a two bolt connection (in one row) on a coped beam, the tension term is as large a percentage of the total as possible. But even then, the reduction in capacity would only be approximately 15% if U_{bs} = 0.5 instead of the 1.0 factor given in the 2005 AISC *Specification*. For longer connections (three or more bolts), this decrease is much less.

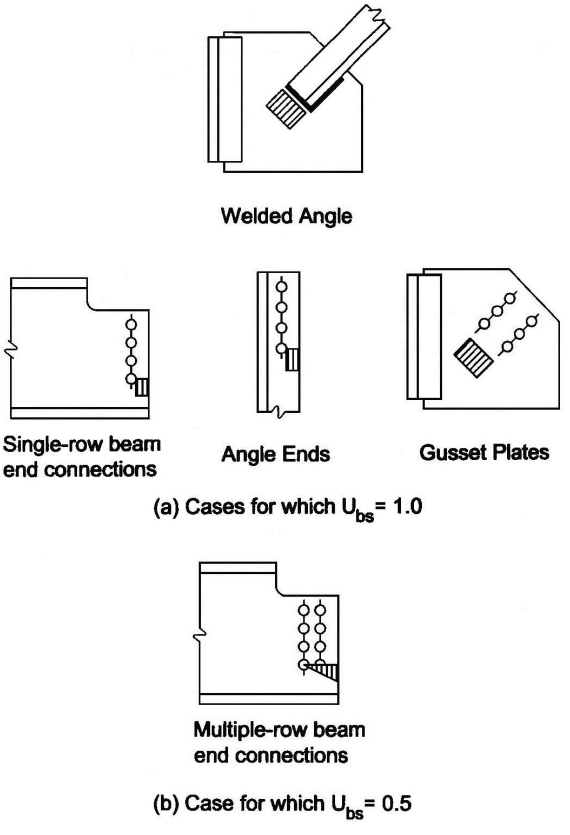

Fig. 4. Values of U_{bs} *as shown in Figure C-J4.2 of the 2005 AISC Specification Commentary (AISC, 2005).*

What about angles (and tees)? Even for one row of bolts in an angle or the stem of a tee, it was reported (Orbison, Wagner and Grondin, 1999) that the smaller the edge distance, the smaller the professional factor. Their tests were for fairly long connections (four bolts) in only one row. Therefore, the tension terms for these tests are a small percentage of the shear term. Even so, reduced edge distance reduced the professional factors, somewhat. The reason for this is fairly obvious. It is not that the stresses along the tension path are nonuniform; it is that their magnitude is increased because of the greater eccentricity of the load and, therefore, the increased effect of the resulting moment on the tension stresses. With only one row of bolts, however, similar to coped beams, it can be argued that using U_{bs} = 1.0 (as shown in Figure 4a) is satisfactory since, again, the tension term is a small fraction of the total.

But what happens with two rows of bolts in one leg of an angle? Note that all of the tests shown in Figure 3 had two rows of bolts. Further note that most of these tests were not included in the study of Driver et al. (2006) because there was stagger between the gage lines. Clearly, the tension term for these tests represents a larger percentage of the block shear capacity than when there is only a single row of bolts. So, the specifying of U_{bs} as significantly less than 1.0 appears to be appropriate.

As far as tees are concerned, Driver et al. show a reduction factor of 0.9. However, it does not appear that this was meant to apply to both situations of web-(referred to as "stem" by Driver et al.) connected and flange-connected tees because they do not include the latter in their list of investigations. For stem-connected tees, there is in-plane eccentricity, but for flange-connected tees there is out-of-plane eccentricity and the block shear failure for these usually extends into the web. For the flange-connected case, based on many tests (Epstein and Stamberg, 2002), it does not appear that the proposed reduction is sufficient. For tees that fail in block shear along the alternate path, the tension term is a significant fraction of the total block shear. Driver et al. did not report on these block shear failures when presenting their "unified" block shear equation.

CONCLUSIONS

Block shear treatment by AISC has undergone several revisions since 1978, where it first appeared, through the latest, 2005 equations. In the opinion of the authors, either the definition of U_{bs} must change or the figures in the Commentary need to include more cases where U_{bs} is not equal to 1.0. As a minimum, two gage lines in one leg of an angle as well as tees connected by their flanges and, probably, W sections connected by their flanges should be added to the cases in Figure 4b. The statement in the 2005 *Specification* that, "Where the tension stress is uniform, U_{bs} = 1.0; Where the tension stress is nonuniform, U_{bs} = 0.5 in., in conjunction with the limited cases shown in the Commentary, is not particularly helpful in pointing to cases where the use of U_{bs} = 1.0 may not be conservative. It is not that the tension stresses need to be nonuniform, but the magnitude of the stresses, as influenced by the eccentricity of the load, is what reduces the efficiency of the connection.

REFERENCES

Adidam, N. (1990), "Analysis of Block Shear Experiments for Structural Steel Angles in Tension," Thesis presented to the University of Connecticut, in partial fulfillment of the requirements for the degree of Master of Science.

Aleksiewicz, L.J. (2004), "A Review of the Capacity of Angles in Tension," Thesis presented to the University of Connecticut, in partial fulfillment of the requirements for the degree of Master of Science.

AISC (1978), *Specification for the Design, Fabrication and Erection of Structural Steel for Buildings*, American Institute of Steel Construction, Inc., Chicago, IL.

AISC (1986a), *Load and Resistance Factor Design Specification for Structural Steel Buildings*, American Institute of Steel Construction, Inc., Chicago, IL.

AISC (1986b), *Manual of Steel Construction, Load and Resistance Factor Design*, 1st Edition, American Institute of Steel Construction, Inc., Chicago, IL.

AISC (1989), *Specification for the Design, Fabrication and Erection of Structural Steel for Buildings*, American Institute of Steel Construction, Inc., Chicago, IL.

AISC (1993), *Load and Resistance Factor Design Specification for Structural Steel Buildings*, American Institute of Steel Construction, Inc., Chicago, IL

AISC (1999), *Load and Resistance Factor Design Specification for Structural Steel Buildings*, American Institute of Steel Construction, Inc., Chicago, IL.

AISC (2005), *Specification for Structural Steel Buildings*, American Institute of Steel Construction, Inc., Chicago, IL.

Birkemoe, P. and Gilmor, M. (1978), "Behavior of Bearing Critical Double-angle Beam Connections," *Engineering Journal*, AISC, Vol. 15, No. 4, 4th Quarter, pp. 109–115.

Driver, R.G., Grondin, G.Y. and Kulak, G.L. (2006), "Unified Block Shear Equation for Achieving Consistent Reliability," *Journal of Constructional Steel Research*, Vol. 62, Issue 3, pp. 210–222.

Epstein, H. (1992), "An Experimental Study of Block Shear Failure of Angles in Tension," *Engineering Journal*, AISC, Vol. 29, No. 2, 2nd Quarter, pp. 75–84.

Epstein, H.I. and Chamarajanagar, R. (1996), "Finite Element Studies for Correlation with Block Shear Tests," *Computers and Structures*, Vol. 61, No. 5, pp. 967–974.

Epstein, H.I. (1996a), "Effects of the Latest LRFD Block Shear Code Change," *Engineering Journal*, AISC, Vol. 33, No.1, 1st Quarter, pp. 30–33.

Epstein, H. (1996b), "Block Shear of Structural Tees in Tension - Alternate Paths," *Engineering Journal*, AISC, Vol. 33, No. 4, 4th Quarter, pp. 147–152.

Epstein, H. and D'Aiuto, C. (2002), "Using Moment and Axial Interaction Equations to Account for Moment and Shear Lag Effects in Tension Members," *Engineering Journal*, AISC, Vol. 39, No. 2, 2nd Quarter, pp. 91–99.

Epstein, H. and McGinnis, M. (2000), "Finite Element Modeling of Block Shear in Structural Tees," *Computers and Structures*, Vol. 77, No. 5, pp. 571–582.

Epstein, H. and Thacker, B. (1991), "The Effect of Bolt Stagger for Block Shear Tension Failures in Angles," *Computers and Structures*, Vol. 39, No. 5, pp. 571–576.

Epstein, H. and Stamberg, H. (2002), "Block Shear and Net Section Capacities of Structural Tees in Tension: Test Results and Code Implications," *Engineering Journal*, AISC, Vol. 39, No. 4, 4th Quarter, pp. 228–239.

Grondin, G. (2005), Discussion of "Using Moment and Axial Interaction Equations to Account for Moment and Shear Lag Effects in Tension Members," *Engineering Journal*, AISC, Vol. 42, No. 1, 1st Quarter, pp. 45–50.

Gross, J.M. (1994), "A Study of Block Shear Failure in Bolted Connections in High-strength Steel Angles," Master of Science Thesis, Bucknell University, Lewisburg, PA.

Hardash, S. and Bjorhovde, R. (1985), "New Design Criteria for Gusset Plates in Tension," *Engineering Journal*, AISC, Vol. 22, No. 2, 2nd Quarter, pp. 77–94.

Kulak, G.L. and Grondin, G.Y. (2001), "AISC LRFD Rules for Block Shear – A Review," *Engineering Journal*, AISC, Vol. 38, No. 4, 4th Quarter, pp. 199–203.

Orbison, J.G., Wagner, M.E. and Grondin, G.Y. (1999), "Tension Plate Behavior in Single-row Bolted Connections Subject to Block Shear," *Journal of Constructional Steel Research*, Vol. 49, Issue 3, pp. 225–239.

Ricles, J. and Yura, J. (1983), "Strength of Double-row Bolted Web Connections," *Journal of Structural Engineering*, ASCE, Vol. 109, No. 1, ST1, pp. 488–490.

Designing Compact Gussets with the Uniform Force Method

LARRY S. MUIR

In 1991 an AISC task group endorsed the uniform force method (UFM) as the preferred method for determining the forces that exist at gusset interfaces. Since that time it has been included in the AISC *Manual of Steel Construction*. The UFM provides a standardized way to obtain economical, statically admissible force distributions for vertical bracing connections. One criticism of the method is that it sometimes results in oddly shaped or disproportionately large gusset plates. To overcome this perceived limitation of the UFM, designers have been seeking out alternate methods.

This paper demonstrates that removing one unnecessary geometrical constraint from the formulation of the UFM will allow greater freedom in gusset geometry, while maintaining the efficiencies that result from the method. A new formulation of the UFM is presented, and the strengths and weaknesses of other proposed design methods are also explored.

THE UNIFORM FORCE METHOD

The uniform force method has been included in the AISC *Manual of Steel Construction* since 1992. The UFM was originally proposed by Thornton (1991) and was based on observations from Richard's (1986) research. In the commonly accepted form, the UFM produces the following force distribution:

$$H_b = \frac{\alpha}{r} P \tag{1a}$$

$$V_b = \frac{e_b}{r} P \tag{1b}$$

$$H_c = \frac{e_c}{r} P \tag{1c}$$

$$V_c = \frac{\beta}{r} P \tag{1d}$$

where

$$r = \sqrt{\left(\alpha + e_c\right)^2 + \left(\beta + e_b\right)^2} \tag{2}$$

$$\alpha = \tan\theta \left(\beta + e_b\right) - e_c \tag{3}$$

In order to satisfy the relationship between α and β, the designer is often forced to use either an oddly shaped or disproportionately large gusset plate. Alternately, moments can be introduced at the connection interfaces. Neither approach is ideal.

ALTERNATIVES TO THE UNIFORM FORCE METHOD

Any viable alternative sought to replace the UFM should meet the following criteria: (1) it must provide a clear procedure to satisfy equilibrium and conform to the basic assumptions made during the analysis and design of the main members (the most important criterion); (2) since the UFM readily accommodates a wide range of geometries and boundary conditions, any alternate method should also be able to accommodate such situations; and (3) it must result in economical designs.

Several alternatives to the UFM have been proposed. Chief among the alternatives are the KISS Method, the parallel force method and the truss analogy method. None of these methods suffer from the constrictive relationship between α and β that exists in the UFM. In other words, these methods can be used with any gusset geometry and do not force the use of oddly shaped or large gusset plates. The strengths and weaknesses of these methods will be explored. In all of the discussions the work-point of the brace is assumed to be located at the intersection of the centerlines of the beam and the column, since this is the typical case.

Larry S. Muir is president of Cives Engineering Corporation and chief engineer of Cives Steel Company, Roswell, GA.

The KISS Method

KISS (Figure 1) is an acronym for "keep it simple stupid," and the method is simple, as the name implies, and foolproof, though uneconomical. The method involves delivering the entire horizontal brace component directly to the beam through the beam-to-gusset connection and the entire vertical brace component directly to the column through the column-to-gusset connection. To satisfy equilibrium, moments must be introduced. At the beam-to-gusset the moment is equal to He_b, and at the column-to-gusset the moment is equal to Ve_c.

The KISS Method satisfies two of the three criteria for a viable alternative to the UFM. It satisfies equilibrium and the design and analysis assumptions, and it is universally applicable to all geometries and boundary conditions. However, the presence of the large moments at the connection interfaces makes it an uneconomical choice in practice.

The Parallel Force Method

In the parallel force method, sometimes referred to as the component method (Figure 2), the reactions of the gusset at the beam and column interfaces are assumed to act parallel to the brace force. Since the forces are parallel, they obviously do not intersect at a common point, as is the case with the UFM. Therefore, in order to maintain rotational equilibrium, two choices are available. Either the magnitude of the parallel forces are set so that they balance each other about the work-line of the brace, or moments are added at the beam and/or column interfaces. The additional moments, though lesser in magnitude than the KISS method, adversely impact the economy of the connection.

If the former approach is taken, rotational equilibrium of the beam and column will not generally be satisfied. A moment connection will then have to be added between the beam and the column. Since this will normally be a field-welded connection, this is considered to be an uneconomical alternative in most parts of the country.

In terms of applicability to a variety of boundary conditions, the parallel force method suffers from a major shortcoming. Since the forces at both the beam-to-gusset and the column-to-gusset interfaces are assumed parallel to the brace force, a horizontal component will always exist at the column-to-gusset connection. When framing to a column web, this presents a significant design challenge, which will usually be overcome by the addition of column stiffening local to the connection, further reducing the economy of the method.

The parallel force method only satisfies one of the three criteria for a viable alternative to the UFM. It satisfies equilibrium and the design and analysis assumptions, but it is not as economical as the UFM and is not suited to connections made to column webs.

The Truss Analogy Method

The truss analogy method (Figure 3) determines the force distribution on the gusset by modeling the interface forces as a pinned "truss" node located at the center of the brace-to-gusset connection. The truss analogy method suffers the same problem as the parallel force method when attaching to column webs. Additionally, the truss analogy method can result in counterintuitive and uneconomical force distributions. This is illustrated in Figure 3 where the gusset-

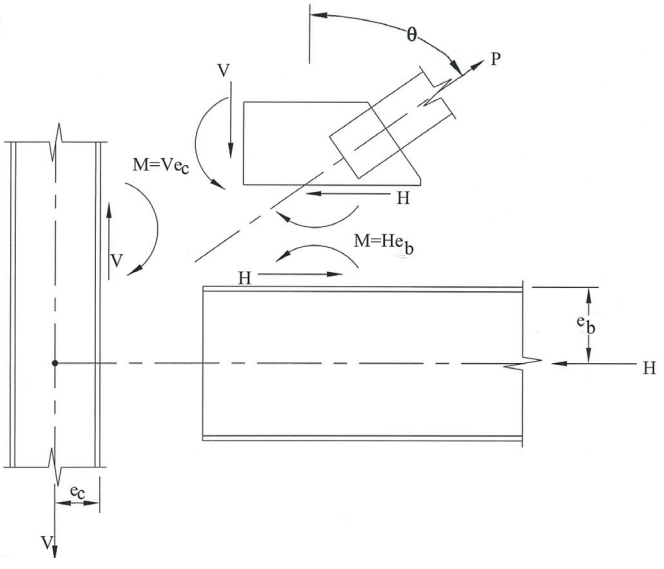

Fig. 1. KISS method.

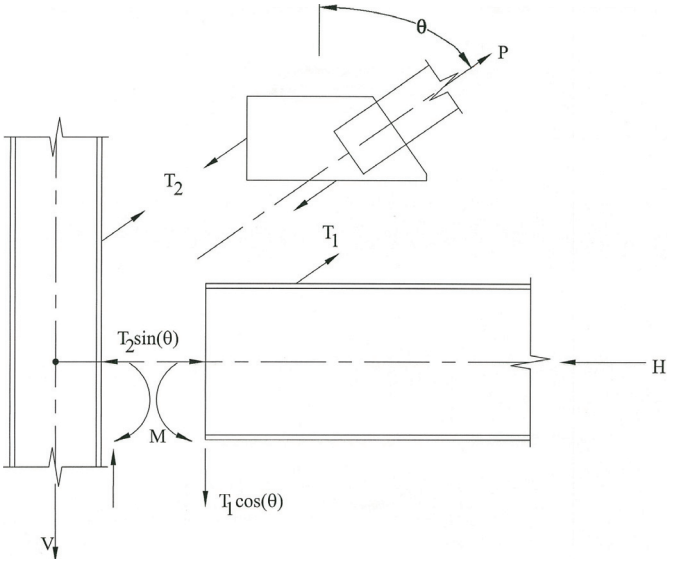

Fig. 2. Parallel force method.

to-column connection delivers only a horizontal component to the column. A formalized treatment of the equilibrium requirements for the beam and column has never been presented and is therefore left to the designer. Often moments are required at all of the connection interfaces in order to satisfy equilibrium.

The truss analogy method satisfies none of the criteria for a viable alternative to the UFM.

A GENERALIZED UFM

Since none of the alternatives investigated appear to provide better results than the UFM, it is advantageous to make adjustments to the formulation of the UFM to make it more applicable to compact gussets.

The goal of the UFM was to derive a procedure to obtain statically admissible force distributions, which would produce no moments at the connection interfaces and would be applicable to a wide range of geometries and boundary conditions. However, the procedure includes an additional constraint that unnecessarily limits its applicability. The force at the gusset-to-column interface, $\sqrt{V_c^2 + H_c^2}$, is forced to pass through a point that lies a distance, e_b, above the work-point.

Since there is a perceived problem with the UFM that can be overcome by removing this constraint, it is advantageous to eliminate it from the method. In order to do so, the problem must first be defined. There are essentially three elements involved: the beam, the column, and the gusset. The brace is neglected since it is assumed to carry only axial force and is not part of the indeterminate system. Each of the three members is subjected to three forces. In order for moments to be eliminated from the interfaces the forces applied to each element must intersect at a single point. These points of intersection are referred to as control points.

The Beam

It is easiest to begin with the beam (Figure 4), since the location of its control point is evident. The three forces applied to the beam are the horizontal component of the brace, H, the beam-to-gusset force, $\sqrt{V_b^2 + H_b^2}$, and the beam-to-column force, $\sqrt{V_b^2 + H_c^2}$. The horizontal component of the brace is resisted along the centerline of the beam and intersects the beam-to-column force at the point (e_c, 0). Therefore, the beam-to-gusset force must also pass through this point. From this we find that

$$\frac{V_b}{H_b} = \frac{e_b}{\alpha} \tag{4}$$

The Gusset

The three forces applied to the gusset (Figure 5) are the brace force, P, the beam-to-gusset force, $\sqrt{V_b^2 + H_b^2}$, and the gusset-to-column force, $\sqrt{V_c^2 + H_c^2}$. In order to eliminate moments at the interfaces, these three forces must intersect at a single point. Since the slope of the brace force, $1/\tan(\theta)$, and the slope of the beam-to-gusset force, e_b/α, are known, the intersection can be determined. The gusset control point is:

$$\left(\frac{e_b e_c \tan(\theta)}{e_b \tan(\theta) - \alpha}, \frac{e_b e_c}{e_b \tan(\theta) - \alpha} \right)$$

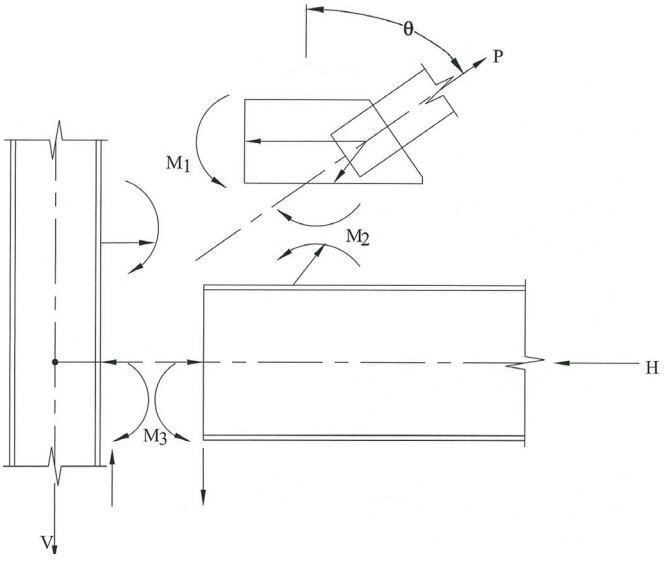

Fig. 3. Truss analogy method.

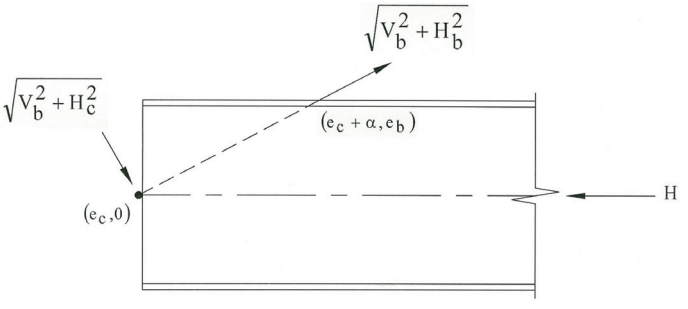

Fig. 4. Beam free body diagram.

The Column

The three forces applied to the column (Figure 6) are the vertical component of the brace, *V*, the column-to-gusset force, $\sqrt{V_c^2 + H_c^2}$, and the beam-to-column force, $\sqrt{V_b^2 + H_c^2}$. Knowing that the gusset-to-column force must pass through the gusset control point, the slope of the gusset-to-column force is:

$$\frac{V_c}{H_c} = \frac{\beta}{e_b}\left[\frac{e_b}{\beta}\left(1 - \frac{\tan(\theta)(e_b+\beta) - e_c}{\alpha}\right) + 1\right] \tag{5}$$

From this, since the column-to-gusset force and the beam-to-column force must intersect at the centerline of the column, the slope of the beam-to-column force is:

$$\frac{V_b}{H_c} = \frac{e_b}{e_c}\left(\frac{\tan(\theta)\left(e_b+\beta\right) - e_c}{\alpha}\right) \tag{6}$$

The point of intersection of the column-to-gusset force and the beam-to-column force, the column control point, is:

$$\left(0, e_b\left(\frac{\tan(\theta)\left(e_b+\beta\right) - e_c}{\alpha}\right)\right)$$

Force Distribution

Having established the geometrical constraints required to eliminate moments at all connection interfaces, the forces at the interfaces can be derived. Since the column must be in equilibrium, the following can be established:

$$\sum F_y = 0 = P\cos(\theta) - \left(V_b + V_c\right) \tag{7}$$

$$\sum F_x = 0 = H_c - H_c \tag{8}$$

$$\sum M = 0 = H_c\left(e_b + \beta\right) - P\cos(\theta)e_c \tag{9}$$

From this

$$H_c = \frac{\cos(\theta)e_c}{\left(e_b+\beta\right)}P \tag{10}$$

To satisfy the requisite geometry for the beam-to-gusset and beam-to-column forces, the following must be true:

$$V_b = \left[\frac{e_b\left(\sin(\theta)\left(e_b+\beta\right) - \cos(\theta)e_c\right)}{\alpha\left(e_b+\beta\right)}\right]P \tag{11}$$

The remaining forces are apparent:

$$H_b = P\sin(\theta) - H_c \tag{12}$$

$$V_c = P\cos(\theta) - V_b \tag{13}$$

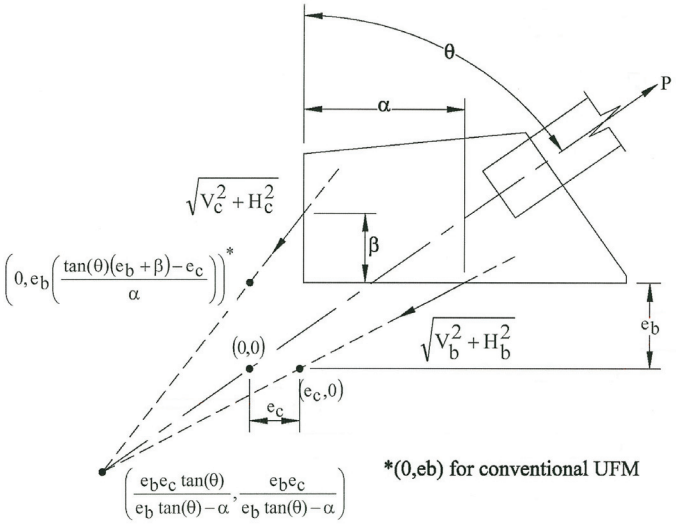

Fig. 5. Gusset free body diagram.

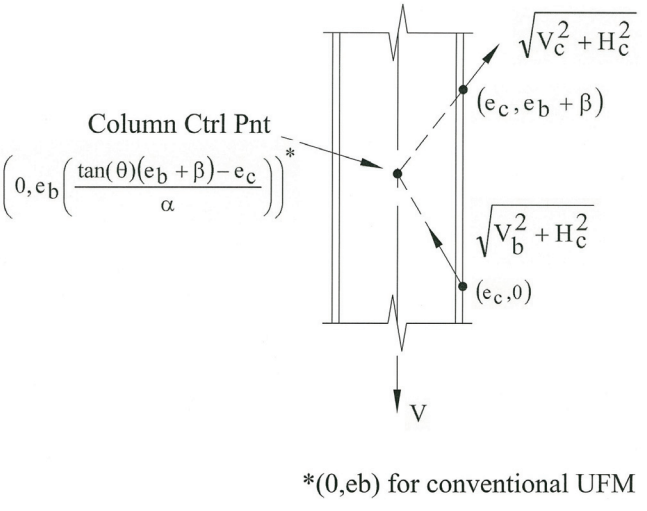

Fig. 6. Column free body diagram.

With the geometry and force distribution established, a new form of the UFM has been derived without the somewhat arbitrary constraint on the location of the column control point. Without this constraint, α and β can be set to any convenient values. This removes the need to consider the moments caused by $\bar{\alpha}$ and $\bar{\beta}$, where $\bar{\alpha}$ is the actual distance from the face of the column flange to the centroid of the gusset-to-beam connection, and $\bar{\beta}$ is the actual distance from the face of the beam flange to the centroid of the gusset-to-column connection.

However, there may still be a need to redistribute the vertical reaction delivered to the beam, V_b. This counteracting force is referred to as ΔV_b. ΔV_b can be introduced into this new formulation easily to produce the full spectrum of force distributions that can exist in the connection while maintaining column-to-gusset and beam-to-column connections free of moments. It is assumed that moments at the column-to-gusset and beam-to-column connections are uneconomical and therefore undesirable.

Of course the introduction of ΔV_b disrupts the established equilibrium and adjustments must be made. The adjustment involves introducing a moment at the beam-to-gusset interface. This moment can be calculated as:

$$M_b = H_b e_b - \left(V_b - \Delta V_b\right)\alpha \tag{14}$$

Column Moment

A moment gradient will exist in the column whether using the original formulation or the new formulation of the UFM presented in this paper. Using the original formulation, the moment will be zero at the intersection of the top of steel elevation and the centerline of the column. In the new formulation, the moment may be either positive or negative throughout the section of the column bounded by the connection or the moment may be zero at some section similar to the original formulation. In either case the maximum moment the column will be subjected to can be determined as:

$$M_c = \max\left\{V_c e_c, \left(V_c e_c - H_c\left(e_b + \beta\right)\right)\right\} \tag{15}$$

Since the choice of column section will usually be governed by buckling and the column is restrained from buckling local to the brace connection, it is normal practice to neglect this moment. For this reason, the moment internal to the column is not mentioned in the AISC *Steel Construction Manual* (AISC, 2005) discussion of the UFM.

An Example

The forces on the connection shown in Figure 7 will be calculated to demonstrate the new formulation.

$$\alpha = \frac{27.75}{2} + 0.5 = 14.375 \text{ in.}$$

$$\beta = \frac{13}{2} = 6.5 \text{ in.}$$

$$H_c = \frac{\cos\left(55^o\right)\left(7\right)}{\left(12+6.5\right)}100 = 21.7 \text{ kips}$$

$$V_b = \left[\frac{\left(12\right)\left(\sin(55^o)\left(12+6.5\right) - \cos(55^o)\left(7\right)\right)}{\left(14.375\right)\left(12+6.5\right)}\right]\left(100\right)$$

$$= 50.3 \text{ kips}$$

$$H_b = 100\sin\left(55^o\right) - 21.7 = 60.2 \text{ kips}$$

$$V_c = 100\cos\left(55^o\right) - 50.3 = 7.06 \text{ kips}$$

Summing moments on the beam about the beam control point produces:

$$V_b\alpha - H_b e_b = 50.3(14.375) - 60.2(12) \approx 0 \text{ kip-in.}$$

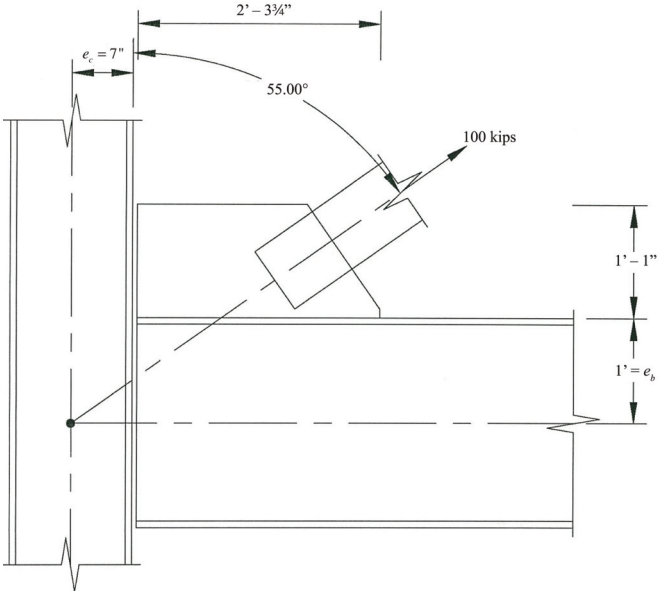

Fig. 7. Example.

Summing moments on the gusset about the work-point produces:

$$V_b\left(\alpha+e_c\right)-H_be_b+V_ce_c-H_c\left(e_b+\beta\right)=50.3(14.375+7)-$$

$$60.2(12)+7.06(7)-21.7(12+6.5)\approx 0\text{ kip-in.}$$

Summing moments on the column about the beam-to-column connection produces:

$$P\cos(\theta)e_c-H_c\left(e_b+\beta\right)=100\cos(55^o)(7)-21.7(12+6.5)$$

$$\approx 0\text{ kip-in.}$$

Note that:

$$\tan(\theta)\left(\beta+e_b\right)-e_c=\tan(55^o)\left(6.5+12\right)-7=19.4\neq\alpha$$

For completeness the vertical coordinate of the column control point can be calculated as:

$$y_{ccp}=e_b\left(\frac{\tan(\theta)\left(e_b+\beta\right)-e_c}{\alpha}\right)$$

$$=(12)\left(\frac{\tan(55^o)\left(12+6.5\right)-7}{14.375}\right)=16.2\text{ in.}$$

It may be noted that for this case the term V_b is significantly larger than would be obtained using the traditional UFM. As is the case with the traditional UFM, a ΔV_b can be introduced to manipulate the distribution of vertical force. Taking ΔV_b equal to 13.1 kips produces the same distribution of vertical force that is obtained from the UFM when all parameters except α are held constant.

As can be seen from Table 1, which presents a comparison of the traditional UFM to the modified UFM, each can be modified to produce identical results. This is to be expected since each must satisfy equilibrium. The primary advantage to the new formulation is that it eliminates the need for the modifiers $\bar{\alpha}$ and $\bar{\beta}$. Also the new formulation makes it easier to overcome the perceived limitations of the UFM.

Table 1. Comparison of the Traditional and the Modified Uniform Force Methods

Parameters	Traditional UFM		Modified UFM	
	without $\bar{\alpha}$	with $\bar{\alpha}$	without ΔV_b	with ΔV_b
α	19.4	19.4	14.4	14.4
$\bar{\alpha}$	–	14.4	–	–
β	6.5	6.5	6.5	6.5
V_b	37.2	37.2	50.3	37.2
H_b	60.2	60.2	60.2	60.2
V_c	20.2	20.2	7.06	20.2
H_c	21.7	21.7	21.7	21.7
ΔV_b	–	–	–	13.1
M_b	–	188	–	188

OTHER PRACTICES THAT CAN REDUCE THE GUSSET PROFILE

Having eliminated the geometrical constraints on gusset size from the UFM, attention can be turned to other steps that can be taken to reduce the gusset profile.

The Whitmore Section

The Whitmore section is commonly accepted to be an area, which extends at a 30° angle from the edges of the brace-to-gusset connection along the length of the connection. The area beyond this section is assumed to be ineffective in terms of gross tension yielding and compression buckling of the gusset. It is common practice to try to include all of the allowed Whitmore section within the gusset, but it is not a requirement to do so. By allowing the edges of the gusset plate to encroach on the Whitmore section, the profile of the gusset can be reduced.

Weld Size

It is common practice to attempt to limit fillet weld sizes to those that can be applied in a single pass, usually 5⁄16 in. This greatly enhances connection economy, since the number of passes required to complete a weld increases disproportionately with the leg size. To maintain a single pass weld, the gusset plate dimensions, particularly at the beam-to-gusset connection, are often increased. The gusset profile can be reduced by allowing multiple pass welds to be used, but only with increased fabrication costs.

Bolt Type

If reducing the gusset profile is of paramount concern, the strongest possible bolt configuration should be employed. Slip-critical connections should be avoided since they will require more bolts and therefore a larger gusset profile. Likewise, if the threads will be excluded from the shear plane, which is usually the case for heavily loaded bracing connections, then the "X-value" for the bolts should be used. Providing a detail that places the bolts in double shear at the brace-to-gusset connection also helps to reduce the gusset profile.

CONCLUSIONS

The UFM, as currently presented in the Manual, contains an unnecessary constraint on the location of the column control point. This constraint often gives designers the perception that the method is ill suited to the design of compact gusset plates.

By eliminating the unnecessary constraint in the new formulation, force distributions can be derived that consist of only shear and axial forces at the connection interfaces. The new formulation also simplifies the UFM by eliminating the need for $\bar{\alpha}$ and $\bar{\beta}$.

By manipulating the term ΔV_b, designers can obtain the full spectrum of force distributions that can exist in the connection while maintaining column-to-gusset and beam-to-column connections free of moments.

NOTATION

e_b = one-half the depth of the beam

e_c = one-half the depth of the column

y_{ccp} = vertical coordinate of the column control point

P = brace load

H = horizontal component of the brace load

H_b = shear force on the beam-to-gusset connection

H_c = axial force on the beam-to-column and gusset-to-column connections (assumes no transfer force)

M_b = moment on the beam-to-gusset connection

V = vertical component of the brace load

V_b = shear force on the beam-to-column connection and axial force on the beam-to-gusset connection

V_c = shear force on the gusset-to-column connection

ΔV_b = change in the distribution of vertical load

α = distance from the face of the column flange or web to the centroid of the gusset-to-beam connection

β = distance from the face of the beam flange to the centroid of the gusset-to-column connection

$\bar{\alpha}$ = actual distance from the face of the column flange to the centroid of the gusset-to-beam connection (This term is not required in the new formulation.)

$\bar{\beta}$ = actual distance from the face of the beam flange to the centroid of the gusset-to-column connection (This term is not required in the new formulation.)

REFERENCES

AISC (2005), *Steel Construction Manual*, 13th Edition, American Institute of Steel Construction, Inc., Chicago, IL.

Richard, R.M. (1986), "Analysis of Large Bracing Connection Designs for Heavy Construction," *National Steel Construction Conference Proceedings*, American Institute of Steel Construction, Inc., Chicago, IL.

Thornton, W.A. (1991), "On the Analysis and Design of Bracing Connections," *National Steel Construction Conference Proceedings*, American Institute of Steel Construction, Inc., Chicago, IL.

Limit State Response of Composite Columns and Beam-Columns Part II: Application of Design Provisions for the 2005 AISC Specification

ROBERTO T. LEON and JEROME F. HAJJAR

The strength of composite beam-columns, including steel sections encased in concrete (also known as SRC) and steel sections filled with concrete (CFT), as presented in the 2005 AISC *Specification for Structural Steel Buildings*, ANSI/AISC 360-05 (AISC, 2005a), hereafter referred to as the 2005 AISC *Specification*, must be computed based on first principles of mechanics and reasonable models for the stress-strain characteristics of the materials. Chapter I of the 2005 AISC *Specification* provides two options to fulfill this requirement: a general approach labeled the strain-compatibility method and a simplified approach labeled the plastic stress distribution method.

The strain-compatibility method is conceptually similar to conducting cross section analysis of a reinforced concrete section, and requires the designer to:

1. Subdivide the cross section into a large number of areas (termed "fibers");
2. Assume a strain distribution across the cross-section and a location of the neutral axis;
3. Compute stresses based on the assumed stress-strain relationships for the different components (unconfined and confined concrete, reinforcing bars, and the steel shape);
4. Integrate the stresses over the cross section to obtain the total axial load and the moment about the plastic neutral axis (or other commonly assumed axis);
5. Iterate steps 2 through 4 to obtain an axial load-moment interaction surface for the column.

Roberto T. Leon is professor, school of civil and environmental engineering, Georgia Tech, Atlanta, GA and former chair, AISC Task Committee 5 on Composite Construction.

Jerome F. Hajjar is professor, department of civil and environmental engineering, University of Illinois, Urbana, IL.

The designer is free to use any reasonable assumptions, including a nonlinear strain distribution in step 2 and nonlinear material properties in step 3, so long as those assumptions are supported by analyses, test data, or other documentation. In general, the analysis is run with an assumption of a linear strain distribution in step 2 and simplified uniaxial material relationships in step 3.

Figure 1 illustrates the strain-compatibility procedure. Figure 1a shows the subdivision of the cross-section into a series of square "fibers" representing four different materials: unconfined concrete outside the ties, confined concrete inside the ties (shaded), reinforcing bar steel, and rolled shape steel. Figure 1b shows a linear strain distribution with an arbitrary location of the neutral axis. Figure 1c shows the material properties. For each material, it shows both the nonlinear stress-strain curves as may be assumed for the strain-compatibility analysis and the bilinear rigid-plastic curves (dashed lines) that would be assumed for a simplified analysis; for example, a plastic strength calculation. Figure 1d shows the stress distributions for the situation usually used to compute the ultimate strength of the cross-section, in other words, when the strain in the concrete, ε_c, has reached 0.003 and the steel strain in the extreme fiber of the steel shape, ε_s, has exceeded its yield strain. The concrete stress blocks are shown separately for clarity. Note that for this case the unconfined stress-strain relationship is shown up to the top edge of the section. Figure 1e shows a stress distribution when the concrete strain has exceeded 0.003 and the steel shape and reinforcing bars are well into the strain-hardening range. In this case the confined concrete stress-strain relationship is used, but limited to the confined section; the unconfined section has spalled off. Figure 1f shows the typical stress distribution used for the plastic stress distribution case. Note that this stress distribution does not correspond exactly to any "real" stress distribution but is considered as a conservative approximation for a section that can sustain concrete strain on the order of 0.005 and steel strains larger than 0.01.

In Figure 2, three qualitative curves are shown for the stress distributions shown in Figures 1d through f. The first curve is for the strength envelope consistent with a concrete strain of 0.003 at the extreme fiber (Figure 1d) while the

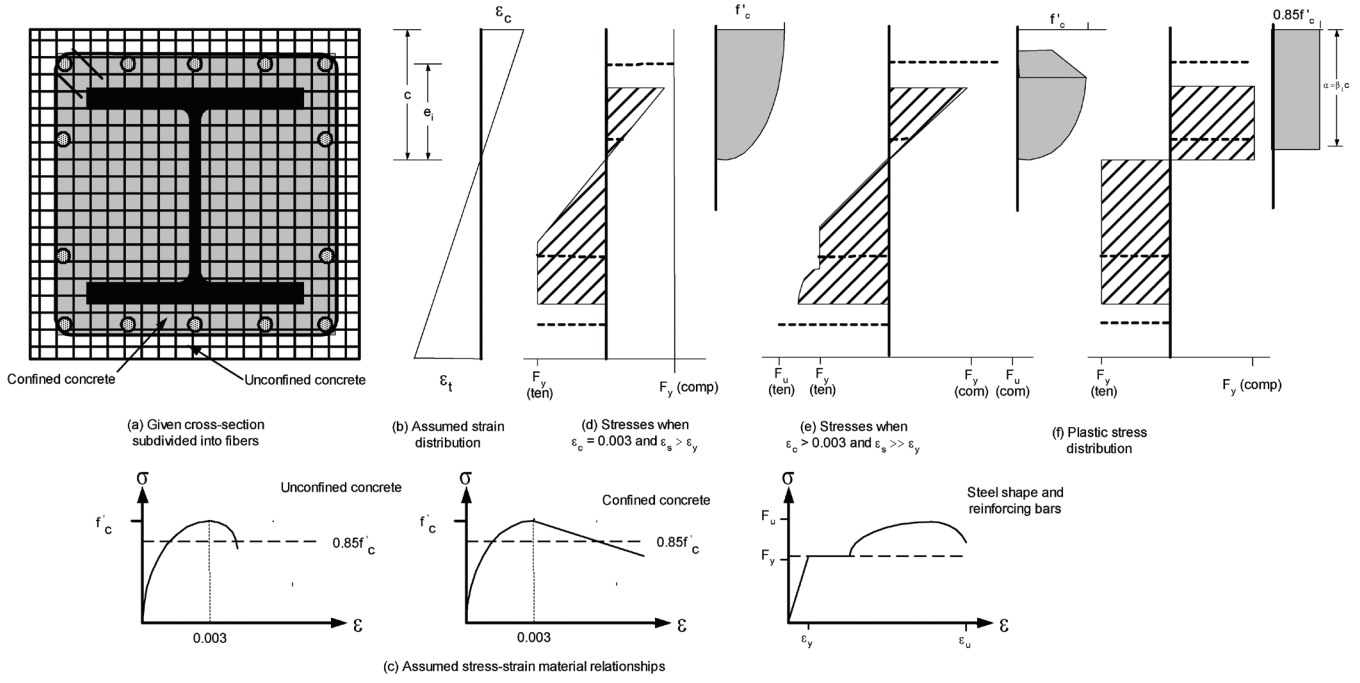

Fig. 1. Development of composite beam-column cross-section strength.

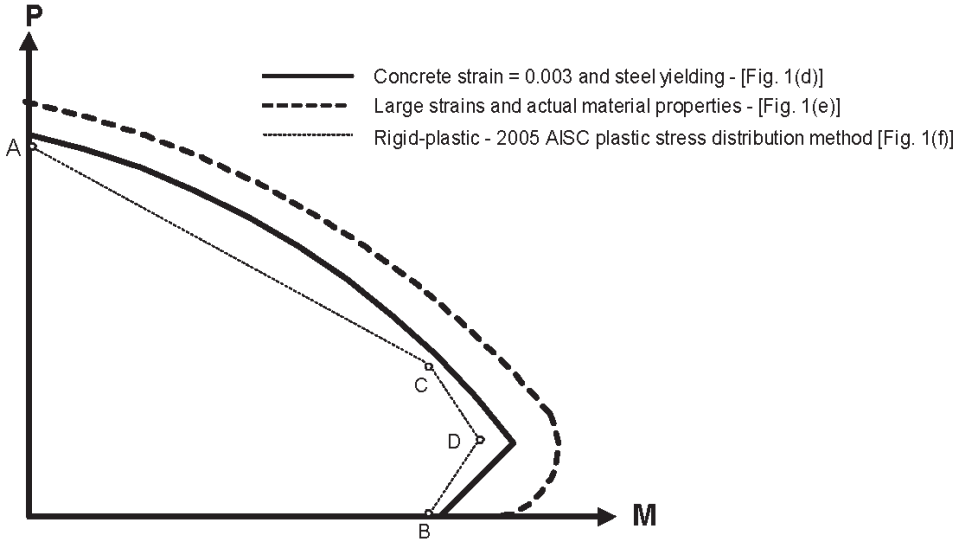

Fig. 2. Interaction diagrams based on the stress distributions shown in Figure 1d through 1f.

second curve is for a concrete strain of approximately 0.005 at the same location (Figure 1e). In the latter case, the effect of the unconfined concrete has been eliminated and only the confined concrete core is contributing. Figure 2 also shows the corresponding strength envelope assuming bilinear rigid-plastic stress-strain curves for the materials and calculated only for the position of the neutral axis at four discrete points (Figure 1f) rather than continuously. The latter corresponds to the simplified approach (plastic stress distribution method) used in the 2005 AISC *Specification*.

It should be noted that the strain-compatibility method discussed here is the only one currently applicable to cases with biaxial loading if one wants to generate interaction points in addition to the anchor points on the coordinate axes of the interaction diagram. For that case the procedure is analogous to that described in Figure 1, except that the section will not be aligned along its principal axes as currently shown in Figure 1a but at some other angle. The calculations will become more laborious and there are only approximate solutions available for the case of CFT columns, which can be treated as reinforced concrete columns with distributed reinforcement and distance between extreme bar layers equal to the section depth. However, the use of the interaction equations of AISC 2005 *Specification* Chapter H (AISC, 2005a), discussed below, provides an alternative procedure in which only the anchor points on the coordinate axes of the interaction diagram need to be computed.

The procedure discussed here is meant for monotonic loading cases; for seismic design further attention to confinement and local buckling phenomena will be needed to sustain the strength envelopes shown in Figure 2 under large cyclic deformations. The strain compatibility method is now embedded in a number of commercial structural analysis and design software packages for reinforced concrete sections and is accessible to most engineers. Thus the 2005 AISC *Specification* explicitly endorses the use of these advanced design tools. However, this approach is time-consuming and not always useful for preliminary design.

The plastic stress distribution method proposed in Chapter I of the 2005 AISC *Specification* is based on the plastic stress distributions shown by the dashed lines in the material properties in Figure 1. This method is intended to provide a design-oriented approach that captures the essential features of the strain compatibility one, but without the associated complexities (Roik and Bergmann, 1992). This approach is described in detail in this paper, which begins with a discussion of the axial compressive strength of different composite cross sections and then moves on to the design of composite beam-columns. The materials are assumed to be elasto-plastic, with no attempt to include deformation capacity (ductility) in the calculations. The assumption is that the confinement required by the AISC *Specification* for encased shapes and that provided by the tubes in CFTs is sufficient to provide the limited ductility required for the steel to yield significantly ($\varepsilon_s > 0.005$) while the concrete compressive strength has not decreased below that given by an assumption of a uniform stress of $0.85f'_c$ for SRCs and rectangular CFTs ($0.95f'_c$ for circular CFTs) over an effective depth similar to that used in conventional reinforced concrete design. These assumptions are well within those made in Section 10.2 and 10.3 of the ACI Code (ACI, 2005), and thus this approach is deemed to satisfy both the current steel and concrete design specifications. Note that the AISC *Steel Construction Manual* (AISC, 2005b) indicates that the 0.95 factor for circular CFTs is for the uniform compression case only. However, the calibrations were conducted assuming 0.95 for any interaction condition and thus that value is used in this paper for all calculations for circular CFTs (Kim, 2005). The confinement resulting from hoop stresses in circular tubes could justify a larger factor in many practical cases, but other checks on the column slenderness and the eccentricity of the load would be required. The 0.95 factor was selected as a reasonable lower bound value that would not require such further checks.

The simplified or plastic stress distribution method is analogous to the strain-compatibility method used to determine the strength of a reinforced concrete column, but rather than solving for a large number of points along the interaction diagram, it relies on linear interpolation between four points for major axis bending for encased composite sections or five points for minor axis bending of encased composite sections and all filled composite sections (Figure 3). Aside from these anchor points, the remaining points are approximations to the exact interaction curve. Designers can use the strain-compatibility method to check the plastic stress distribution method, but similar results will only be obtained if the assumed stress-strain curves for the strain compatibility method are the same as those for the plastic method.

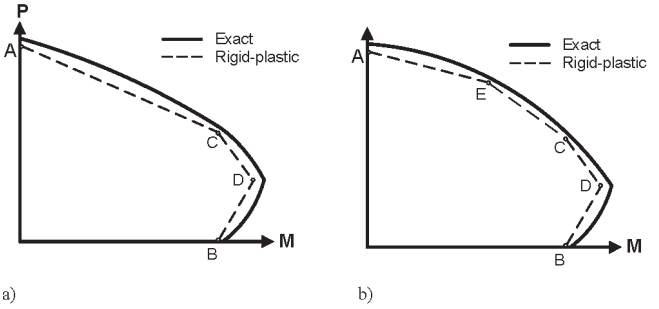

Fig. 3. Interaction diagrams for composite beam-columns: a) encased composite sections, strong axis, and filled composite sections; and b) encased composite sections, weak axis.

PRELIMINARY SIZING OF COMPOSITE SECTIONS FOR AXIAL COMPRESSION

For systems in which the composite columns are assumed to carry primarily gravity loads, or for in assessing composite beam-column strength, the design process outlined below as per the plastic stress distribution method may be used to compute the design axial compressive strength. This may be used with the required strength, P_u, to assess the axial strength of the member.[1] See Leon, Kim and Hajjar (2007) for a summary of all design equations discussed in this procedure.

1. Select the steel shape and reinforcing bars yield strengths, F_y and F_{yr}, respectively, and the concrete compressive strength, f_c'.

2. Select a steel ratio, ρ, for the column. This ratio refers to the area of the steel shape only, A_s, to the gross area of concrete, A_g. The influence of the rebar will be ignored in this design procedure because the AISC *Specification* does not consider them in the calculations of the steel area. For encased composite sections in gravity systems, reasonable and economic sizes result from assuming ρ is in the range of 8 to 12%. For filled composite sections, the range for ρ is typically 6 to 10%.

3. Select a slenderness ratio for the column. Most composite columns are not very slender, so the reduction in the nominal axial strength due to length effects is often smaller than that for regular steel columns of the same length. Most composite columns in gravity frames will have a slenderness parameter $\lambda = \sqrt{P_o / P_e}$ between 0.5 and 1.0 (corresponding to reductions for length effects of 80 to 65%). This reduction value will be termed β and a value of 0.7 is recommended for initial trial designs.

4. Calculate the required gross area of the concrete based on Equation I2-4 from ANSI/AISC 360-05 (AISC, 2005a) [termed in this paper Equation (AISC 2005 I2-4)]:

$$\frac{P_o}{\phi_c \beta} = A_s F_y + A_{sr} F_{yr} + 0.85 A_c f_c', \text{ kips (kN)} \qquad \text{(AISC 2005 I2-4)}$$

In the design of SRCs, one can assume that for this calculation $A_s \approx \rho A_g$, $A_{sr} \approx 0.3\rho A_g$ and $A_c = (1 - 1.3\rho)A_g$. For circular concrete-filled steel tubes (CCFT), assume $A_s \approx \rho A_g$, $A_{sr} = 0$, and $A_c = (1 - \rho)A_g$. For CCFTs, 0.95 may be used in the last term instead of 0.85 to account for the effects of confinement [see Equation (AISC 2005 I2-13)]. For encased sections and rectangular concrete-filled tubes (RCFTs), an approximation of Equations (AISC 2005 I2-4) and (AISC 2005 I2-13) can be used to find the preliminary size of the column as follows (and a similar formula is shown for circular concrete-filled tubes):

$$A_g \approx \frac{P_o}{\phi \beta \left[\rho F_y + 0.3\rho F_{yr} + 0.85 f_c' \left(1 - 1.3\rho\right) \right]} \qquad \text{(SRC and RCFT)}$$

$$A_g \approx \frac{P_o}{\phi_c \beta \left[\rho F_y + 0.95 f_c' \left(1 - \rho\right) \right]} \qquad \text{(CCFT)}$$

5. Assume a preliminary section size and reinforcement based on A_g calculated above and begin the checking procedure. For filled composite sections, first check local buckling of the steel tube as per AISC (2005a).

6. Determine the coefficient C_1 or C_3 from Equation (AISC 2005 I2-7) for encased composite sections or Equation (AISC 2005 I2-15) for filled composite sections:

$$C_1 = 0.1 + 2\left(\frac{A_s}{A_c + A_s} \right) \qquad \text{(AISC 2005 I2-7)}$$

$$\approx (0.1 + 2\rho) \le 0.3$$

$$C_3 = 0.6 + 2\left(\frac{A_s}{A_c + A_s} \right) \qquad \text{(AISC 2005 I2-15)}$$

$$\approx (0.6 + 2\rho) \le 0.9$$

7. Compute the equivalent stiffness (EI_{eff}) from Equation (AISC 2005 I2-6) for encased composite sections or (AISC 2005 I2-14) for filled composite sections:

$$EI_{eff} = E_s I_s + 0.5 E_s I_{sr} + C_1 E_c I_c, \text{ kip-in.}^2 \text{ (N-mm}^2\text{)} \qquad \text{(AISC 2005 I2-6)}$$

$$EI_{eff} = E_s I_s + 1.0 E_s I_{sr} + C_3 E_c I_c, \text{ kip-in.}^2 \text{ (N-mm}^2\text{)} \qquad \text{(AISC 2005 I2-14)}$$

[1] For a complete set of notations, see Appendix A.

8. Compute the elastic Euler buckling load, P_e, from Equation (AISC 2005 I2-5) for buckling about the axis that provides the lower buckling strength:

$$P_e = \pi^2 (EI_{eff}) / (KL)^2, \text{ kips (kN)} \qquad \text{(AISC 2005 I2-5)}$$

9. Calculate the squash load for the columns from Equation (AISC 2005 I2-4) or (AISC 2005 I2-13), where C_2 is 0.85 for rectangular tubes and 0.95 for circular pipes:

$$P_o = A_s F_y + A_{sr} F_{yr} + 0.85 A_c f_c', \text{ kips (kN)} \qquad \text{(AISC 2005 I2-4)}$$

$$P_o = A_s F_y + A_{sr} F_{yr} + C_2 A_c f_c', \text{ kips (kN)} \qquad \text{(AISC 2005 I2-13)}$$

This load corresponds to the stress distribution shown in Part (a) of Table 1, or Point A in Tables 2 through 5. This is the maximum axial compressive load that the cross-section can carry if strain-hardening of the steel and additional strength due to the confinement of the concrete are ignored.

10. For design, this maximum strength needs to be adjusted to account for length effects through either Equation (AISC 2005 I2-2) or (AISC 2005 I2-3). This adjustment is based on the ratio of P_o/P_e for the governing axis of buckling; this ratio corresponds to the slenderness ratio, λ_c^2, used in previous versions of the AISC *Specification*:

(a) When $P_e \geq 0.44P_o$:

$$P_n = P_o \left[0.658^{\left(\frac{P_o}{P_e}\right)} \right], \text{ kips (kN)} \qquad \text{(AISC 2005 I2-2)}$$

(b) When $P_e < 0.44P_o$:

$$P_n = 0.877 P_e, \text{ kips (kN)} \qquad \text{(AISC 2005 I2-3)}$$

11. For design, the value of P_n is then adjusted by the appropriate resistance factor, ϕ_c, or safety factor, Ω_c, for LRFD or ASD:

$$\phi_c = 0.75 \text{ (LRFD)} \quad \Omega_c = 2.00 \text{ (ASD)}$$

Design Examples

Example 1: Encased Concrete Column (SRC)

Design an encased composite column to resist a required axial strength of 4,000 kips (LRFD) with a KL = 24 ft. Use F_y = 50 ksi, F_{yr} = 60 ksi and f_c' = 8 ksi. Assume the column is continuously braced about the minor axis. In Examples 1 through 3, all the material and similar limitations in AISC Sections I1.2, I2.1a and I2.2a are satisfied. Checking of those limits will be illustrated in Example 4.

1. Select an initial steel ratio, ρ, of 10% for the column.

2. Assume $\beta = 0.7$.

3. Calculate the required gross area:

$$A_g \approx \frac{P_o}{\phi_c \beta \left[\rho F_y + 0.3\rho F_{yr} + 0.85 f_c' (1 - 1.3\rho) \right]}$$

$$= \frac{4{,}000}{(0.75)(0.7)\left[(0.1)(50) + 0.3(0.1)(60) + (0.85)(8)(0.87) \right]}$$

$$A_g \approx 599 \text{ in.}^2$$

4. Assuming a square column, this gross area will roughly require a 24 in. × 24 in. column. The steel section will require an $A_s \approx 59.9$ in.^{2} to achieve the desired steel ratio. Select a W14×211 (A_s = 62.0 in.^{2}) buckling about its major axis and assume 16-#8 bars distributed along the perimeter of the section providing a rebar reinforcement ratio of approximately 2.2% (see Figure 4). Many of these reinforcing bars will be needed to maintain confinement and rebar spacing requirements, and will not

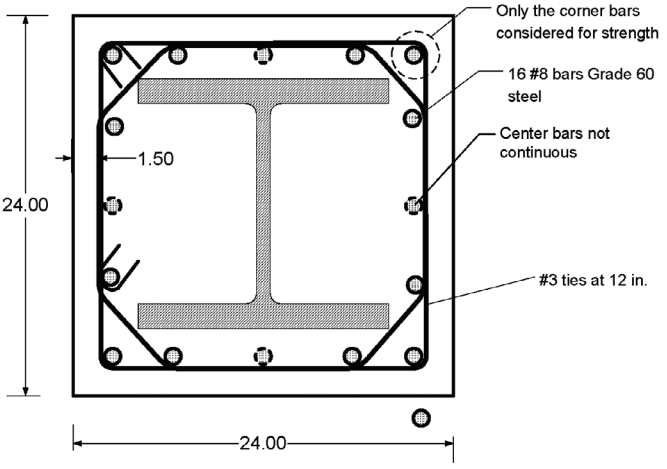

Fig. 4. SSRC section for Example 1.

necessarily be continuous through the joint due to the presence of framing beams. In this example, only the four corner bars, located at a distance of 9.63 in. from the column centerline, will be assumed as continuous and used in the strength calculations [$A_{sr} = 4(0.79 \text{ in.}^2)$]. For this section:

$A_s = 62.0 \text{ in.}^2$
$I_s = I_x = 2{,}660 \text{ in.}^4$
$Z_x = 390 \text{ in.}^3$
$A_{sr} = 3.16 \text{ in.}^2$
$A_c = A_g - A_s - A_{sr} = (24)(24) - 62.0 - 3.16 = 511 \text{ in.}^2$
$e_1 = 9.63$ in. (distance from the column centerline to reinforcing bars)
$I_{sr} \approx (A_{sr})(e_1)^2 = 293 \text{ in.}^4$
$w_c = 148.1 \text{ lb/ft}^3$, assumed

$$E_c = w_c^{1.5}\sqrt{f'_c \text{ (ksi)}} \text{ (AISC)} = 57{,}000\sqrt{f'_c \text{(psi)}} \text{ (ACI)}$$

$$E_c = (148.1 \text{ lb/ft}^3)^{1.5}\sqrt{8 \text{ ksi}} = 5{,}100 \text{ ksi}$$

Assume #3 ties at 12 in.

$\rho_{st} = 0.22 \text{ in.}^2/12 \text{ in.} = 0.0183 \text{ in.}^2/\text{in.} > 0.009 \text{ in.}^2/\text{in.}$ (ANSI/AISC 360-05, Sect. I2.1a)

5. Determine the coefficient C_1 from Equation (AISC 2005 I2-7):

$$C_1 = 0.1 + 2\left(\frac{A_s}{A_c + A_s}\right) = 0.1 + 2\left(\frac{62.0}{511 + 62.0}\right)$$

$= 0.316$ but $C_1 \le 0.3$ so $C_1 = 0.3$

6. Compute the equivalent stiffness, EI_{eff}, from Equation (AISC 2005 I2-6) for encased shapes:

$$EI_{eff} = E_s I_s + 0.5E_s I_{sr} + C_1 E_c I_c$$

$$EI_{eff} = (29{,}000)(2{,}660) + (0.5)(29{,}000)(293) + (0.316)(5{,}100)\left(\frac{24^4}{12} - 2{,}660 - 293\right)$$

$$EI_{eff} = 121 \times 10^6 \text{ kip-in.}^2$$

7. Compute the elastic Euler buckling load, P_e, from Equation (AISC 2005 I2-5):

$$P_e = \frac{\pi^2 EI_{eff}}{(KL)^2} = \frac{\pi^2\left(121 \times 10^6\right)}{\left[(24)(12)\right]^2} = 14{,}400 \text{ kips}$$

8. Calculate the squash load for the column from Equation (AISC 2005 I2-4):

$$P_o = A_s F_y + A_{sr} F_{yr} + 0.85A_c f'_c$$
$$= (62.0)(50) + (3.16)(60) + (0.85)(511)(8)$$
$$= 6{,}760 \text{ kips}$$

9. Adjust for length effects:

$$\frac{P_e}{P_o} = \frac{14{,}400}{6{,}760}$$

$= 2.13 > 0.44$, use ANSI/AISC 360-05 Equation I2-2

$$\frac{P_o}{P_e} = \frac{6{,}760}{14{,}400} = 0.469$$

$$P_n = P_o(0.658)^{\frac{P_o}{P_e}} = 6{,}760(0.658)^{0.469}$$

$= 5{,}560$ kips

10. Finally, for design, the value of P_n is adjusted as:

$\phi_c P_n = (0.75)\ (5{,}560)$
$= 4{,}170$ kips (LRFD) > 4,000 kips **o.k.**

The associated ASD strength is:

$P_n/\Omega_c = (5{,}560 \text{ kips}/2.00) = 2780$ kips (ASD)

This should be compared to the required strength based on ASD load combinations.

The final design is shown in Figure 4.

Example 2: Circular Filled Concrete Column (CCFT)

Design a concrete-filled steel tube column to carry a factored axial load of 1,500 kips (LRFD) with an effective length $KL = 18$ ft. Use $F_y = 42$ ksi, $F_{yr} = 60$ ksi and $f'_c = 5$ ksi.

1. Select a steel ratio, ρ, of approximately 8% for the column.

2. Assume $\beta = 0.7$.

3. Calculate the required gross area:

$$A_g \approx \frac{P_o}{\phi_c \beta\left[\rho F_y + 0.95f'_c(1-\rho)\right]}$$

$$= \frac{1{,}500}{(0.75)(0.7)\left[(0.08)(42) + 0.95(5)(0.92)\right]}$$

$$A_g \approx 370 \text{ in.}^2 = \frac{\pi D^2}{4} \Rightarrow D = 21.7 \text{ in.}$$

4. The computed D exceeds the largest diameter available for circular hollow sections of 20 in. Assuming the same ρ and D = 20 in., the required steel area is $A_s \approx 25.1$ in.^{2} This is about halfway between the areas for a HSS 20.00 × 0.500 and a HSS 20.00 × 0.375. Select the HSS 20.00 × 0.375 and check. For this section:

$A_s = 21.5$ in.^{2}
$I_s = I_x = 1{,}040$ in.^{4}
$Z_x = 135$ in.^{3}
$t = 0.93(0.375) = 0.349$ in. = HSS design thickness
$A_c = \pi[20 - 2(0.349)]^2/4 = 293$ in.^{2}
$E_c = (148.1 \text{ lb/ft}^3)^{1.5}\sqrt{5 \text{ ksi}} = 4{,}030$ ksi

$$\frac{D}{t} = \frac{20}{0.349}$$

$$= 57.3 < 0.15\left(\frac{E}{F_y}\right) = 0.15\left(\frac{29{,}000}{42}\right) = 104 \textbf{ o.k.}$$

5. Determine the coefficient C_3 from Equation (AISC 2005 I2-15) for filled tubes:

$$C_3 = 0.6 + 2\left(\frac{A_s}{A_c + A_s}\right) = 0.6 + 2\left(\frac{21.5}{293 + 21.5}\right)$$

$$= 0.737 \le 0.9 \text{ so } C_3 = 0.737$$

6. Compute the equivalent stiffness, EI_{eff}, from Equation (AISC 2005 I2-14) for concrete-filled tubes:

$$EI_{eff} = E_s I_s + C_3 E_c I_c$$

$$EI_{eff} = (29{,}000)(1{,}040) + (0.737)(4{,}030)\left(\frac{\pi\left[20 - 2(0.349)\right]^4}{64}\right)$$

$$EI_{eff} = 50.4 \times 10^6 \text{ kip-in.}^2$$

7. Compute the elastic Euler buckling load, P_e, from Equation (AISC 2005 I2-5):

$$P_e = \frac{\pi^2 EI_{eff}}{(KL)^2} = \frac{\pi^2(50.4 \times 10^6)}{(18 \times 12)^2} = 10{,}700 \text{ kips}$$

8. Calculate the squash load for the column from Equation (AISC 2005 I2-4):

$$P_o = A_s F_y + 0.95 A_c f'_c = (21.5)(42) + (0.95)(293)(5)$$

$$P_o = 2{,}290 \text{ kips}$$

9. Adjust for length effects:

$$\frac{P_e}{P_o} = \frac{10{,}700}{2{,}290}$$

$= 4.67 > 0.44$ use ANSI/AISC 360-05 Equation I2-2

$$\frac{P_o}{P_e} = \frac{2{,}290}{10{,}700} = 0.214$$

$$P_n = P_o(0.658)^{\frac{P_o}{P_e}} = 2{,}290(0.658)^{0.214} = 2{,}090 \text{ kips}$$

10. Finally, for design, the value of P_n is adjusted as:

$\phi_c P_n = (0.75)(2{,}090)$

$= 1{,}570$ kips (LRFD) > 1,500 kips **o.k.**

The associated ASD strength is:

$P_n/\Omega_c = (2{,}090 \text{ kips}/2.00) = 1{,}050$ kips (ASD)

This should be compared to the required strength based on ASD load combinations.

In the 3rd Ed. AISC *LRFD Manual of Steel Construction* (AISC, 2001), based on the 1999 AISC *LRFD Specification for Structural Steel Buildings*, the tabulated design strength for this section was 1,680 kips; or a difference of –6.5% in strength for the 2005 AISC *Specification* over the 1999 provisions. If the effective length of the column is 40 ft, the ratio of P_o/P_e is 1.06, P_n = 1,470 kips, and ϕP_n = 1,100 kips based on the 2005 AISC *Specification*. The value of ϕP_n = 1220 kips in the 3rd Ed. AISC *LRFD Manual of Steel Construction*, or a difference of –9.8%.

To check the values given for circular columns in the current AISC *Manual* (AISC, 2005b), consider the design of a HSS 18.000 × 0.500 pipe column filled with 4 ksi concrete and an effective length of 24 ft. Repeating the steps above, the key values are:

1. Compute C_3:

$$C_3 = 0.6 + 2\left(\frac{A_s}{A_c + A_s}\right) = 0.6 + 2\left(\frac{25.6}{229 + 25.6}\right)$$

$$= 0.801 \le 0.9 \text{ so } C_3 = 0.801$$

2. Compute the equivalent stiffness, EI_{eff}, from Equation (AISC 2005 I2-14), with $I_{sr} = 0$, for concrete-filled tubes:

$$EI_{eff} = E_s I_s + C_3 E_c I_c$$

$$E_c = (145 \text{ lb/ft}^3)^{1.5}\sqrt{4 \text{ ksi}} = 3{,}490 \text{ l}$$

$$EI_{eff} = (29{,}000)(985) + (0.801)(3{,}490)\left(\frac{\pi\left[18 - 2(0.465)\right]^4}{64}\right)$$

$$EI_{eff} = 40.2 \times 10^6 \text{ kip-in.}^2$$

3. Compute the elastic Euler buckling load, P_e, from Equation (AISC 2005 I2-5):

$$P_e = \frac{\pi^2 EI_{eff}}{(KL)^2} = \frac{\pi^2 (40.2\times 10^2)}{(24\times 12)^2} = 4{,}780 \text{ kips}$$

4. Calculate the squash load for the column from Equation (AISC 2005 I2-13), with $A_{sr} = 0$ and $A_c = \pi[18 - 2(0.465)]^2/4 = 229$ in.^{2}

$$P_o = A_s F_y + 0.95 A_c f_c' = (25.6)(42) + (0.95)(229)(4)$$

$$P_o = 1{,}950 \text{ kips}$$

5. Adjust for length effects:

$$\frac{P_e}{P_o} = \frac{4{,}780}{1{,}950} = 2.45 > 0.44 \text{ use Equation I2-2}$$

$$\frac{P_o}{P_e} = \frac{1{,}950}{4{,}780} = 0.408$$

$$P_n = P_o (0.658)^{\frac{P_o}{P_e}} = 1{,}950(0.658)^{0.408} = 1{,}640 \text{ kips}$$

$\phi_c P_n = (0.75)\ (1{,}640) = 1{,}230$ kips (LRFD)
[= 1,230 kips in AISC Manual (AISC, 2005b)] **o.k.**

One can also compute the associated ASD strength as:

$P_n/\Omega_c = (1640 \text{ kips}/2.00) = 820$ kips (ASD)
[= 821 kips AISC Manual, (AISC, 2005b)] **o.k.**

ANALYSIS OF COMPOSITE SECTIONS FOR COMBINED AXIAL COMPRESSION AND FLEXURAL LOADS

The calculation of the flexural strengths, which follows, is keyed to the stress distributions shown in Table 1. Table 2 shows the applicable formulae for the case of an encased shape (SRC) for strong axis bending and Table 3 those for weak axis bending. Note that in order to keep the tables simple, only some cases are addressed directly. In particular these are cases where continuous reinforcing bars are grouped near the corners of the SRC sections. Modifications to the tables are discussed in the text; for a more general case, see Appendix B in Viest, Colaco, Furlong, Griffis, Leon and Wyllie (1997). Similar tables are given for rectangular concrete-filled tubes (Table 4) and circular concrete-filled sections (Table 5). Note that for Point B in Table 5 changes have been made to the table as it appears in the AISC 13th Ed. *Steel Construction Manual CD Companion* accompanying the AISC *Manual* (AISC, 2005b). These changes correct what appear to be a typographical error in the computation of θ and a discrepancy in the computation of Z_{sB}. The correct expression for θ is

$$\theta = \frac{0.0260K_c - 2K_s}{0.0848K_c} + \frac{\sqrt{\left(0.0260K_c + 2K_s\right)^2 + 0.857K_cK_s}}{0.0848K_c}$$

The correct expression for Z_{sB} is

$$Z_{sB} = \frac{d^3 - h^3}{12}\sin^3\left(\theta/2\right)\left[\frac{\theta}{\theta - \sin\theta} + \frac{\left(2\pi - \theta\right)}{\left(2\pi - \theta\right) - \sin\left(2\pi - \theta\right)}\right]$$

As shown in Table 5 of this paper, Z_{sB} can be approximated by

$$Z_{sB} \approx \frac{d^3 - h^3}{6}\sin^{(4/3)}\left(\theta/2\right)$$

Also note that Tables 4 and 5 for CFTs carry the fifth point (E), which was dropped from the AISC *Manual* tables. Finally these tables also differ from the ones in the CD-Rom in that the intermediate bars at the centroid of the sections are not considered herein.

The generation of axial load-flexure interaction diagrams is a well-documented but tedious procedure (Figure 1), involving the selection of a neutral axis location and a controlling strain (generally 0.003 for the concrete in compression). Assuming a linear distribution of strain (Figure 1b), a corresponding stress distribution can be found based on the stress-strain characteristics assumed for the materials (Figure 1c) and the level of strain (Figures 1d through f). Summing the forces and moments about the assumed reference axis gives a single combination of axial load, P, and moment strength, M. Moving the location of the neutral axis slightly will lead to a different combination of axial load and moment strength, and the interaction surface can be generated by moving the location of the neutral axis methodically (in other words, giving the rounded curves in Figure 3). This is a process that is most easily carried out with the aid of charts, spreadsheets, or subroutines directly embedded within commercial structural analysis software packages.

It is important to recognize some characteristics of diagrams such as that shown in Table 1, particularly the difference between the assumed neutral axis and the reference axis about which moments are calculated. The latter is an arbitrary choice, usually taken at the centroid of the symmetric section. For that case, it is easy to see that insofar as the summation of axial forces is concerned, the contributions of the longitudinal bars and steel flanges in Figure 5 cancel each other out, leaving only the contributions of the web of the steel shape and the rectangular concrete block. Tables 2 through 5 make extensive use of these simplifications, and what may appear to be missing terms in some of the equations shown are actually the result of cancellation of terms as discussed above.

A careful choice of the location of the neutral axis leads to the rapid generation of an interaction surface very close to the more refined one described above through the use of the expressions in these tables. The location of those points is shown in Figure 3, corresponding to the positions in Table 1. Because of the concavity in the curve between Points A and B for the case of minor axis bending of SRC sections, an additional Point E is used.

The four points in Figure 3a and Table 1 correspond to:

- Point A: pure axial load case, with the cross-section under uniform compression corresponding to $\varepsilon_c = 0.003$.
- Point B: pure flexure case, with all steel in tension and compression yielding, ignoring concrete tensile contribution, and $\varepsilon_c = 0.003$. The neutral axis is located at a distance h_n above the centroid.
- Point C: intermediate case, with the neutral axis located at a distance h_n below the centroid. This approach assumes that the interaction diagram (Figure 3a) is roughly symmetrical about the axial load at the balance point (Point D) up to a moment equal to the plastic strength of the section (Point B). Thus Point C has been selected as an arbitrary but convenient point given that it has the same moment as Point B and twice the axial strength of the balance point. This choice considerably simplifies calculations without appreciable error for symmetrical sections.
- Point D: balance point, or point of maximum moment, corresponding to the neutral axis at the centroid as this gives the largest flexure contribution from the concrete portion.

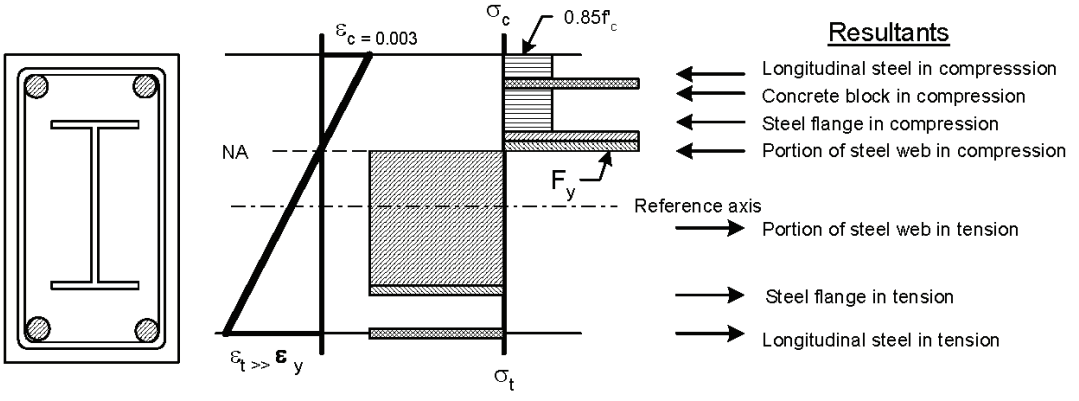

Fig. 5. Calculation of axial load and flexural strength for a given position of the NA.

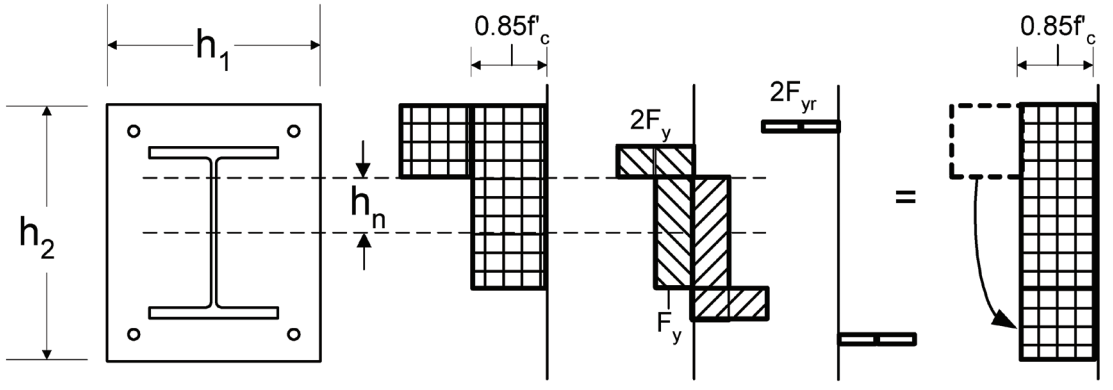

Fig. 6. Axial strength at Point C obtained by adding cases (b) and (c) from Table 1.

The fifth point (Point E), used for SRC bent about its weak axis and concrete-filled tubes (Figure 3b), is computed by selecting an arbitrary position of the neutral axis between Points A and C. For SRC bent about the weak axis, this point is usually taken with the neutral axis at the flange tips.

In the computations that follow, as with the prior examples, the materials are assumed as rigid perfectly-plastic and assumed to have reached high strains so that the elastic contribution is small. The design does not include any explicit checks to ascertain that these large strains can be achieved. It is assumed that the requirements for local buckling and transverse reinforcement implicitly satisfy this requirement. All the steel is assumed to be yielding in tension or compression and strain hardening is ignored. The concrete is assumed to reach its strength at a strain of 0.003, and its nonlinear stress distribution is assumed to be well-represented by an equivalent rectangular block with a stress at $0.85f'_c$. There is currently some discussion of whether this is the best representation for high strength concrete, but this assumption has provided reasonable results for composite columns with concrete strengths up to approximately 10 ksi. The differences in performance between confined and unconfined concrete are ignored, except that for the case of concrete-filled circular pipes, where the stress can be increased from $0.85f'_c$ to $0.95f'_c$ as mentioned earlier.

Steel Reinforced Concrete (SRC) Major Axis Bending

The development of the unfactored interaction diagram for a SRC column bent about its major axis (Table 2) requires the following steps (Roik and Bergmann, 1992):

1. Point A is the squash load for the column, P_o, obtained by setting all the materials at their plastic axial strength. Thus:

$$P_A = P_o = A_s F_y + A_{sr} F_{yr} + 0.85 f'_c A_c$$

2. The axial force at Point C is obtained next by adding the stress distributions from Cases (b) and (c) in Table 1 and integrating the resulting stresses across the cross section. The summation is purely a mathematical artifice to obtain the axial load at C, since Case (b) corresponds to the case of no axial load while Case (c) corresponds to the axial load needed for Point C. The resultant stress blocks from this sum are shown in Figure 6.

   As can be seen from Figure 6, all the forces in the steel section and reinforcing bars cancel each other out when computing the resultant axial force, leaving only the concrete portions as the axial force resultant. As only axial force is to be computed using this diagram, it is possible to move the concrete compression block from Case (b) to a location below that of Case (c). Thus the concrete compression area can be represented by a rectangular distribution across the entire section, simplifying the calculation of the axial force:

$$P_C = 0.85 f'_c (h_1 h_2 - A_s - A_{sr}) = \ 0.85 f'_c (h_1 h_2 - A_s - A_{sr})$$

3. The axial force at Point D corresponds to one-half of that at Point C, as the stress blocks corresponding to Point D will result from subtracting an area equal to $h_n\, h_2$ from the axial force at Point C. Subtracting an additional $h_n\, h_2$ from Point D will lead to Point B, in other words, the zero axial load case. Thus:

$$P_D = 0.425 f'_c (h_1 h_2 - A_s - A_{sr}) = 0.425 f'_c A_c$$

$$P_B = 0$$

4. The moment at Point D corresponds to the summation of all plastic section moduli times their yield stress, with the exception that the concrete contribution is halved because only the portion in compression contributes. The moment at Point D is thus:

$$M_D = Z_s F_y + Z_r F_{yr} + \tfrac{1}{2} Z_c \left(0.85 f'_c\right)$$

   where

$$Z_s = \frac{(d - 2t_f) t_w^2}{4} + b_f t_f (d - t_f), \text{ or}$$

   or as given in Part 1 of the AISC Manual

$$Z_r = \sum_{i=1}^{R} A_{sr_i} e_i, \text{ where } R \text{ is the total number of bars}$$

$$Z_c = \frac{h_1 h_2^2}{4} - Z_s - Z_r$$

   In these formulas A_{sr_i} is the area of reinforcing bar i and e_i is its distance from the plastic neutral axis.

5. To calculate the moments at B and C, another mathematical trick is used. The stress distribution for Point C is subtracted from that of Point B. Most of the forces cancel out, leading to the stress blocks shown in Figure 7. Because these remaining stress blocks result in a zero net moment about the centroid, the moments at B and C must be equal. In addition, since we know from Step 2 (above) what the value of P_C is, the distribution shown in Figure 7 allows the value of h_n to be calculated. In the calculations for Figure 7, the steel stress is decreased by $0.85f'_c$ for consistency with the uniform stress used in Step 2. In addition, one must check that $h_n < (d/2 - t_f)$ to insure that the location of h_n is within the web of the steel section. Finally, note that there are no reinforcing

bars within the $2h_n$ zone near the middle of the beams; if there were, the force in those bars, equal to $A_{sr}(2F_{yr}\text{-}0.85f'_c)$, must be subtracted from the numerator of the expression for h_n. Thus:

$$M_C = M_B$$

$$P_C = 0.85f'_cA \quad \text{(from Step 2)}$$

$$P_C = 2h_n\left(0.85f'_ch_1 + t_w(2F_y - 0.85f'_c)\right) \quad \text{(from Figure 7)}$$

$$h_n = \frac{0.85f'_ch_1h_2}{2(0.85f'_ch_1 + t_w(2F_y - 0.85f'_c))} \le \left(\frac{d}{2} - t_f\right)$$

6. Once h_n has been obtained, the moments at B and C can be calculated using either of the given stress distributions. Alternatively, this moment can be obtained by subtracting the contribution of the portions within the central $2h_n$ region from the maximum moment (M_D). Thus:

$$M_C = M_B = M_D - Z_{sn}F_y - \tfrac{1}{2}Z_{cn}(0.85f'_c)$$

$$Z_{sn} = t_wh_n^2$$

$$Z_{cn} = h_1h_n^2 - Z_{sn}$$

$$Z_r = \sum_{i=1}^{N} A_{sr_i}e_i, \text{ where } N \text{ is the number of bars within } 2h_n$$

7. If step (5) resulted in the location of h_n not being in the web, the next assumption is that it will be within the flange. For this case, the expressions for h_n and Z_s become:

$$h_n = \frac{0.85f'_c\left(A_c + A_s - db_f\right) - 2F_y\left(A_s - db_f\right)}{2\left[0.85f'_c\left(h_1 - b_f\right) + 2F_yb_f\right]}$$

$$Z_{sn} = Z_s - b_f\left(\frac{d}{2} - h_n\right)\left(\frac{d}{2} + h_n\right), \frac{d}{2} - t_f \le h_n \le \frac{d}{2}$$

8. Finally, if the location of h_n is outside the steel shape, the expressions for h_n and Z_s become:

$$h_n = \frac{0.85f'_c\left(A_c + A_s\right) - 2F_yA_s}{2\left(0.85f'_ch_1\right)}$$

$$Z_{sn} = Z_{sx}$$

Steel Reinforced Concrete (SRC) Minor Axis Bending

The procedure for determining the axial load-flexure interaction diagram for minor axis bending is the same as that for major axis bending with two exceptions:

1. There are only two possible locations of h_n (either within or outside the steel section – see Table 3).

2. Another location of h_n is needed to determine Point E. A convenient location to choose is the tip of the flanges. This is the case shown in Table 3 as Point E. The expressions derived for the cases where the plastic neutral axis is within the steel section (Points B and C) are valid for the calculation of the values at Point E, except that $h_n = b_f/2$.

Rectangular Concrete-Filled Steel Tube (RCFT)

The procedure for determining the axial load-flexure interaction diagram for rectangular concrete-filled tubes is similar to that described above for SRC, and the resulting values are shown in Table 4.

Circular Concrete-Filled Steel Tube (CCFT)

The resulting values for CCFT sections are shown in Table 5. Note again that in the definitions of θ and Z_s for Point B, changes have been made to correct errors in the table that appear in the AISC 13th Ed. *Steel Construction Manual CD Companion* accompanying the AISC *Manual* (AISC, 2005b).

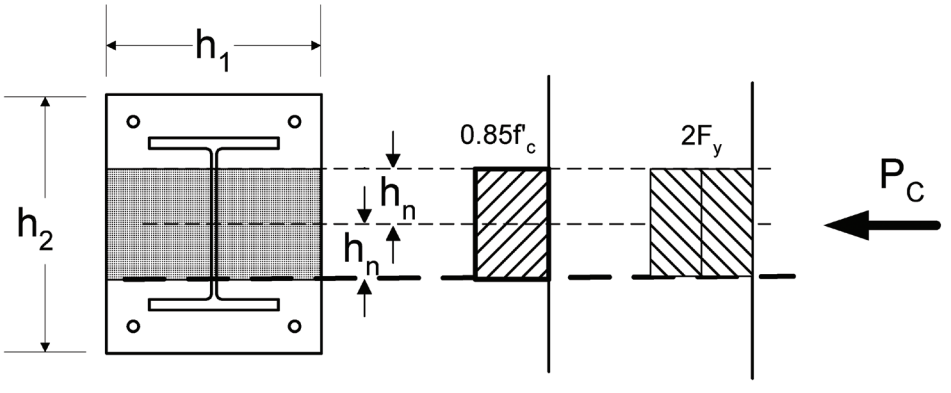

Fig. 7. Moment at Points B and C: stress resultants corresponding to the subtraction of cases (b) and (c) in Table 1 and leading to the calculation of h_n.

STABILITY CONSIDERATIONS

Once the cross-sectional strength has been established, this interaction surface needs to be reduced to account for: (a) stability effects and (b) design strength as opposed to nominal strength. To account for stability, the usual column formula has been used in conjunction with an equivalent moment of inertia. This is straightforward, although it results in a substantial difference in the approach to stability from that given, for example, in ACI 318 (ACI, 2005) for composite columns. The next step, the reduction from nominal to design loads, is not so simple due to the fact that as the failure shifts from tension yielding at low axial loads to compression at loads above the balance point, it will seem that the overall factor for the member should change. In reinforced concrete design this is achieved by changing the resistance factor from 0.90 to 0.65 as the strain in the extreme tensile fiber goes from 0.0005 to the yield strain of the steel. This factor is applied to both the moment and axial force components. AISC has chosen not to use that approach and to retain separate resistance factors and safety factors for axial loads and flexure. This, and the desire to provide simplified approaches for design, has resulted in three separate approaches to checking the strength of a composite beam-column: (1) an approach based on the use of the existing interaction formulas in AISC 2005 *Specification* Chapter H (AISC, 2005a); (2) a more complex approach based on the complete polygonal interaction diagram; and (3) a simplified version of the polygonal approach that uses only one intermediate point. A description of these approaches follows.

Method 1: Approach Based on AISC 2005 Chapter H

For this case, only the nominal axial strength including stability effects, P_n, and the nominal flexural strength of the section, M_n, need to be computed. This makes this approach particularly useful for biaxial bending cases where the engineer does not want to compute additional interaction points for combined axial force and flexure. The anchor points (for uniaxial flexure) can be based on the equations for Points A and B given in Tables 2 through 5, with the stability reduction included in P_n. The interaction Equations H1-1a and H1-1b from Chapter H (AISC, 2005a) are then used directly (Figure 8):

(a) For $\frac{P_r}{P_c} \geq 0.2$

$$\frac{P_r}{P_c} + \left(\frac{M_{rx}}{M_{cx}} + \frac{M_{ry}}{M_{cy}}\right) \leq 1.0 \qquad \text{(AISC H1-1a)}$$

(b) For $\frac{P_r}{P_c} < 0.2$

$$\frac{P_r}{2P_c} + \left(\frac{M_{rx}}{M_{cx}} + \frac{M_{ry}}{M_{cy}}\right) \leq 1.0 \qquad \text{(AISC H1-1b)}$$

where

P_r = required compressive strength, kips (N)
P_c = available compressive strength, kips (N)
M_r = required flexural strength, kip-in. (N-mm)
M_c = available flexural strength, kip-in. (N-mm)
x = subscript relating symbol to strong axis bending
y = subscript relating symbol to weak axis bending

For this case, the safety and resistance factors from Section I4 are applicable:

$\phi_c = 0.75$ (LRFD) $\qquad \Omega_c = 2.00$ (ASD)

$\phi_b = 0.90$ (LRFD) $\qquad \Omega_b = 1.67$ (ASD)

Similar equations may be used for the case of axial tension plus flexure.

Method 2: Full Plastic Strength Approach Based on Polygonal Interaction Envelope

This approach requires the calculation of the full interaction diagram or a reduced set thereof (for example, the four or five points shown in Tables 2 through 5). The axial load values

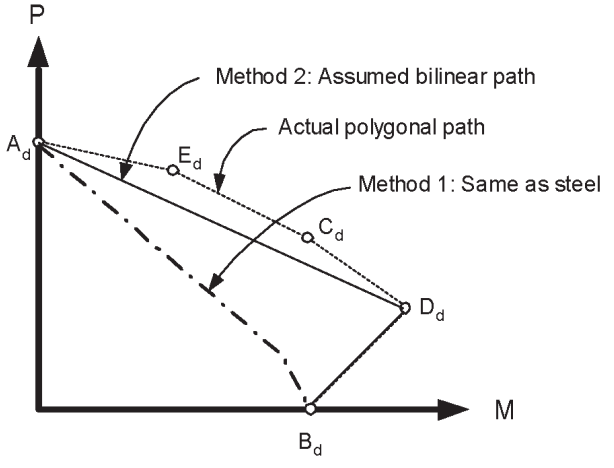

Fig. 8. Schematic representations of Methods 1 and 2 for checking axial load and flexure interaction.

are then reduced to take into account stability effects and also reduced by the following safety and resistance factors:

$\phi_c = 0.75$ (LRFD) $\quad \Omega_c = 2.00$ (ASD)

$\phi_b = 0.90$ (LRFD) $\quad \Omega_b = 1.67$ (ASD)

The corresponding interaction diagram is shown in Figure 8, where the subscript *d* indicates that the values are the design ones (in other words, including a slenderness reduction and the resistance factor). The number of checks and equations needed increase substantially as the number of points used to define the envelope increases. The complete set of equations needed for the case of checking the resistance between the five points is too lengthy to be included here and thus only a simplified case will be illustrated. For a possible polygonal approach to the interaction diagram using Points A, B, and D only, the checks then become:

If $P_n < P_D$

and if $\frac{M_{rx}}{M_{cx}} \le 1$ and $\frac{M_{ry}}{M_{cy}} \le 1$ then

$$\frac{M_{rx}}{M_{cx}} + \frac{M_{ry}}{M_{cy}} \le 1 \qquad (1)$$

otherwise if $\frac{M_{rx}}{M_{cx}} > 1$ and $\frac{M_{ry}}{M_{cy}} \le 1$ then

$$\frac{P_r}{P_{cb}} + \frac{M_{cbx} - M_{rx}}{M_{cbx} - M_{cx}} + \frac{M_{ry}}{M_{cy}} \le 1 \qquad (2)$$

otherwise if $\frac{M_{rx}}{M_{cx}} \le 1$ and $\frac{M_{ry}}{M_{cy}} > 1$ then

$$\frac{P_r}{P_{cb}} + \frac{M_{rx}}{M_{cx}} + \frac{M_{cby} - M_{ry}}{M_{cby} - M_{cy}} \le 1 \qquad (3)$$

otherwise if $\frac{M_{rx}}{M_{cx}} > 1$ and $\frac{M_{ry}}{M_{cy}} > 1$ then

$$\frac{P_r}{P_{cb}} + \frac{M_{cbx} - M_{rx}}{M_{cbx} - M_{cx}} + \frac{M_{cby} - M_{ry}}{M_{cby} - M_{cy}} \le 1 \qquad (4)$$

If $P_r \ge P_{cb}$

$$\frac{P_r - P_{cb}}{P_c - P_{cb}} + \frac{M_{rx}}{M_{cbx}} + \frac{M_{ry}}{M_{cby}} \le 1 \qquad (5)$$

where

P_r = required compressive strength, kips (N)
P_c = available compressive strength, kips (N)
P_{cb} = axial compressive strength at balanced moment, M_{cb}, kips (N)
M_r = required flexural strength, kip-in. (N-mm)
M_c = available flexural strength, kip-in. (N-mm)
M_{cb} = balanced moment, kip-in. (N-mm)
x = subscript relating symbol to strong axis bending
y = subscript relating symbol to weak axis bending

Similar equations as those given for Method 1 may be used for the case of axial tension plus flexure.

One issue with using a different set of resistance and safety factors for flexure and axial force is the possibility that upon the application of the stability reduction coupled with the resistance or safety factors, the resulting available strength envelope may fall outside the cross section strength envelope in the area immediately below the balance point (Figure 9). A simple way has not yet been determined for including this added strength without encountering this potential unconservative design area within the context of accounting for stability using the current AISC *Specification*.

Method 3: Simplified Approach Based on Polygon Values

To maintain some of the substantial strength gains from the strain compatibility approach but to simplify the design process, a third approach has been proposed. In this approach, a third anchor point, C_d, is used in addition to points A_d and B_d as seen in Figure 10. The new Point C_d is derived from the flexural design strength of the member (M_n from Point B) and the corresponding axial strength from Point C (See Figure 3), with appropriate reduction taken to account for slenderness effects and resistance or safety factors as per Leon et al. (2007). Similar equations as those given for Method 2 may be used for the case of axial tension plus flexure.

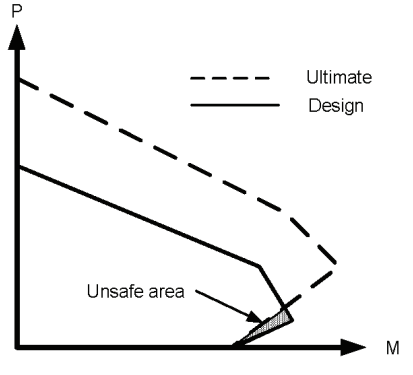

Fig. 9. Possible breaching of ultimate strength envelope by design envelope due to application of resistance and stability reduction factors.

Design Examples

Example 3: SRC Beam-Column

In this example, a simplified axial load-moment envelope is developed for an 18 in. × 18 in. SRC beam-column with an embedded W14×48 section. Additional reinforcement consists of four #7 corner bars and #3 ties spaced at 12 in. Materials used include F_y = 50 ksi, F_{yr} = 60 ksi, and f_c' = 3 ksi. Flexure is about the major axis, the effective length is 24 ft, and buckling is restrained about the minor axis.

Limitations:

1) Normal weight concrete 10 ksi $\geq f_c' \geq$ 3 ksi; in this case f_c' = 3 ksi **o.k.**

2) $F_{yr} \leq$ 75 ksi; in this case, F_{yr} = 60 ksi **o.k.**

3) The cross-sectional area of the steel core shall comprise at least 1% of the total composite cross section.

   A_s = 14.1 in.^{2} > (0.01)(324 in.^{2}) = 3.24 in.^{2} **o.k.**

4) Concrete encasement of steel core shall be reinforced with continuous longitudinal bars and lateral ties or spirals. The minimum transverse reinforcement shall be at least 0.009 in.^{2} of tie spacing:

   ρ_{st} = 0.22 in.^{2}/12 in. = 0.0183 in.^{2}/in. > 0.009 in.^{2}/in. **o.k.**

5) The minimum steel ratio for continuous longitudinal reinforcing, ρ_{sr}, shall be 0.004:

$$\rho_{sr} = \frac{A_{sr}}{A_g} = \frac{(4 \times 0.6)}{324} = 0.0074 > 0.004 \text{ o.k.}$$

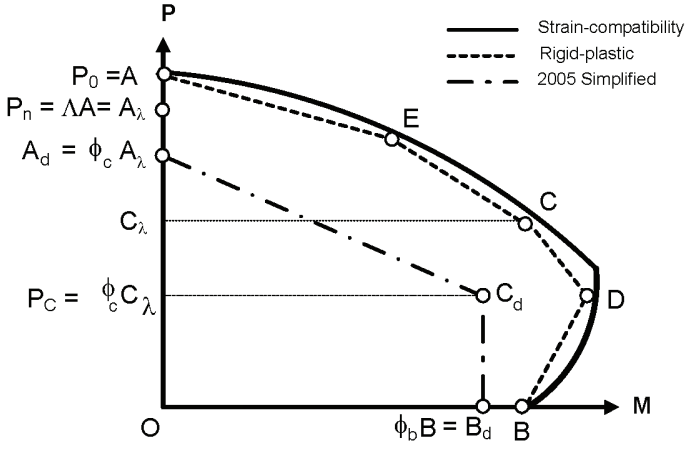

Fig. 10. Simplified interaction diagram for LRFD design.

Point A in Table 2 (M = 0)

Determine the available compressive strength and moment strength.

$$A_c = (324 - 14.1 - 2.40) = 308 \text{ in.}^2$$

$$P_o = A_s F_y + A_{sr} F_{yr} + 0.85 A_c f_c'$$

$$P_o = (14.1)(50) + (2.40)(60) + 0.85(308)(3)$$
$$= 1{,}630 \text{ kips}$$

$$C_1 = 0.1 + 2\left(\frac{A_s}{A_c + A_s}\right) = 0.1 + 2\left(\frac{14.1}{308 + 14.1}\right)$$
$$= 0.188 \leq 0.3$$

$$e_1 = \left(\frac{\text{overall depth} - 2\text{ (cover)} - 2\text{(stirrup)} - \text{bar diameter}}{2}\right)$$

$$e_1 = \left(\frac{18 - (2)(1.5) - (2)(0.375) - 0.875}{2}\right) = 6.69 \text{ in.}$$

$$I_{sr} \approx \sum \left(A_{sr_i}\right)(e_i)^2 = 2(1.20)(6.69)^2 = 107 \text{ in.}^3$$

$$I_c = \left(\frac{h_1 h_2^3}{12}\right) - I_s - I_{sr}$$

$$= \left(\frac{(18)(18)^3}{12}\right) - 484 - 107 = 8{,}160 \text{ in.}^4$$

$$E_c = \left(148.1 \text{ lb/ft}^3\right)^{1.5} \sqrt{3 \text{ ksi}} = 3{,}122 \text{ ksi}$$

$$EI_{eff} = E_s I_s + 0.5 E_s I_{sr} + C_1 E_c I_c$$

$$EI_{eff} = (29{,}000)(484) + (0.5)(29{,}000)(107)$$
$$+ (0.188)(3{,}122)(8{,}160)$$

$$EI_{eff} = 20.4 \times 10^6 \text{ kip-in.}^2$$

Note that if buckling had not been prevented about the minor axis, the I_s to be used in the computation of I_{eff} would have been I_y rather than I_x.

$$P_e = \frac{\pi^2 EI_{eff}}{(kL)^2} = \frac{\pi^2 (20.4 \times 10^6)}{(24 \times 12)^2} = 2{,}430 \text{ kips}$$

$$\frac{P_o}{P_e} = \frac{1{,}630}{2{,}430} = 0.67 \leq 2.25$$

or

$$\frac{P_e}{P_o} = \frac{2{,}430}{1{,}630} = 1.49 > 0.44$$

∴ Use Equation (AISC 2005 I2-2)

$$P_n = P_o\left[0.658^{\left(\frac{P_o}{P_e}\right)}\right] = (1{,}630 \text{ kips})\left[0.658^{(0.67)}\right] = 1{,}230 \text{ kips}$$

$\phi_c P_n = (0.75)(1{,}230) = 923$ kips (LRFD)

$P_n/\Omega_c = (1{,}230 \text{ kips}/2.00) = 615$ kips (ASD)

Point B in Table 2 ($P_B = 0$)

Determine the location of h_n

1) Above the flange or $\left(h_n > \frac{d}{2} = \frac{13.8 \text{ in.}}{2}\right) = h_n > 6.90$ in.

$$h_n = \frac{0.85f_c'\left(A_c + A_s\right) - 2F_yA_s}{2\left(0.85f_c'h_1\right)}$$

$$= \frac{0.85\left(3.0\right)\left(308 + 14.1\right) - 2\left(50\right)\left(14.1\right)}{2\left(0.85\right)\left(3.0\right)\left(18\right)}$$

$= -6.41$ in. < 6.90 in., so h_n is not outside the steel section

2) For h_n within the flange $\left[\left(\frac{d}{2} - t_f\right) < h_n \le \frac{d}{2}\right]$

or $6.31\text{in.} < h_n \le 6.90$ in.

$$h_n = \frac{0.85f_c'\left(A_c + A_s - db_f\right) - 2F_y\left(A_s - db_f\right)}{2\left[0.85f_c'\left(h_1 - b_f\right) + 2F_yb_f\right]}$$

$$= \frac{\left[0.85(3)\left(308 + 14.1 - (13.8)(8.03)\right)\right]}{2\left[0.85(3)\left(18 - 8.03\right) + 2(50)(8.03)\right]}$$

$$- \frac{\left[2(50)\left(14.1 - (13.8)(8.03)\right)\right]}{2\left[0.85(3)\left(18 - 8.03\right) + 2(50)(8.03)\right]}$$

$= 6.16$ in., so h_n is in the web

Since h_n is within the web and thus no rebars are present within h_n ($A_{sr} = 0$):

$$h_n = \frac{0.85f_c'A_c}{2\left[0.85f_c'\left(h_1 - t_w\right) + 2F_yt_w\right]}$$

$$= \frac{0.85\left(3\right)(308)}{2\left[0.85(3)\left(18 - 0.340\right) + 2(50)(0.340)\right]}$$

$= 4.96$ in.

$Z_{sn} = t_w h_n^2 = (0.340)(4.96)^2 = 8.36$ in.^{3}

$Z_{cn} = h_1h_n^2 - Z_{sn} = (18)(4.96)^2 - 8.37 = 434$ in.^{3}

Before computing M_b, M_D must be computed:

$$M_D = Z_sF_y + Z_rF_{yr} + \tfrac{1}{2}Z_c\left(0.85f_c'\right)$$

$$Z_r = \sum A_{sr_i}\left(\frac{h_2}{2} - c\right) = \sum\left(A_{sr_i}e_i\right) = 4(0.6)(6.69)$$

$= 16.1$ in.^{3}

$$Z_c = \left(\frac{h_1h_2^2}{4}\right) - Z_s - Z_r = \left(\frac{(18)(18)^2}{4}\right) - 78.4 - 16.1$$

$= 1{,}360$ in.^{3}

$$M_D = (78.4)(50) + (16.1)(60) + \tfrac{1}{2}(1{,}360)\left(0.85\right)(3)$$

$= 6{,}620$ kip-in.

$$M_B = M_D - Z_{sn}F_y - \tfrac{1}{2}Z_{cn}\left(0.85f_c'\right)$$

$$= (6{,}620) - (8.36)(50) - \tfrac{1}{2}(434)(0.85)(3)$$

$= 5{,}650$ kip-in.

$\phi_bM_B = (0.90)(5{,}650) = 5{,}090$ kip-in.

$M_B/\Omega_b = (5{,}650/1.67) = 3{,}380$ kip-in.

Point C ($M_C = M_B$; $P_C = 0.85f_c'A_c$)

$$P_C = A_c\left(0.85f_c'\right)$$

$$= \left(308 \text{ in.}^2\right)\left(0.85\right)\left(3.0 \text{ ksi}\right) = 785 \text{ kips}$$

$\phi P_{C_d} = 0.75(785)(0.658)^{0.67} = 445$ kips

$P_{C_d}/\Omega = (784)(0.658)^{0.67}/2.00 = 296$ kips

$M_C = M_B = 5{,}650$ kip-in.

$\phi M_C = \phi M_B = (0.9)5{,}650$ kip-in. $= 5{,}090$ kip-in.

$M_C/\Omega = M_B/\Omega = 5{,}650/1.67$ kip-in. $= 3{,}380$ kip-in.

Point D

$$P_D = \frac{A_c\left(0.85f_c'\right)}{2}$$

$$= \frac{\left(308 \text{ in.}^2\right)\left(0.85\right)\left(3.0 \text{ ksi}\right)}{2}$$

$= 393$ kips

$\phi P_{D_d} = 0.75(393)(0.658)^{0.67} = 223$ kips

$P_{D_d}/\Omega = (393)(0.658)^{0.67}/2.00 = 148$ kips

$M_D = 6{,}620$ kip-in.

$\phi M_D = (0.9)6{,}620 = 5{,}960$ kip-in.

$M_D/\Omega = 6{,}620/1.67 = 3{,}960$ kip-in.

The results are summarized in Figure 11.

Example 4: RCFT Beam-Column

Develop a simplified axial load-moment envelope for a HSS16 in.×16 in.×⅝ in. filled with $f'_c = 4$ ksi concrete. The effective length of the member is 24 ft. Assume A500 Grade B ($F_y = 46$ ksi and $F_u = 58$ ksi). Note that the design thickness for a 0.625 in. nominal value is 0.581 in.

Limitations:

1) The cross-sectional area of the steel core shall comprise at least 1% of the total composite cross-section.

   $A_s = 35.0$ in.$^2 > (0.01)(16)^2 = 2.56$ in.^{2} **o.k.**

   Note that $\rho = \frac{35}{256} = 0.137$, or 13.7% which is very high.

2) The slenderness of the tube wall is:

$$\left(\frac{b}{t}\right) = \frac{16(2)(0.581)}{0.581}$$

$$= 25.5 < 2.26\sqrt{\frac{E}{F_y}} = 2.26\sqrt{\frac{29{,}000}{46}} = 56.7 \textbf{ o.k.}$$

Point A in Table 4 ($M_A = 0$)

Determine the available compressive strength and flexural strength.

In the following calculations the symbol "≈" is used to indicate that the effect of the corner radii is not being accounted for exactly; this effect is small and can generally be neglected.

$$P_o = A_s F_y + A_{sr} F_{yr} + 0.85 A_c f'_c$$

$$A_c \approx 256 - 35.0 = 221 \text{ in.}^2$$

$$P_o = (35.0)(46) + 0.85(221)(4)$$

$$= 2{,}360 \text{ kips}$$

$$C_3 = 0.6 + 2\left(\frac{A_s}{A_c + A_s}\right) = 0.6 + 2\left(\frac{35}{(221+35)}\right)$$

$$= 0.873$$

$$I_s = 1{,}370 \text{ in.}^4$$

$$I_c \approx \left(\frac{d^4}{12}\right) - I_s = \left(\frac{(16)^4}{12}\right) - 1{,}370 = 4{,}090 \text{ in.}^4$$

$$E_c = (148.1 \text{ lb/ft}^3)^{1.5}\sqrt{4 \text{ ksi}} = 3{,}605 \text{ ksi}$$

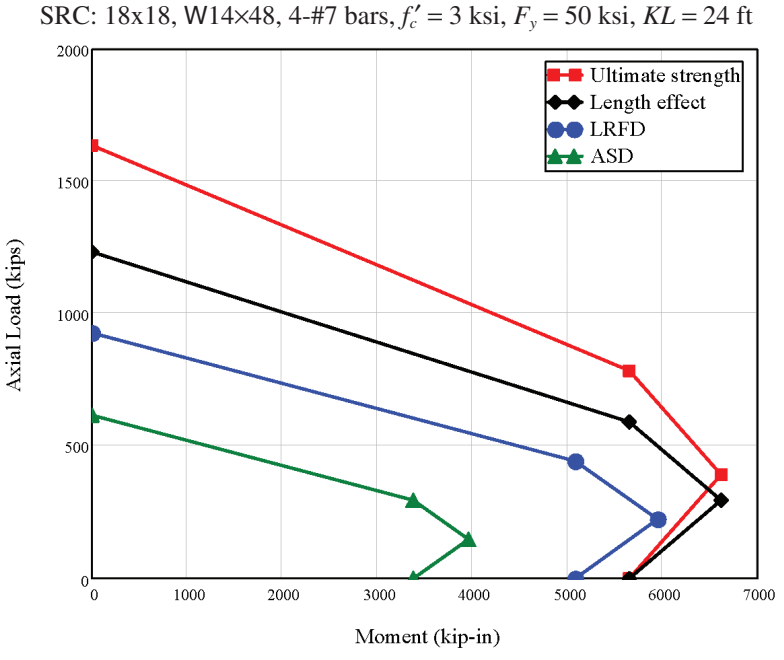

Fig. 11. Interaction diagrams for column in Example 3.

$$EI_{eff} = E_s I_s + 0.5E_s I_{sr} + C_3 E_c I_c$$
$$= (29{,}000)(1{,}370) + (0.873)(3{,}605)(4{,}090)$$
$$= 52.6 \times 10^6 \text{ kip-in.}^2$$

$$P_e = \frac{\pi^2 EI_{eff}}{(KL)^2} = \frac{\pi^2 (52.6 \times 10^6)}{(24 \times 12)^2} = 6{,}260 \text{ kips}$$

$$\frac{P_o}{P_e} = \frac{2{,}360}{6{,}260} = 0.38 < 2.25$$

or $$\frac{P_e}{P_0} = \frac{6{,}260}{2{,}360} = 2.65 > 0.44$$

$\therefore$ Use Equation (AISC 2005 I2-2)

$$P_n = P_o \left[0.658^{\left(\frac{P_o}{P_e}\right)} \right] = (2{,}360)\left[0.658^{(0.38)}\right]$$
$$= 2{,}010 \text{ kips}$$

$\phi_c P_n = (0.75)\ (2{,}010) = 1{,}510$ kips (LRFD)

$P_n/\Omega_c = (2{,}010/2.00) = 1{,}010$ kips (ASD)

Point B in Table 4 ($P_B = 0$)

Determine location of h_n

$$h_n = \frac{0.85 f_c' A_c}{2\left[0.85 f_c' h_1 + 4 t_w F_y\right]} \le \frac{h_2}{2}$$

$$= \frac{0.85(4)(221)}{2\left[0.85(4)[16-(2)(0.581)] + 4\ (0.581)(46)\right]}$$

$$= 2.39 \text{ in.} \le \frac{(16-(2)(0.581))}{2} = 7.42 \text{ in.}$$

Before computing M_B, M_D must be computed.

$Z_s = 200$ in.^{3}

$$Z_c = \frac{h_1 h_2^2}{4} - 0.192 r_i^3 \approx \left(\frac{\left[\left(16-(2)(0.581)\right)\right]^3}{4} \right) = 817 \text{ in.}^3$$

$$M_D = Z_s F_y + \tfrac{1}{2} Z_c \left(0.85 f_c'\right)$$
$$= (200)(46) + \tfrac{1}{2}(817)(0.85 \times 4)$$
$$= 10{,}600 \text{ kip-in.}$$

$Z_{sn} = 2 t_w h_n^2 = 2\ (0.581)(2.39)^2 = 6.64$ in.^{3}

$Z_{cn} = h_1 h_n^2 = [16-(2)(0.581)](2.39)^2 = 84.8$ in.^{3}

$$M_B = M_D - Z_{sn} F_y - \tfrac{1}{2} Z_{cn}\left(0.85 f_c'\right)$$
$$= 10{,}600 - (6.64)(46) - \tfrac{1}{2}(84.8)(0.85)(4)$$
$$= 10{,}200 \text{ kip-in.}$$

$\phi_b M_B = (0.9)\ (10{,}200) = 9{,}180$ kip-in.

$M_B/\Omega_b = (10{,}200/1.67) = 6{,}110$ kip-in.

Point C in Table 4 ($M_C = M_B$; $P_C = 0.85 f_c' A_c$)

$$P_C = A_c\left(0.85 f_c'\right)$$
$$P_C = \left(221 \text{ in.}^2\right)\left(0.85\right)\left(4.0 \text{ ksi}\right) = 751 \text{ kips}$$
$$\phi P_{C_d} = (0.75)(751)(0.658)^{0.38} = 480 \text{ kips}$$
$$P_{C_d}/\Omega = 751(0.658)^{0.38}/2.00 = 320 \text{ kips}$$
$$M_C = M_B = 10{,}200 \text{ kip-in.}$$
$$\phi M_C = (0.9)(10{,}200) = 9{,}180 \text{ kip-in.}$$
$$M_C/\Omega = 10{,}200/1.67 = 6{,}110 \text{ kip-in.}$$

Point D in Table 4

$$P_D = \frac{A_c\left(0.85 f_c'\right)}{2}$$
$$= \frac{\left(221\right)\left(0.85\right)\left(4.0 \text{ ksi}\right)}{2}$$
$$= 376 \text{ kips}$$
$$\phi P_{D_d} = (0.75)(376)(0.658)^{0.38} = 241 \text{ kips}$$
$$P_{D_d}/\Omega = (376)(0.658)^{0.38}/2.00 = 160 \text{ kips}$$
$$M_D = 10{,}600 \text{ kip-in.}$$
$$\phi M_D = (0.9)(10{,}600) = 9{,}540 \text{ kip-in.}$$
$$M_D/\Omega = 10{,}600/1.67 = 6{,}350 \text{ kip-in.}$$

The results are summarized in Figure 12.

Example 5: CCFT Beam-Column

Determine the interaction diagram for a 20 in. diameter, ⅜ in. thick circular concrete-filled tube column with a $KL = 13$ ft. Assume $F_y = 42$ ksi and $f_c' = 5$ ksi.

Basic geometrical properties:

$d = 20$ in.

$t = 0.349$ in.

$h = d - 2t = 19.3$ in.

$$r_m = \frac{d-t}{2} = 9.83 \text{ in}$$

$$A_s = 2\pi r_m t = 21.6 \text{ in.}^2$$

$$A_c = \frac{\pi h^2}{4} = 293 \text{ in.}^2$$

$$A_g = A_c + A_s = 315 \text{ in.}^2$$

$$E_c = (148.1)^{1.5}\sqrt{5} = 4{,}030 \text{ ksi}$$

$$I_s = \frac{\pi}{64}\left[d^4 - h^4\right] = 1{,}040 \text{ in.}^4$$

$$I_c = \frac{\pi h^4}{64} = 6{,}810 \text{ in.}^4$$

$$I_g = I_s + I_c = 7{,}850 \text{ in.}^4$$

The cross-sectional area of the steel core shall comprise at least 1% of the total composite cross-section.

$$\frac{A_s}{A_c + A_s} = 0.07 > 0.010 \quad \textbf{o.k.}$$

The slenderness of the tube wall is:

$$\frac{D}{t} = 57.3 < 0.15\left(\frac{E_s}{F_y}\right) = 104 \quad \textbf{o.k.}$$

Point A in Table 5 ($M_A = 0$)

Determine the available compressive strength using the properties determined above.

$C_2 = 0.95$

$$C_3 = \min\left[0.9,\ 0.6 + 2\left(\frac{A_s}{A_c + A_s}\right)\right] = 0.74$$

$EI_{eff} = E_s I_s + E_s I_{sr} + C_3 E_c I_c = 351{,}000$ kip-ft^2

$P_o = A_s F_y + A_{sr} F_{yr} + C_2 A_c f_c' = 2{,}300$ kips

$$P_e = \frac{\pi^2 EI_{eff}}{(KL_c)^2} = 20{,}500 \text{ kips}$$

$$\frac{P_o}{P_e} = \frac{2{,}300}{20{,}500} = 0.112$$

RCFT: $16 \times 16 \times \frac{5}{8}$, $f_c' = 4$ ksi, $F_y = 46$ ksi, $KL = 24$ ft

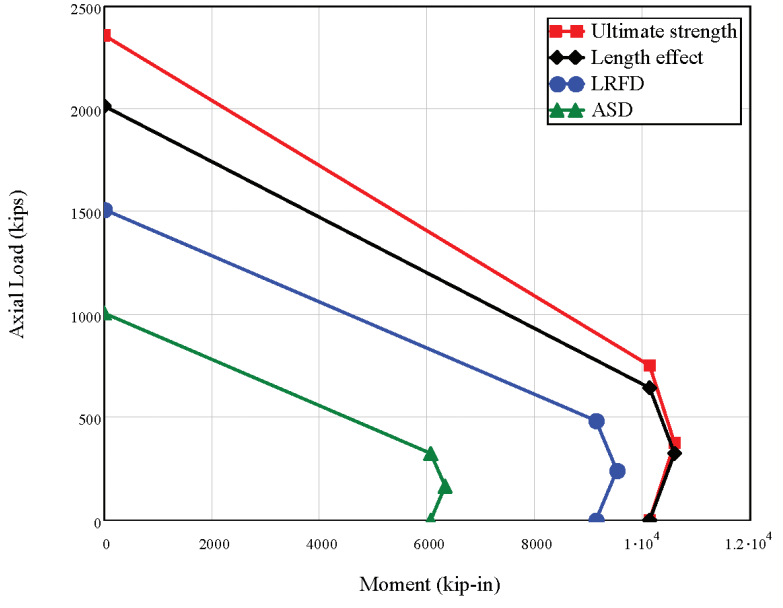

Fig. 12. Interaction diagrams for column in Example 4.

If $P_e > 0.44P_o$, $P_n = \left(0.658^{\frac{P_o}{P_e}}\right)P_o = 2{,}190$ kips

$\phi_c P_n = (0.75)(2{,}190) = 1{,}640$ kips

$P_n/\Omega_c = (2{,}190 \text{ kips}/2.00) = 1{,}100$ kips

Point B in Table 5 ($P_B = 0$)

From definitions of Point B in Table 5:

$K_c = f_c' h^2 = 1{,}860$ kips

$K_s = F_y r_m t = 144$ kips

$$\theta = \frac{0.0260K_c - 2K_s}{0.0848K_c} + \frac{\sqrt{\left(0.0260K_c + 2K_s\right)^2 + 0.857K_cK_s}}{0.0848K_c}$$

$= 2.19$ rad

$$Z_{cB} = \frac{h^3 \sin^3\left(\theta/2\right)}{6} = 842 \text{ in.}^3$$

$$Z_{sB} \approx \frac{d^3 - h^3}{6}\sin^{(4/3)}\left(\theta/2\right) = 116 \text{ in.}^3$$

$$M_B = Z_{sB}F_y + \frac{Z_{cB}\left(0.95f_c'\right)}{2} = 6{,}870 \text{ kip-in.}$$

$\phi_b M_B = (0.9)(6{,}870) = 6{,}180$ kip-in.

$M_B/\Omega_b = (6{,}870/1.67) = 4{,}110$ kip-in.

Point C in Table 5

$P_C = 0.95f_c'A_c = 1{,}390$ kips

$M_C = M_B = 6{,}870$ kip-in.

Slenderness reductions on the axial strength and application of resistance and safety factors to axial and flexural strength should be taken as per Example 4 and Leon et al. (2007).

Point D in Table 5

$$P_D = \frac{\left(0.95f_c'\right)A_c}{2} = 696 \text{ kips}$$

$Z_c = h^3/6 = 1{,}200$ in.^{3}

$Z_s = \left(d^3/6\right) - Z_c = 133$ in.^{3}

$$M_D = Z_sF_y + \frac{Z_c\left(0.95f_c'\right)}{2} = 8{,}440 \text{ kip-in.}$$

Slenderness reductions on the axial strength and application of resistance and safety factors to axial and flexural strength should be taken as per Example 4 and Leon et al. (2007).

The results are summarized in Figure 13.

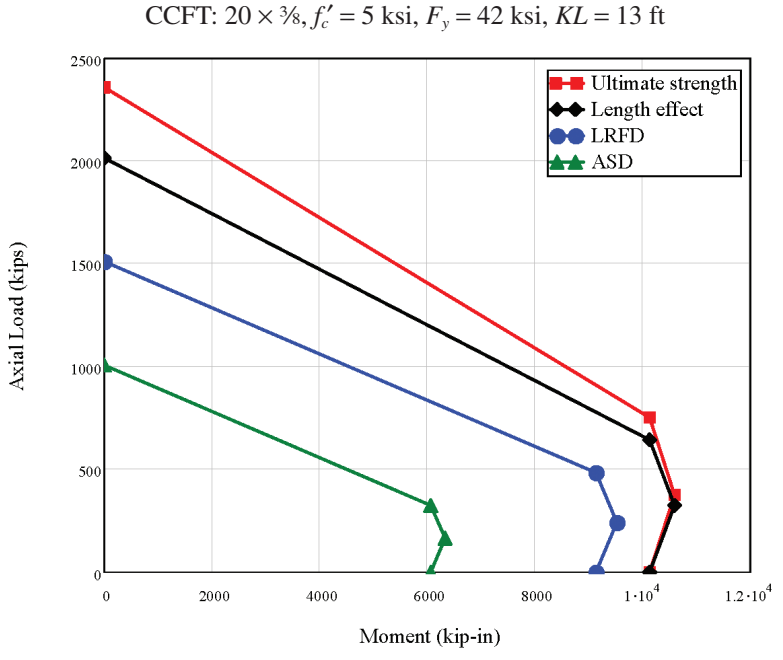

Fig. 13. Interaction diagrams for column in Example 5.

CONCLUSIONS

This paper presents the background on the step-by-step procedures available in the 2005 AISC *Specification* (AISC, 2005a) for computing composite column and beam-column strength, including accounting for stability effects on members subjected to biaxial flexure plus axial compression. The new procedures highlighted in the 2005 AISC *Specification* are discussed, including the use of a plastic stress distribution method that accounts for the beneficial effects of the concrete to the strength of the cross-section. Several examples are given for calculating the design strength of encased composite sections (SRC) as well as filled composite sections, both rectangular (RCFT) and circular (CCFT).

ACKNOWLEDGMENTS

This research was sponsored by the National Science Foundation under Grant No. CMS-0084848, the American Institute of Steel Construction, the Georgia Institute of Technology, the University of Minnesota, and the University of Illinois at Urbana-Champaign. The authors would like to thank the members of AISC Specification Task Committee 5 on Composite Construction for their contributions to this research. The assistance of Tiziano Perea, Cenk Tort, Matthew Eatherton, Arvind Goverdhan and William Jacobs with verifying the design examples is gratefully acknowledged.

APPENDIX A

NOMENCLATURE

A_s = area of the steel section, in.^{2} (mm^2)

A_c = area of concrete, in.^{2} (mm^2) $= A_{gross} - A_s - A_{sr}$

A_{sr} = area of continuous longitudinal reinforcing bars, in.^{2} (mm^2)

A_{sr} = area of a longitudinal bar, in.^{2} (mm^2)

A_{srn} = area of longitudinal bars within the $2h_n$ region, in.^{2} (mm^2)

A_{gross} = total area of member, in.^{2} (mm^2) $= h_1\, h_2$

b_f = flange width, in. (mm)

c = cover to centroid of longitudinal bars, in. (mm)

d = depth of steel section, in. (mm)

e_i = eccentricity of bar i with respect to centroid, in. (mm)

E_c = modulus of elasticity of concrete $= w_c^{1.5}\sqrt{f'_c}$ ksi $(= 5000\sqrt{f'_c}$, MPa)

E_s = modulus of elasticity of steel, which shall be taken as 29,000 ksi (210 MPa)

EI_{eff} = effective stiffness of composite section, kip-in.^{2} (N-mm^2)

f'_c = specified minimum concrete compressive strength, ksi (MPa)

F_y = yield strength of steel section, ksi (MPa)

F_{yr} = specified minimum yield strength of reinforcing bars, ksi (MPa)

h_1 = depth of the section

h_2 = width of the section

I_c = moment of inertia of the concrete section, in.^{4} (mm^4)

I_s = moment of inertia of steel shape, in.^{4} (mm^4)

I_{sr} = moment of inertia of reinforcing bars, in.^{4} (mm^4)

K = effective length factor determined in accordance with Chapter C

L = laterally unbraced length of the member, in. (mm)

N = number of longitudinal reinforcing bars

t_f = flange thickness, in. (mm)

t_w = depth of steel section, in. (mm)

w_c = weight of concrete per unit volume ($90 \le w_c \le 150$, lb/ft^3 or $1{,}440 \le w_c \le 2{,}450$, kg/m^3)

REFERENCES

ACI (2005), *Building Code Requirements for Structural Concrete*, ACI 318-05, American Concrete Institute, Farmington Hills, MI.

AISC (1999), *Load and Resistance Factor Design Specification for Structural Steel Buildings*, American Institute of Steel Construction, Chicago, IL.

AISC (2001), *LRFD Manual of Steel Construction*, 3rd Edition, American Institute of Steel Construction, Chicago, IL.

AISC (2005a), *Specification for Structural Steel Buildings*, ANSI/AISC 360-05, American Institute of Steel Construction, Chicago, IL.

AISC (2005b), *Steel Construction Manual*, 13th Edition, American Institute of Steel Construction, Chicago, IL.

Kim, D.K. (2005), "A Database for Composite Columns," M.S. Thesis, School of Civil and Environmental Engineering, Georgia Institute of Technology, Atlanta, GA.

Leon, R.T., Kim, D.K., and Hajjar, J.F. (2007), "Limit State Response of Composite Columns and Beam-Columns: Formulation of Design Provisions for the 2005 AISC Specification," *Engineering Journal*, AISC, No. 4, 4th Quarter, pp. 341–358.

Roik, K. and Bergmann, R. (1992),. "Composite Columns," in *Constructional Steel Design*, Dowling, P., Harding, J.E. and Bjorhovde, R. (eds.), Elsevier Science Publishers, New York, pp. 443–470.

Viest, I.M., Colaco, J.P., Furlong, R.W., Griffis, L.G., Leon, R.T., and Wyllie, L.A., Jr. (1997), *Composite Construction: Design for Buildings*, McGraw-Hill, New York, NY.

TABLE 1 - STRESS DISTRIBUTIONS FOR ANCHOR POINTS IN THE INTERACTION CURVE

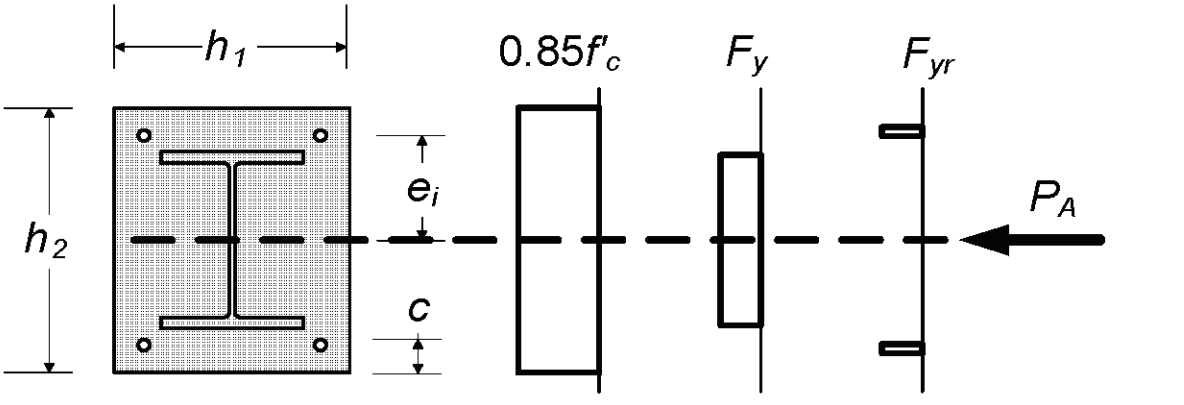

(a) Axial load capacity (Point A)

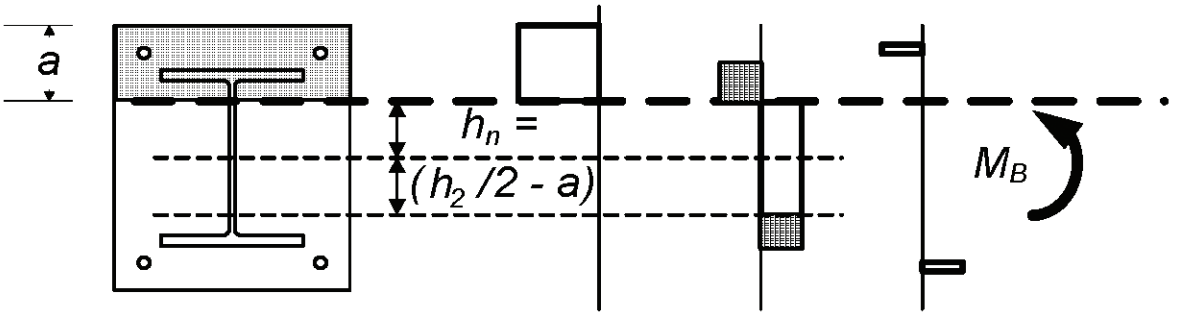

(b) Flexural capacity (Point B)

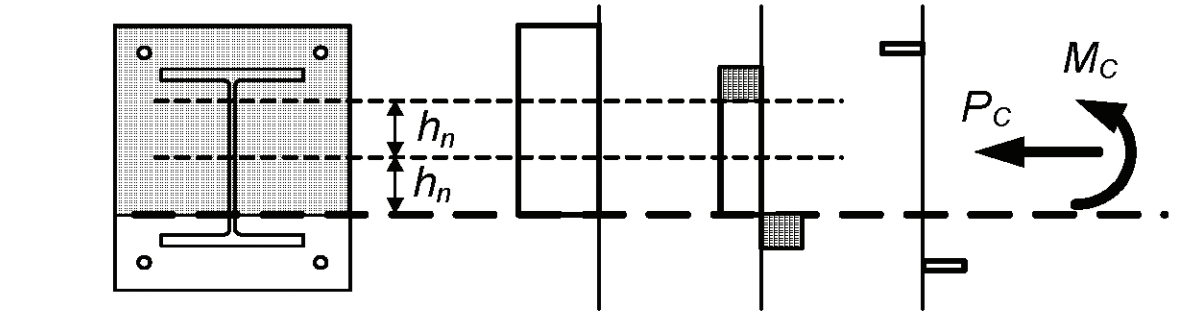

(c) Intermediate point (Point C)

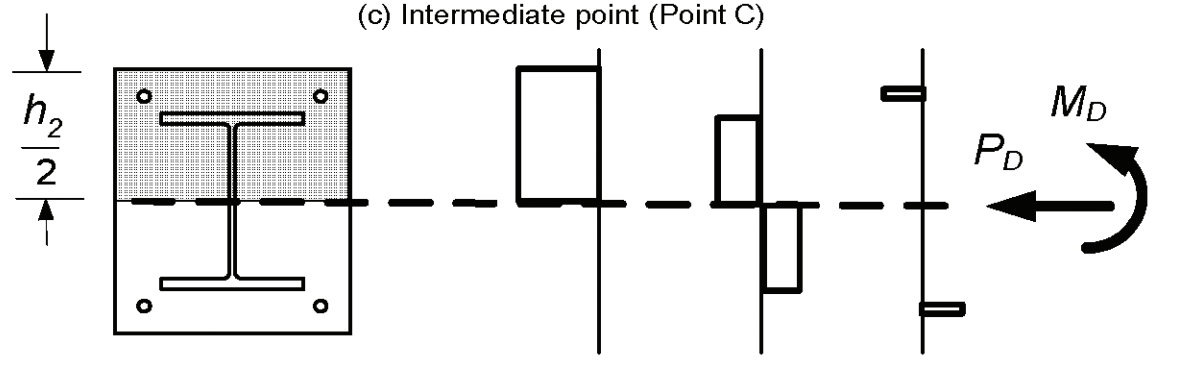

(d) Balance point (Point D)

TABLE 2 - PLASTIC CAPACITIES FOR RECTANGULAR,ENCASED W-SHAPES BENT ABOUT THE X-X AXIS

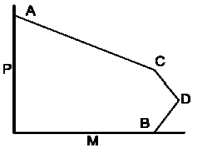

Section	Stress Distribution	Point	Defining Equations
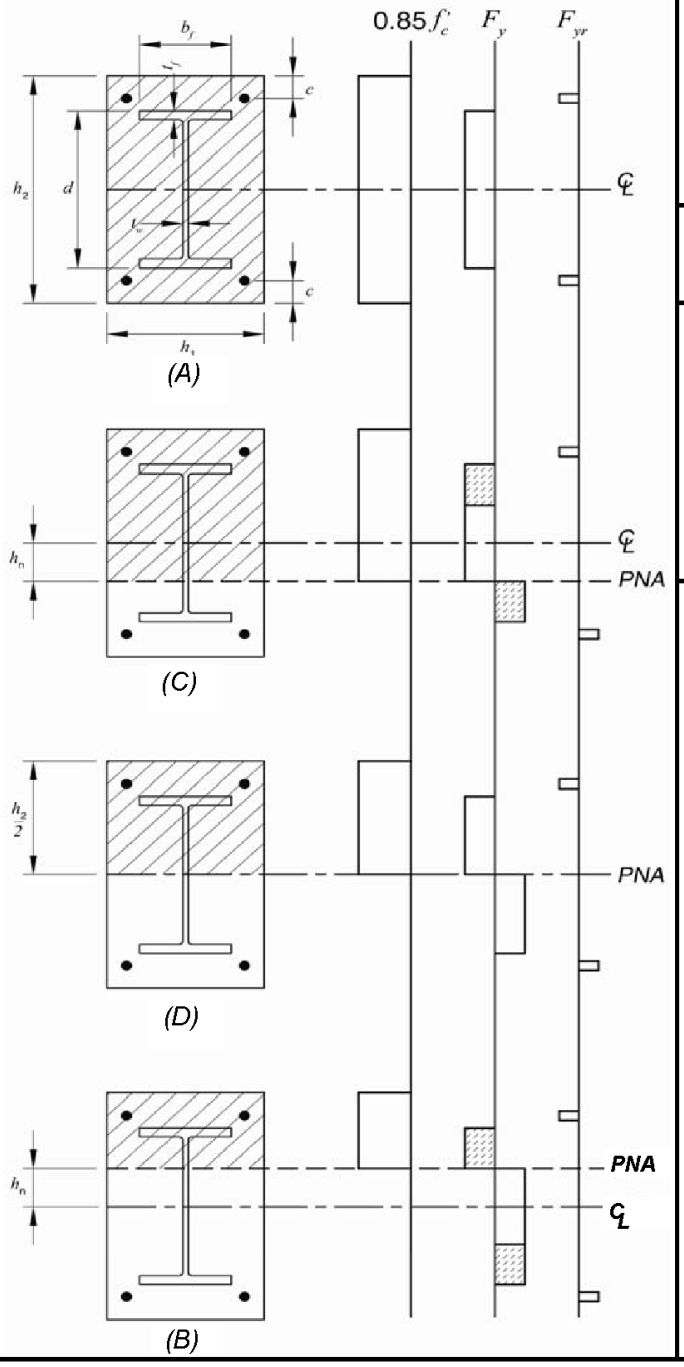		A	$P_A = A_s F_y + A_{sr} F_{yr} + 0.85 f_c' A_c$ $M_A = 0$ A_s = area of steel shape A_{sr} = area of continuous reinforcing bars $A_c = h_1 h_2 - A_s - A_{sr}$
		C	$P_C = 0.85 f_c' A_c$ $M_C = M_B$
		D	$P_D = \frac{0.85 f_c' A_c}{2}$ $M_D = Z_s F_y + Z_r F_{yr} + \frac{1}{2} Z_c (0.85 f_c')$ $Z_r = A_{sr}\left(\frac{h_2}{2} - c\right)$ $\quad Z_s = b_f t_f (d - t_f) + \frac{(d - 2t_f) t_w^2}{4}$ $Z_c = \frac{h_1 h_2^2}{4} - Z_s - Z_r$
		B	$P_B = 0$ $M_B = M_D - Z_{sn} F_y - \frac{1}{2} Z_{cn} (0.85 f_c')$ $Z_{cn} = h_1 h_n^2 - Z_{sn}$ $\quad Z_{sn} = t_w h_n^2$ For h_n below the flange $\left(h_n < \frac{d}{2} - t_f\right)$: $h_n = \frac{0.85 f_c' A_c}{2\left[0.85 f_c' (h_1 - t_w) + 2 t_w F_y\right]}$ For h_n within the flange $\left(\frac{d}{2} - t_f < h_n < \frac{d}{2}\right)$: $h_n = \frac{0.85 f_c' \left(A_c + A_s - d b_f\right) - 2F_y \left(A_s - d b_f\right)}{2\left[0.85 f_c' (h_1 - b_f) + 2 F_y b_f\right]}$ $Z_{sn} = Z_s - b_f \left(\frac{d}{2} - h_n\right)\left(\frac{d}{2} + h_n\right)$ For h_n above the flange $\left(h_n > \frac{d}{2}\right)$: $h_n = \frac{0.85 f_c' \left(A_c + A_s\right) - 2 F_y A_s}{2\left(0.85 f_c' h_1\right)}$ $Z_{sn} = Z_s$ = x-axis plastic section modulus

TABLE 3 - PLASTIC CAPACITIES FOR RECTANGULAR, ENCASED W-SHAPES BENT ABOUT THE Y-Y AXIS

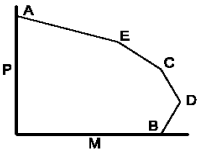

Section	Stress Distribution	Point	Defining Equations
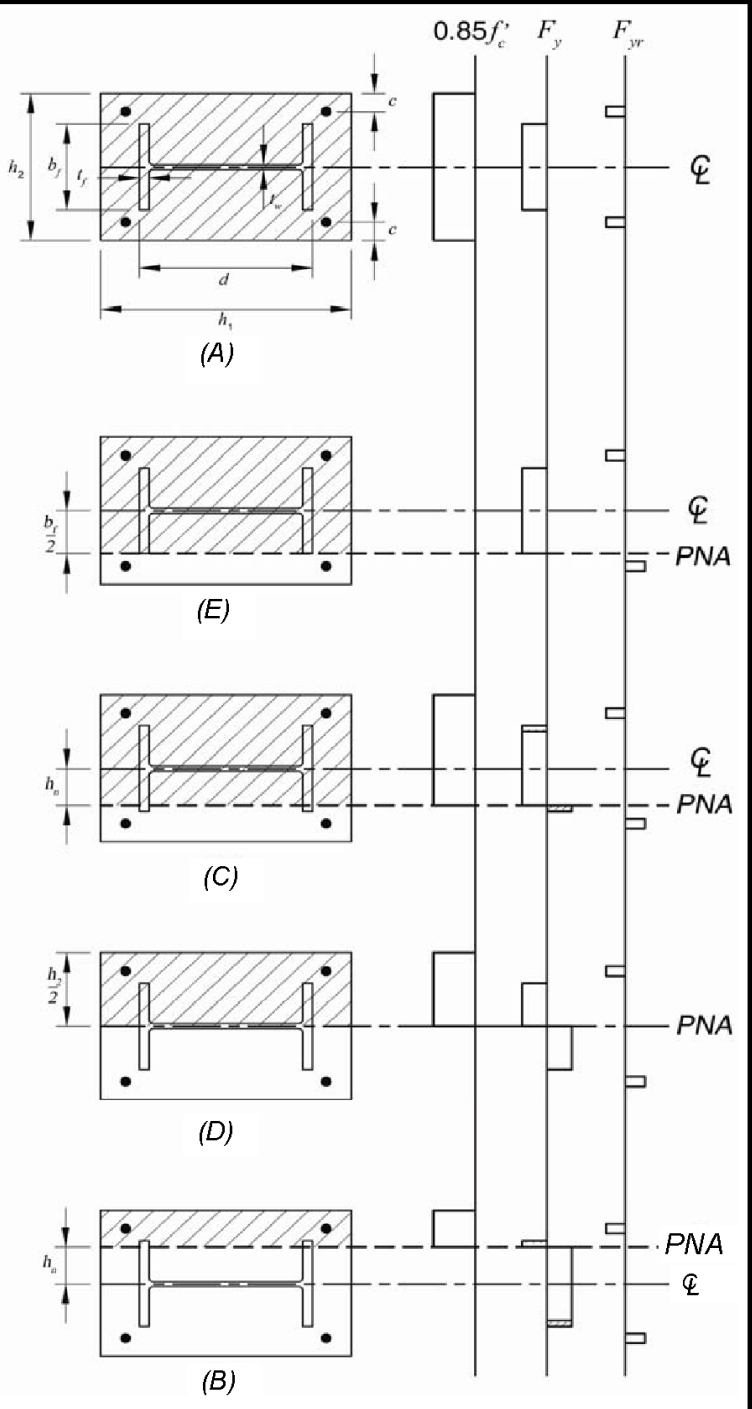		A	$P_A = A_s F_y + A_{sr} F_{yr} + 0.85 f_c' A_c \qquad M_A = 0$ A_s = area of steel shape A_{sr} = area of continuous reinforcing bars $A_c = h_1 h_2 - A_s - A_{sr}$
		E	$P_E = A_s F_y + (0.85 f_c') \left[A_c - \frac{h_1}{2}(h_2 - b_f) + \frac{A_{sr}}{2} \right]$ $M_E = M_D - Z_{sE} F_y - \frac{1}{2} Z_{cE} (0.85 f_c')$ $Z_{sE} = Z_{sy}$ = y-axis plastic section modulus $Z_{cE} = \frac{h_1 b_f^2}{4} - Z_{sE}$
		C	$P_C = 0.85 f_c' A_c$ $M_C = M_B$
		D	$P_D = \frac{0.85 f_c' A_c}{2}$ $M_D = Z_s F_y + Z_r F_{sr} + \frac{1}{2} Z_c (0.85 f_c')$ Z_s = full y-axis plastic section modulus $Z_r = A_{sr} \left(\frac{h_2}{2} - c \right) \qquad Z_s = \frac{t_f b_f^2}{2} + \frac{(d - 2t_f) t_w^2}{4}$ $Z_c = \frac{h_1 h_2^2}{4} - Z_s - Z_r$
		B	$M_B = M_\Delta - Z_{sn} F_y - \frac{1}{2} Z_{cn} (0.85 f_c') \qquad P_B = 0$ $Z_{cn} = h_1 h_n^2 - Z_{sn}$ For h_n below the flange $\left(\frac{t_w}{2} < h_n < \frac{b_f}{2} \right)$: $h_n = \frac{0.85 f_c' \left(A_c + A_s - 2 t_f b_f \right) - 2 F_y \left(A_s - 2 t_f b_f \right)}{2 \left[4 t_f F_y + 0.85 f_c' (h_1 - 2 t_f) \right]}$ For h_n above the flange $\left(h_n > \frac{b_f}{2} \right)$: $h_n = \frac{0.85 f_c' \left(A_c + A_s \right) - 2 F_y A_s}{2 \left[0.85 f_c' h_1 \right]}$ $Z_{sn} = Z_{sy}$ = y-axis plastic section modulus

TABLE 4 - PLASTIC CAPACITIES FOR COMPOSITE, FILLED HSS BENT ABOUT THE X-X AXIS

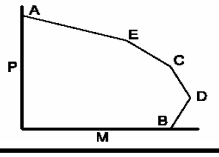

Section	Stress Distribution	Point	Defining Equations
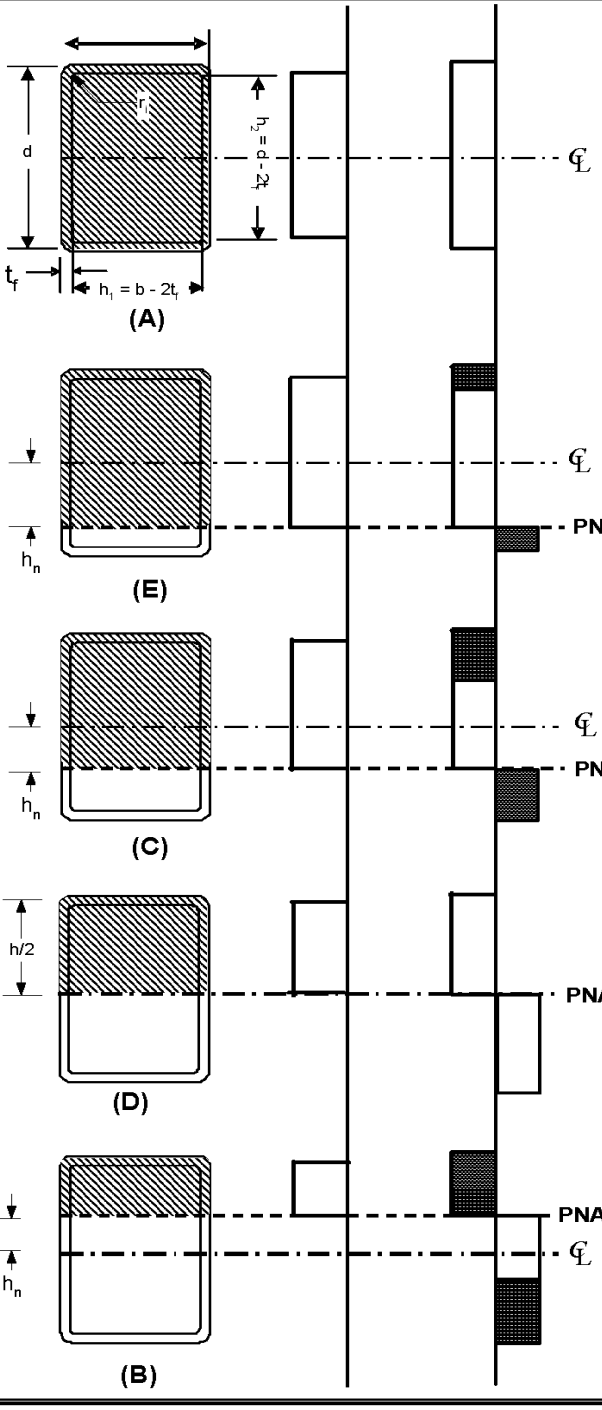		A	$P_A = A_s F_y + A_c\left(0.85 f_c'\right)$ $M_A = 0$ A_s = area of steel shape $A_c = h_1 h_2 - 0.858 r_i^2$ $h_1 = b - 2t_f$ $h_2 = d - 2t_f$
		E	$P_E = \frac{1}{2}\left(0.85 f_c'\right)A_c + 0.85 f_c' h_1 h_E + 4 F_y t_w h_E$ $M_E = M_{max} - \Delta M_E$ $Z_{sE} = b h_E^2 - Z_{cE}$ $\quad Z_{cE} = h_1 h_E^2$ $\Delta M_E = Z_{sE} F_y + ½ Z_{cE}\left(0.85 f_c'\right)$ $h_E = \frac{h_n}{2} + \frac{d}{4}$
		C	$P_C = A_c\left(0.85 f_c'\right)$ $M_C = M_B$
		D	$P_D = \frac{0.85 f_c' A_c}{2}$ $M_D = Z_s F_y + ½ Z_c\left(0.85 f_c'\right)$ Z_s = full y-axis plastic section modulus of steel shape $Z_c = \frac{h_1 h_2^2}{4} - 0.192 r_i^3$
		B	$P_B = 0$ $M_B = M_D - Z_{sn} F_y - ½ Z_{cn}\left(0.85 f_c'\right)$ $Z_{sn} = 2 t_w h_n^2$ $Z_{cn} = h_1 h_n^2$ $h_n = \frac{0.85 f_c' A_c}{2\left[0.85 f_c' h_1 + 4 t_w F_y\right]} \le \frac{h_2}{2}$

TABLE 5 - PLASTIC CAPACITIES FOR COMPOSITE, FILLED ROUND HSS BENT ABOUT ANY AXIS

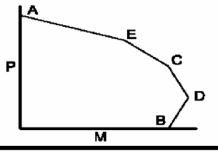

Section	Stress Distribution	Point	Defining Equations
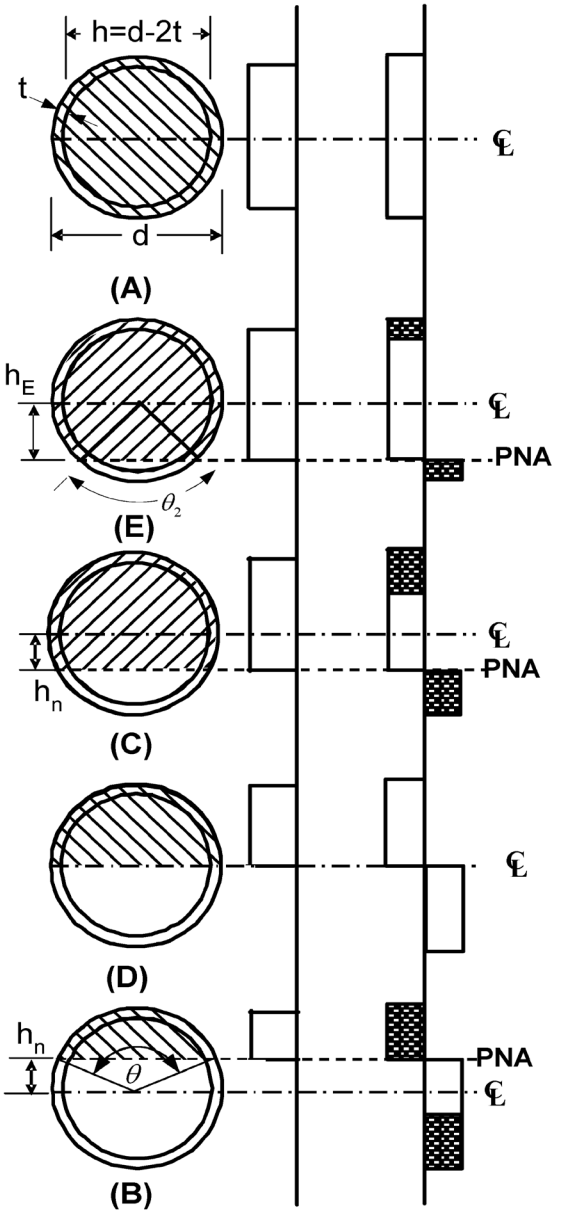		A	$P_A = A_s F_y + 0.95 f_c' A_c$ * $M_A = 0$ $A_s = 2\pi r_m t$ $r_m = \frac{d - t}{2}$ $A_c = \frac{\pi h^2}{4}$ * 0.95 instead of 0.85 can be used for the coefficient on the concrete compressive stress for all cases
		E	$h_E = \frac{h_n}{2} + \frac{h}{4}$ (h_n from Point B) $\theta_2 = \pi - 2\arcsin\left(2h_E/h\right)$ $Z_{sE} = \frac{d^3 - h^3}{6}\sin^3\left(\theta_2/2\right)X$ $X = \left[\frac{\theta_2}{\theta_2 - \sin\theta_2} + \frac{(2\pi - \theta_2)}{(2\pi - \theta_2) - \sin(2\pi - \theta_2)}\right]$ $Z_{sE} \approx \frac{d^3 - h^3}{6}\sin^{(4/3)}\left(\theta_2/2\right)$ $Z_{cE} = \frac{h^3}{6}\sin^3\left(\theta_2/2\right)$ $M_E = Z_{sE}F_y + \frac{1}{2}Z_{cE}(0.95f_c')$ $P_E = (0.95f_c'A_c + F_yA_s) -$ $\frac{1}{2}\left[F_y(d^2 - h^2) + \frac{1}{2}(0.95f_c')\,h^2\right][\theta_2 - \sin\theta_2]$
		C	$P_C = 0.95f_c'\,A_c$ $M_C = M_B$
		D	$P_D = \frac{0.95f_c'A_c}{2}$ $M_D = Z_s F_y + \frac{1}{2}Z_c(0.95f_c')$ Z_s = plastic section modulus of steel shape = $\frac{d^3}{6} - Z_c$ $Z_c = \frac{h^3}{6}$
		B	$P_B = 0$ $M_B = Z_{sB}F_y + \frac{Z_{cB}(0.95f_c')}{2}$ $Z_{cB} = \frac{h^3\sin^3(\theta/2)}{6}$ $Z_{sB} = \frac{d^3 - h^3}{12}\sin^3(\theta/2)\left[\frac{\theta}{\theta - \sin\theta} + \frac{(2\pi - \theta)}{(2\pi - \theta) - \sin(2\pi - \theta)}\right]$ $Z_{sB} \approx \frac{d^3 - h^3}{6}\sin^{(4/3)}(\theta/2)$ $\theta = \frac{0.0260K_c - 2K_s}{0.0848K_c} + \frac{\sqrt{(0.0260K_c + 2K_s)^2 + 0.857K_cK_s}}{0.0848K_c}$ $K_c = f_c'h^2$ $K_s = F_y\,r_m\,t$ $h_n = \frac{h}{2}\sin\left(\frac{\pi - \theta}{2}\right)$ (to be used in computing values for Point E)

Investigation of Flange Local Bending Under Flexible Patch Loading

LYLE P. CARDEN, GOKHAN PEKCAN and AHMAD M. ITANI

When a rigid patch or line load is applied to a beam, the flange is only able to deform as allowed by deformation of the web, thus the capacity of the web controls the design. However, in applications where a patch load is flexible, it is possible for the flange to bend around the web, which may limit the capacity of the beam. A flexible patch load is considered one where the load is able to deform as the loaded member deforms, resulting in a more uniform distribution of applied stress than when a load is applied through a rigid element. A recent study by the authors (Carden, Pekcan and Itani, 2005) has shown that flange bending may be the critical limit state in applications such as bridge falsework where timber posts bear on unstiffened steel beams. The resulting damage mechanism illustrated in Figure 1 has the potential to lead to instabilities and collapse of bridge falsework during construction.

Past studies on the effect of patch loading (Roberts and Rockey, 1979; Roberts and Markovic, 1983; Elgaaly, 1983; Roberts and Newark, 1997; Shahabian and Roberts, 1999; Graciano and Edlund, 2003) have generally assumed rigid patch loads which have not resulted in flange bending other than that required for deformation of the web. The case of a flexible patch load provided by a timber post has not been considered, thus there is currently no design methodology to assess flange bending capacity under this loading condition.

The AISC *Specification for Structural Steel Buildings* (AISC, 2005), hereafter referred to as the AISC *Specification*, allows for the calculation of flange bending capacity in beam-column joints. The ultimate flange bending capacity in the column flange assumes that a tensile line load is applied to the column flange from the beam flange. A yield line pattern in the column flange and a uniform stress distribution from the beam flange is assumed in order to derive an equation to calculate the ultimate capacity of the flange (Graham, Sherbourne and Khabbaz, 1959). However, this equation, which is based on the need to limit tensile stresses in the connection of the beam flange at the column web, is conservative if applied to a compressive patch load. The conservatism is in part because a patch load is able to engage a larger region in resisting bending of the flange than a linearly applied load from an adjoining flange. In addition weld fracture is not the concern resulting from flange bending in this application.

Two methods that account for the effect of patch loading from timber and steel posts on beams were developed elsewhere (Carden et al., 2005) and are summarized in what follows. In the first, the interaction between the flange bending capacity and the post compression capacity was considered. If the flange is significantly weaker than the post, it will tend to dictate the strength of the joint region. On the other hand,

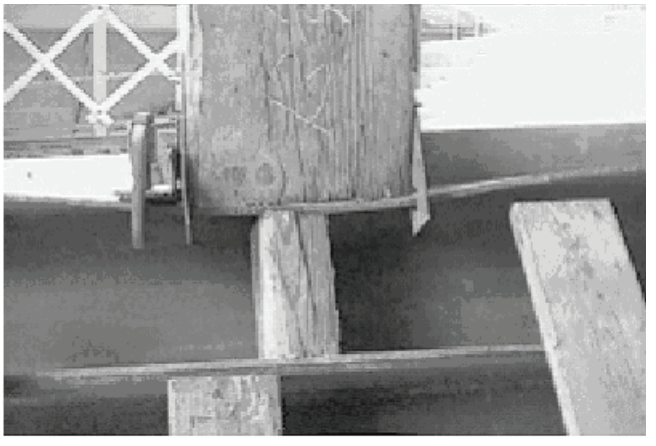

Fig. 1. Flange bending in sill beam (courtesy of J. Lammers, Caltrans).

Lyle P. Carden is a structural engineer, Martin & Chock, Inc., Honolulu, HI.

Gokhan Pekcan is assistant professor, department of civil and environmental engineering, University of Nevada, Reno, NV.

Ahmad M. Itani is professor, department of civil and environmental engineering, University of Nevada, Reno, NV.

if the post compression strength is notably lower than the beam flange capacity then the post will dictate the overall response. If the flange and post have similar strengths then the joint capacity will tend to be smaller than the capacity of either component. The second method uses an effective bearing area for the post, which accounts for flange bending capacity in a secondary manner by reducing the effective area of the post depending on the thickness of the flange. The first method was found to be most effective for predicting the flange-post bearing joint strength with a timber post; however, with a steel post, which is axially rigid, the second method leads to more accurate assessment of the joint strength.

The above methods were developed assuming a concentric loading, without the use of any blocking, which is sometimes used in attempts to strengthen the joint region. This paper describes a series of experiments and finite element analyses to investigate the effectiveness of the above methodologies for predicting the flange-post joint capacity; considering eccentricities between the centroids of the beam and post, and the use of blocking. The methodologies are then developed into a form appropriate for design using load and resistance factor design (LRFD) and allowable stress design (ASD) procedures.

FLANGE-POST CAPACITY

Interaction Method

The flange bending capacity, R_f, due to a flexible patch load similar to that associated with bearing of a timber post can be described as

$$R_f = \beta t_f^2 F_{yf} \quad (1)$$

where

β = a constant determined from a yield line analysis (Carden et al., 2005)
t_f = thickness of the flange
F_{yf} = specified minimum yield stress of the flange

Expressions for β were developed assuming a uniform and triangular stress distribution for the patch load, as shown in Figure 2. However, for a nominal 12×12 in. post, a β value equal to 18 was found to be appropriate for calculating the flange bending capacity for a range of beams with flange thicknesses between 0.44 and 0.94 in. subjected to concentric patch loading.

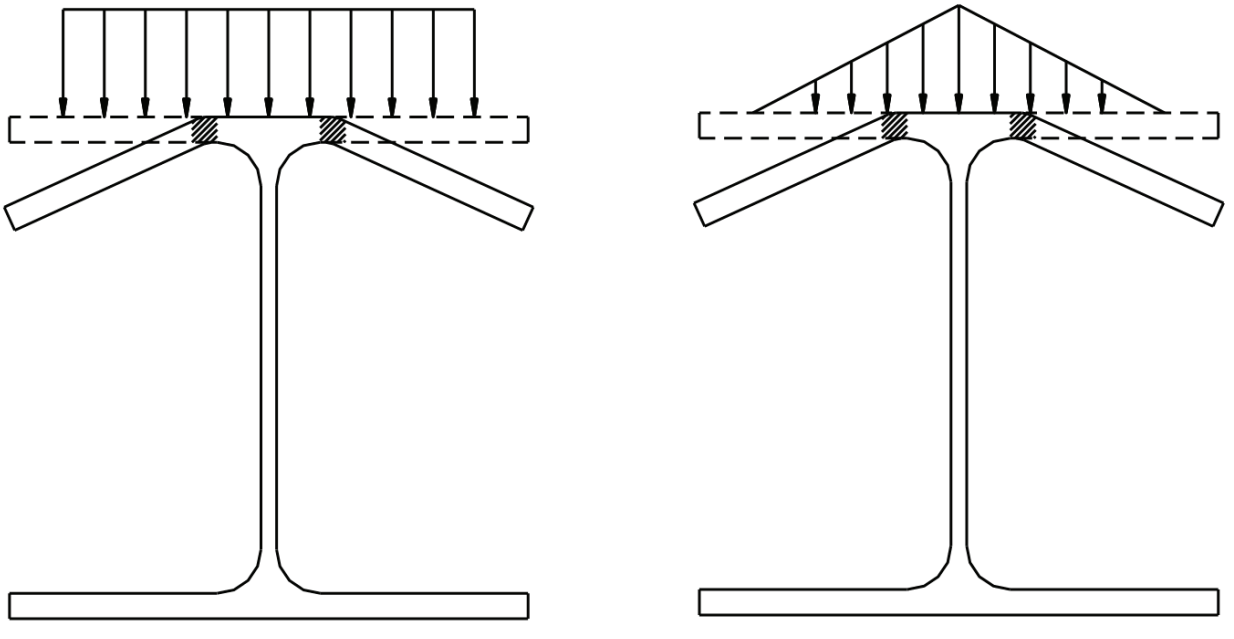

(a) (b)

Fig. 2. Patch load assuming: (a) a uniform stress distribution and (b) a triangular stress distribution.

In order to calculate the capacity of the flange-post bearing region it is also necessary to consider the compression capacity of a short timber post which is given by

$$P_p = F_c' A_p \tag{2}$$

where

A_p = nominal cross-sectional area of the post
F_c' = specified minimum compression stress of the timber blocking after applicable modification factors are applied (AFPA, 1996)

As the compression capacity in the bearing joint region is considered over a short length, the post stability factor in this calculation is equal to 1.0. It is noted that stability of the post should be considered as a separate limit state in the design of the post.

The strength of the joint region can then be determined from the interaction of the flange bending and post compressive strength using the following relationship

$$\left(\frac{P_u}{R_f}\right)^2 + \left(\frac{P_u}{P_p}\right)^2 \leq 1 \tag{3}$$

where

P_u = applied axial load in the post

Bearing Area Method

This method focuses on the post capacity for calculating the ultimate load, with the impact of flange bending inherent but not explicitly considered in the formulation. The method is found to be more effective for a steel post where the post is axially rigid and thus does not allow the flange to deform before failure of the post, unlike a more flexible timber post (Carden et al., 2005). For this model an effective cross-sectional area of the steel post is considered to carry the entire axial load, as shown in Figure 3, and can be calculated using similar assumptions to those used in the web yielding equation given by the AISC *Specification* (AISC, 2005). The effective area of the post is determined by the width of the post that is effective in carrying the load multiplied by the thickness of the post walls. An equation for the capacity of a steel post is given by

$$P_p = \left[\alpha\left(t_f + t_{bp}\right) + 2k_1\right] 2t_p F_{yp} \tag{4}$$

where

α = constant which depends on the slope of the stress gradient assumed through the flange
t_{bp} = thickness of the base plate of the post
k_1 = distance from the center of the web to the edge of the fillet
F_{yp} = specified minimum yield stress of the post
t_p = wall thickness of the round hollow steel section

The $2t_p$ allows for the transfer of axial load on two sides of the round hollow steel post section.

Strength of Blocking

Falsework design typically avoids the use of stiffeners, as beams are reused and construction is temporary. However, in some cases timber blocking is used in an attempt to stiffen the beam flanges. Generally timber blocks sized between 4×4 in. and 6×8 in. are used, the capacity of which can be calculated based on the axial compression capacity of a short timber member. However, experimental and analytical studies showed that the full capacity of the blocking is generally not effective, particularly for a steel post, thus the capacity of the timber blocking, P_b, can be given by

$$P_b = \gamma F_c' A_b \tag{5}$$

where

γ = blocking effectiveness factor
A_b = combined cross-sectional area of the blocking on both sides of the web

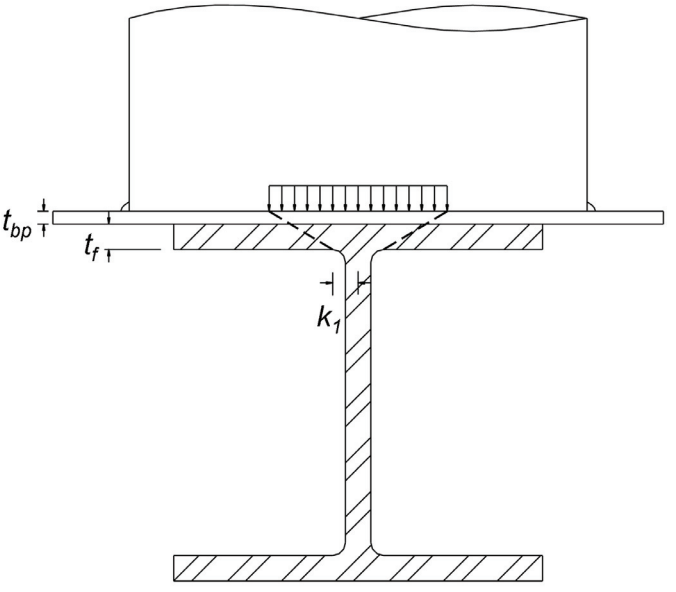

Fig. 3. Effective area of steel post for calculating the ultimate post load.

EXPERIMENTAL STUDIES

Experimental Setup

A series of experiments were performed to study different limit states in a flange-post bearing joint region. A total of 15 experiments focused on quantifying the flange-post joint capacity; 13 with timber posts and two with steel posts. The experimental setup with a timber post and steel beam is shown in Figure 4 as an example of one configuration. The flanges were restrained at the ends of the 48 in. long beam segments by the steel frame shown in the figure, preventing lateral instability of the beams for studying the flange and post limit states. Loads were applied to the end of the 48 in. long posts through a slider to limit lateral deformation at the end of the post, which was attached to a displacement controlled hydraulic actuator. The instrumentation consisted of displacement transducers and strain gages, as well as a machine-vision camera that allowed the measurement of strains and deformations. Three different beam sections were used, including ASTM A572 Gr. 50 HP12×53 and HP14×73 beams, and ASTM A992 W14×90 beams. Number 2 Douglas Fir 12 × 12 in. timber members were used for the posts and corbels. An 18-in.-diameter ⅜-in.-thick A500 Gr. B (42 ksi) round hollow steel section with a ½-in.-thick base plate was used to simulate a steel post. In some of the experiments, 6 × 8 in. Number 2 Douglas Fir timber blocking was also placed between the flanges on both sides of the web. The effects of eccentric patch loading were also investigated experimentally by introducing eccentricities ranging from 1/12 to ⅙ of the flange width. The failure load of the joints between the beams and steel posts could not be directly obtained from the two experiments, as timber corbels (members located under the sill beam in typical bridge falsework and located between the beam and reaction plate in experiments similar to that shown in Figure 4) were included in these experiments and governed the failure response.

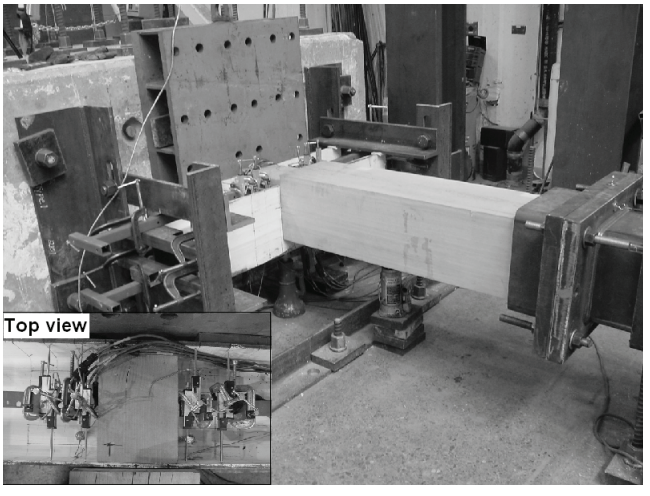

Fig. 4. Experimental setup with a timber post and steel beam with blocking and an eccentricity between the centroid of the beam and post.

Experimental Results

The force measured in the actuator was plotted against the axial displacement at the slider end of the post for each experiment. A typical force-displacement curve for a beam concentrically loaded through a timber post without any blocking is shown in Figure 5a, and that for a beam with blocking is shown in Figure 5b. These figures show that the stiffness initially increases as any gaps due to lack of fit between the

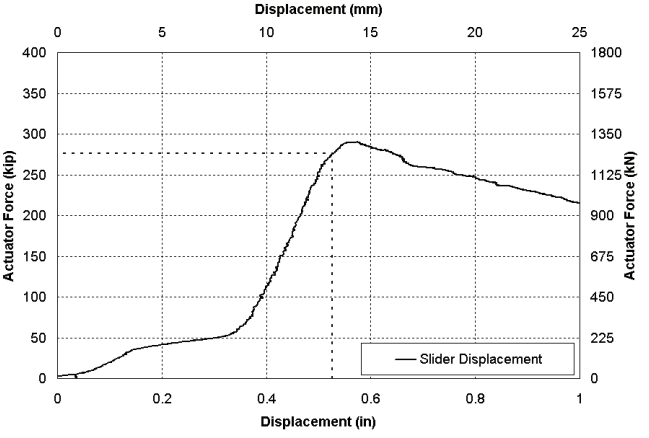

(a)

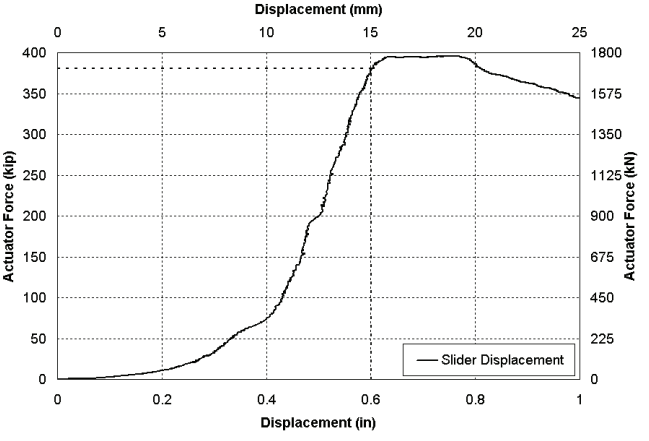

(b)

Fig. 5. Force displacement curve for HP14×73 beams: (a) concentrically loaded with no blocking and (b) concentrically loaded with blocking.

various components close, after which the maximum stiffness is reached. The stiffness decreases and load then starts to drop as crushing of the post and plastic deformation in the flange occurs. Comparison of Figures 5a and 5b shows that blocking resulted in slightly improved capacity.

The ultimate load was defined as the load at which the stiffness reduces to 50% of the initial stiffness, where the initial stiffness was defined as the stiffness between 25% and 75% of the ultimate load. Accordingly, the ultimate load, determined iteratively, is shown by the dashed lines in Figure 5 and is typically within 10% of the maximum load where post crushing and flange bending occurred.

A mixture of suspended lime and water was painted onto each beam and was observed to flake off once the steel started to yield. For each of the beams, the observed load where flaking occurred on the beam flange was recorded, with flaking typically located initially at the edge of the fillet between the flange and web under the post. Figure 6 compares the load at which flaking was observed with the estimated ultimate load based on the relative stiffness of the beams with timber posts. With the steel posts, flaking was not observed in the beams until after the posts had already yielded and thus is not included in the figure. Comparisons for different beam sizes and different configurations with and without blocking, and with different eccentricities between the post and beam are plotted in Figure 6. There are only 12 points for 13 experiments with timber posts as flaking was not observed at the appropriate time in one of the beams due to premature failure of the timber post. As can be seen in the figure, observed and estimated ultimate force is different by no more than 13% for each beam, with an average difference of 2%. The comparison therefore indicates that the estimated ultimate load, based on a 50% reduction in stiffness, is similar to the load at which yielding is first observed, and thus, is an appropriately defined ultimate load.

Along with the subassembly experiments, component experiments were performed to determine the axial capacity of three timber posts, three timber blocks, and a steel post. The resulting axial capacity of the timber post, based on an average from the experiments, was 352 kips. The average axial capacity of the timber blocks was 163 kips and the capacity of the steel post was 888 kips. In addition, eight coupon tests were performed on samples of steel from the beams resulting in an average yield stress of 53 ksi and a range between 50 and 58 ksi.

For the beams with timber posts, the capacity of the flange-post joint region was calculated using Equations 1, 2, 3 and 5, when blocking was used, using the actual strengths of the post, blocking and steel material from the component experiments. Equation 1, with a β value of 18, was used to estimate the flange bending capacity. The timber blocking was assumed to be 100% effective, thus a γ value of 1.0 was assumed in Equation 5 and the effective blocking capacity was directly added to the flange bending capacity. The blocked or unblocked flange capacity was then combined with the timber post strength from Equation 2 using Equation 3. The experimental data show that there is a relatively small reduction in capacity when the post is eccentric to the centroid of the beam. Thus it is assumed that the above equations apply equally when there is an eccentricity equal to or less than ⅙ of the width of the flange. The resulting calculated capacity of the flange-post region for the beams with timber posts is compared in Figure 7 to the estimated ultimate force from the experimental data, based on a 50% reduction in stiffness. The estimated forces are approximately equal to or less than the observed forces, at between 71% and 105% of

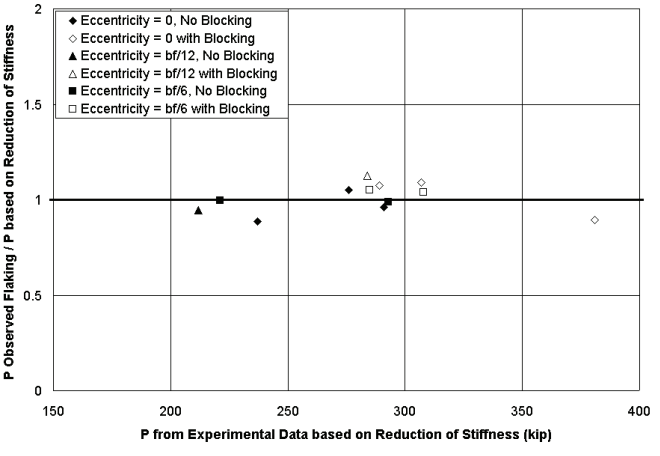

Fig. 6. Comparison of ultimate force observed due to flaking on the flange and ultimate force calculated at a 50% reduction in initial stiffness from force displacement curve.

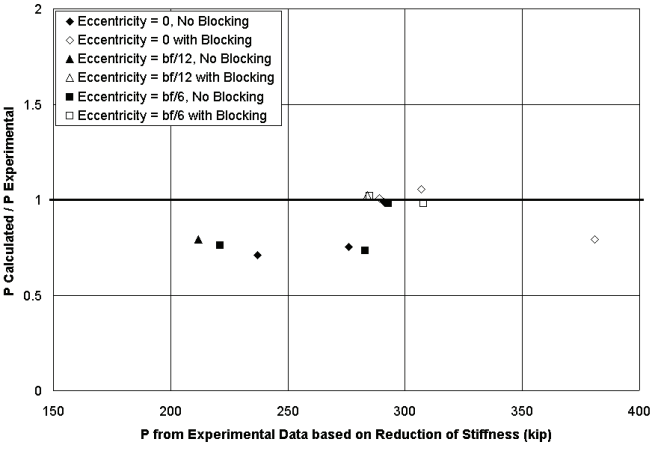

Fig. 7. Comparison of calculated ultimate force to experimental ultimate force based on a 50% reduction in stiffness.

that observed, for all members. The stagger in the observed capacities is mainly attributed to the variability of material properties, particularly for the timber members. The lime flaking pattern observed in the beams after considerable inelastic flange bending was very similar to the yield pattern assumed in developing Equation 1. Therefore, this method is appropriate for predicting the capacity of the flange-post joint region with a timber post.

The effective post bearing area method was used to estimate the capacity of the flange-post joint region with a steel post, based on Equation 4. The observed failure mode in the experiments with the steel post was consistent with the effective bearing area assumed for calculating the ultimate load, with yielding and crippling of the post occurring in the region where the post was bearing on the beam in line with the web. Unfortunately, the calculated ultimate load could not be directly compared to the experimental data as timber corbels were also used in experiments with the steel posts and these affected the ultimate load of the system. Thus, finite element analyses were used for comparison with the calculated ultimate load for cases with steel posts.

FINITE ELEMENT ANALYSES

Models

A series of finite element models of the different experimental configurations were developed and verified using the experimentally recorded response data. These finite element models allowed a larger range of beams and configurations to be considered, without material variability affecting the results. HP12×53, HP14×73, HP12×89 and W14×90 beams were modeled with timber posts (Figure 8a), and W14×90, HP14×117 and W14×120 beams were modeled with steel posts (Figure 8b).

The beams, posts and blocking were modeled with linear three-dimensional eight node elements in ABAQUS (Hibbett, Karlson and Sorensen, 2003), meshed typically as shown in Figure 8. The steel members were modeled with a plastic isotropic material using an expected yield strength of 55 ksi for the A572 Gr. 50 and A992 steel beams (approximately equal to the 53 ksi average strength measured from coupon tests) and 46 ksi for the A500 Gr. 42 steel posts. The timber posts were modeled with a multi-linear material model to fit the observed force-displacement relationships resulting from both material and geometric nonlinearities. Experiments on the 11.5 in. square Douglas Fir timber posts resulted in a calculated nominal post strength of 2.7 ksi, which was assumed as the first-yield stress in the finite element model. The stress was assumed to increase linearly by 20% to allow for material and geometric stiffening up to 2 times the yield strain. The stress was then assumed to gradually decrease to zero at a strain of 10% to reflect the reduction in strength due to crushing. Based on measured values from experiments, the elastic modulus was equal to 550 ksi. The multi-linear model was found to compare better to the experimental data than pre-defined material models in ABAQUS. The 7.5 × 5.5 in. blocking elements were modeled with a similar model using a 4.0 ksi initial yield stress and a 330 ksi elastic modulus, as determined from the component experiments.

Loads were applied axially to the top of the post in displacement control until after the maximum load in the system was reached. The interfaces between the beams and other components were modeled with surfaces which are assumed to be connected by maintaining a constant geometric relationship between adjacent nodes. This is similar to a contact model with a high friction coefficient between nodes, but was found to be significantly more computationally efficient with comparable results. The nodes under the beams were completely restrained, while at the end of the post, the nodes were restrained to allow axial deformation only. Both flanges at the ends of the beam were also restrained to prevent out-of-plane deformation of the flanges.

For each configuration considered, the axial force in the post was plotted against the axial displacement at the free end of the post or patch load. The ultimate load was defined from the force-displacement curve at a point where the tangential stiffness reduced to 50% of the initial stiffness, consistent with the experimental data.

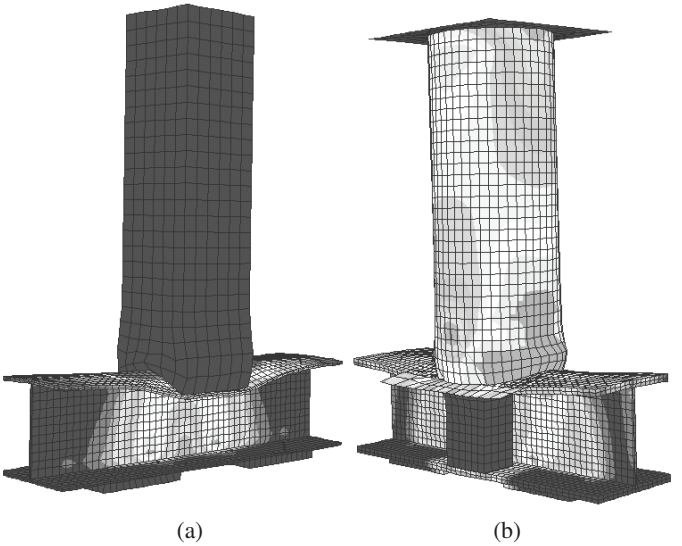

(a) (b)

Fig. 8. Finite element models for: (a) a timber post and beam and (b) a steel post and beam with blocking.

Results from Analyses

Comparisons of the force-displacement curves from the finite element model and experimental data for two typical beams with and without blocking are shown in Figures 9a and 9b, respectively. The displacement from the experimental data was offset so that extrapolation of the maximum stiffness passed through the origin, to allow comparison with the finite element results. The comparisons show that the initial slope and maximum load were similar between the finite element and experimental models. A comparison between the ultimate loads calculated from the finite element model and experimental data is given in Figure 10. The load obtained from the finite element analysis is between 76% and 121% of the experimental load. Therefore, there is good correlation between the experimental and finite element results, with the variability attributed primarily to the variability in the capacity of the different posts and blocking.

The finite element results show that blocking resulted in a 20 to 70% increase in the flange-post joint capacity when using a timber post, depending on the flange bending capacity. With a steel post, blocking allowed only a 20 to 25% increase in the joint capacity. An eccentricity between the centroids of the flange and post equal to a maximum of ⅙ of the flange width, resulted in a relatively small reduction in the flange-post capacity of 10 to 15% when using a timber post. With a steel post, each eccentric case resulted in an almost identical flange-post capacity to the concentric case.

The calculated flange-timber post capacity based on the interaction equation (Equation 3), as a ratio of the capacity calculated from the finite element analysis, is plotted in Figure 11a, for different beam sizes, with and without blocking and with different eccentricities. The blocking was considered to be 100% effective ($\gamma = 1.0$) with the timber posts, as described previously. Figure 11a shows that for the beams with timber posts, the calculated capacity is between 80% and 105% of the capacity calculated from the finite element model, with just two exceptions. These exceptions are for the larger beams with a large eccentricity where the calculated capacity is up to 119% of that from the finite element model. This level of eccentricity is unlikely to occur in a real situation; therefore, these cases are not of particular concern. Furthermore, when appropriate factors and nominal strengths instead of expected strengths are used in design, these cases are expected to be conservative as well. In practice, the maximum eccentricity should be limited to ⅙ of

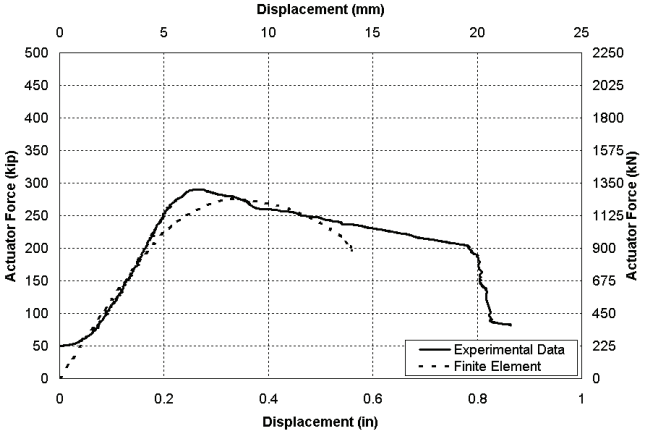

(a)

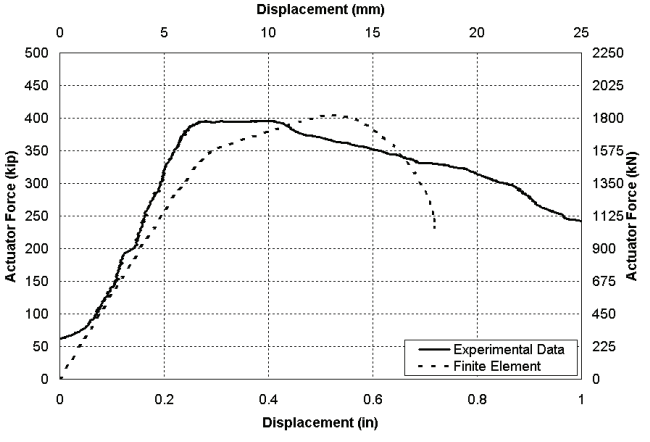

(b)

Fig. 9 Comparison of force-displacement curve for HP14×73 beams: (a) concentrically loaded with no blocking and (b) concentrically loaded with blocking from experimental data and finite element analysis.

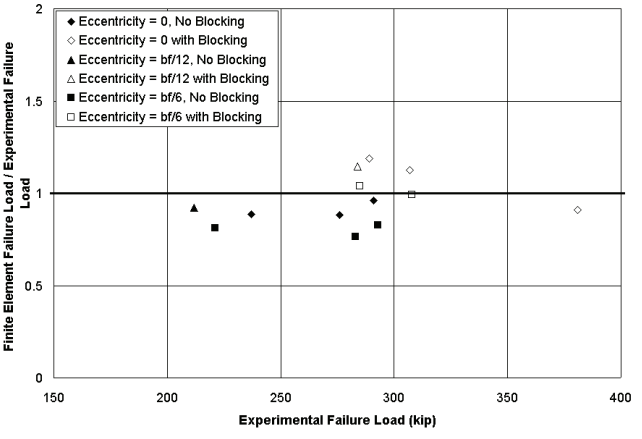

Fig. 10. Comparison of ultimate force from experimental data and finite element analysis.

the flange width. The calculated capacity based on the interaction equation appears to be relatively accurate and generally conservative for all cases including those with timber blocking.

With the steel posts, the ultimate capacity of the flange-post joint region is calculated using the effective bearing area method (Equation 4). As the stiffness of the post is greater than the stiffness of the blocking, the effectiveness of the blocking is reduced to 30% ($\gamma = 0.3$). While the blocking can be loaded further and the force carried by the joint continues to increase, significant flange bending and post yielding occurs resulting in significant permanent deformations in both beam and post. Thus, the effectiveness of timber blocking with a steel post is limited. Comparisons between the calculated capacity using the effective post bearing area and effective blocking capacity (Equations 4 and 5) and the finite element analyses are shown in Figure 11b. The method is shown to be accurate and conservative, with calculated capacities between 81% and 105% of those from the finite element model. The use of a 30% effectiveness factor for the timber blocking gives a ratio of calculated to finite element capacity with the timber blocking relatively consistent to that without the timber blocking.

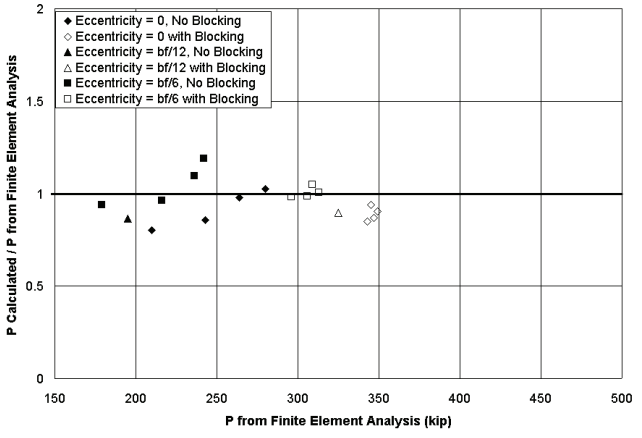

(a)

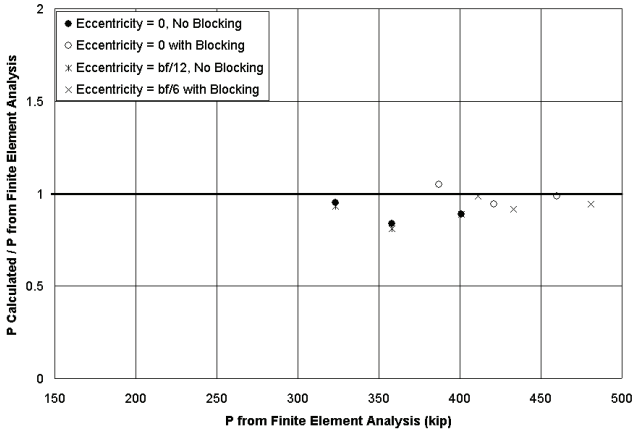

(b)

Fig. 11. Comparison of finite element analysis with calculated ultimate force using: (a) the interaction equation (Equation 3) and (b) the effective bearing area (Equation 4).

DESIGN OF FLANGE-POST BEARING JOINT REGIONS

Design Strength with a Timber Post

It is noted that the actual strength of the posts and beams were used in the comparisons discussed earlier. Clearly, the use of minimum specified stresses along with application of load factors and resistance factors for LRFD, or allowable stresses for ASD, will result in additional conservatism in the design equations. In LRFD format, for a steel beam with a patch load from a timber post, the factored applied load in the post, P_u, should be less than a combination of flange bending capacity, including blocking, and the post compression capacity for a short length of post, such that

$$P_u < \left(\frac{1}{\phi R_{nf}^{\ 2}} + \frac{1}{\phi P_{np}^{\ 2}} \right)^{-\frac{1}{2}} \tag{6a}$$

where

ϕR_{nf} = design strength of the flange including blocking

ϕP_{np} = design strength of the post

The design strength of the flange, including blocking (when used), is given by

$$\phi R_{nf} = \phi_b 18 t_f^{\ 2} F_{yf} + \lambda \phi_c F_c' A_b \tag{6b}$$

where

ϕ_b = resistance factor for flange bending, equal to 0.90 (AISC, 2005)

ϕ_c = resistance factor for compression in the blocking, equal to 0.90 (AFPA, 1996)

λ = time effect factor, equal to 1.0 for a typical falsework duration

The design strength of the post is given by

$$\phi P_{np} = \phi_c F_c' A_p \tag{6c}$$

where

ϕ_c = resistance factor for compression in the post, equal to 0.90

In ASD format, the applied stress in the post, f_c, should be less than the combination of allowable effective stress from flange bending capacity, F_{cf}, and allowable stress in the post, F'_{cp}, such that

$$f_c < \left(\frac{1}{F_{cf}^{\ 2}} + \frac{1}{F'^{2}_{cp}} \right)^{-\frac{1}{2}} \quad (7a)$$

The effective stress from flange bending capacity, including the capacity provided by timber blocking, can be determined from

$$F_{cf} = \frac{18 t_f^{\ 2} F_f}{A_p} + \frac{F'_{cb} A_b}{A_p} \quad (7b)$$

where

F_f = allowable flange stress, equal to 22 ksi for A36 steel or 30 ksi for A572 Gr. 50 or A992 steel beams if the allowable stress safety factor (1.67) is applied as defined by the AISC *Specification* (AISC, 2005)

F'_{cb} = allowable compression stress in the timber blocking (AFPA, 2001)

F'_{cp} = allowable stress in the post, due to post compression over a short length of the post, with applicable modification factors, is taken directly from the ASD specifications (AFPA, 2001)

Design Strength with a Steel Post

The design capacity of the flange-post bearing joint region with a steel post can be most accurately determined using the effective bearing area. Therefore, using the LRFD format, design of the flange-post region should ensure that

$$P_u < \phi R_n \quad (8a)$$

where

P_u = factored applied load

ϕR_n = design strength of the post in bearing, including the strength provided by blocking

ϕR_n is given by

$$\phi R_n = \phi_{cp} \left[5\left(t_f + t_{bp} \right) + 2k_1 \right] 2 t_p F_{yp} + \phi_{cb} 0.3 F'_c A_b \quad (8b)$$

where

ϕ_{cp} = resistance factor for compression in the post, which, to be consistent with that used for web yielding, equal to 1.00 (AISC, 2005)

ϕ_{cb} = resistance factor for the blocking, equal to 0.90

In ASD format the flange-post connection region for a steel post should be designed such that

$$f_{cp} < F'_{cpb} \quad (9a)$$

where

f_{cp} = applied compression stress in the gross cross-sectional area of the post

$$f_{cp} = \frac{R}{\left[5\left(t_f + t_{bp} \right) + 2k_1 \right] 2 t_p} \quad (9b)$$

where

R = applied force in the post

The allowable stress in the post including blocking is given by

$$F_{cpb} = F_{cp} \left(1 + \frac{0.3 F'_{cb} A_b}{F_{cp} \left[5\left(t_f + t_{bp} \right) + 2k_1 \right] 2 t_p} \right) \quad (9c)$$

where

F_{cp} = 28 ksi for an A500 Gr. B round hollow steel section based on an allowable stress safety factor of 1.50, as for web yielding (AISC, 2005)

F'_{cb} = allowable stress in the timber blocking (AFPA, 2001)

SUMMARY AND CONCLUSIONS

The capacity of the beam-post joint region for an unstiffened beam supporting or supported by a timber or steel post, similar to those found in bridge falsework, may be governed by a combination of flange bending and post crushing or yielding. A series of experiments and finite element analyses were conducted to investigate potential failure mechanisms and to quantify the flange-post joint capacity. Also considered in the study was the effect of: i) blocking placed between the top and bottom flanges, and ii) eccentricity between the centroids of the beam and post. Accordingly, the following observations were made:

1. The ultimate capacity of the joint is defined at a point where the stiffness of the force-displacement curve reduces to 50% of the initial stiffness. This definition of the ultimate capacity provided consistent correlation with the experimental observations; namely onset of flange bending.

2. Depending on the size of the beam, timber blocking is found to increase flange-post joint capacity by 20 to 70%.

3. When used under a steel post with large beam sections, timber blocking is less effective resulting in a maximum likely increase of 25% in joint capacity.

4. An eccentricity between the flange and a timber post, which should be limited to ⅙ of the flange width results in a reduction of flange-post strength of 10 to 15%.

5. The effect of eccentricity, which should be limited to ⅙ of the flange width, on the joint capacity when steel posts are used is negligible.

Two methods were developed for predicting the flange-post joint capacity; namely, the interaction method and the effective bearing area method. The interaction method accounted for a combination of flange bending and post crushing capacities. Based on the experimental and analytical observations, this method is found appropriate and recommended for use in calculating the capacity of joints that consist of a timber post bearing onto a beam flange. Blocking can be considered "100% effective" ($\gamma = 1.0$ in Equations 5 and 7b) with respect to increasing the flange bending capacity when a timber post is used. The effective bearing area method is recommended for calculating the flange-post joint capacity with a steel post and is derived based on assumptions similar to those used in the calculation of web yielding capacity. It is noted that timber blocking has a relatively low stiffness when used under a steel post. Therefore, a blocking effectiveness factor of 30% ($\gamma = 0.3$ in Equation 5) is recommended based on the experimental and analytical findings. Finally, design equations are presented in both LRFD and ASD format for calculating flange-post capacity with and without blocking.

ACKNOWLEDGMENTS

The authors would like to extend their gratitude to the California Department for Transportation for funding of this study under contract number 59A0445, with special thanks to John Lammers and Peter Lee for their assistance and direction.

REFERENCES

AFPA (1996), *Load and Resistance Factor Design – Manual for Engineered Wood Construction*, American Forest and Paper Association, Washington, DC.

AFPA (2001), *National Design Specification for Wood Construction*, American Forest and Paper Association, Washington, DC.

AISC (2005), *Specification for Structural Steel Buildings*, American Institute of Steel Construction, Inc., Chicago, IL.

Carden, L.P., Pekcan, G. and Itani, A.M. (2005), "Recommendations for the Design of Beams and Posts in Bridge Falsework," *Research Report CCEER 05-15,* Center for Civil and Earthquake Engineering Research, University of Nevada, Reno, NV.

Elgaaly, M. (1983), "Web Design Under Compressive Edge Loads," *Engineering Journal*, AISC, 4th quarter, pp. 153–171.

Graciano, C. and Edlund, B. (2003), "Failure Mechanism of Slender Girder Webs with a Longitudinal Stiffener under Patch Loading," *Journal of Constructional Steel Research*, Vol. 59, No. 1, pp. 27–45.

Graham, J.D., Sherbourne, A.N. and Khabbaz, R.N. (1959), *Welded Interior Beam-to-Column Connections,* American Iron and Steel Institute, Inc., Chicago, IL.

Hibbett, Karlson and Sorensen, Inc. (2003), "ABAQUS – Finite Element Program," Hibbett, Karlson & Sorensen, Inc., Fremont, CA.

Roberts, T.M. and Markovic, N. (1983), "Stocky Plate Girders Subjected to Edge Loading," *Proc. Instn. Civ. Engrs.,* Vol. 75, No. 2, pp. 539–550.

Roberts, T.M. and Newark, A.C.B. (1997), "Strength of Webs Subjected to Compressive Edge Loading," *Journal of Structural Engineering,* Vol. 123, No. 2, pp. 176–183.

Roberts, T.M. and Rockey, K.C. (1979), "A Mechanism Solution for Predicting the Collapse Loads for Slender Plate Girders when Subjected to In-Plane Patch Loading," *Proc. Instn. Civ. Engrs.,* Vol. 67, No. 2, pp. 155–175.

Shahabian, F. and Roberts, T.M. (1999), "Buckling of Slender Web Plates Subjected to Combinations of In-Plane Loading," *Journal of Constructional Steel Research,* Vol. 51, No. 2, pp. 99–121.

Capacity Design of Vertical Boundary Elements in Steel Plate Shear Walls

JEFFREY W. BERMAN and MICHEL BRUNEAU

Design requirements now appear in the 2005 AISC *Seismic Provisions for Structural Steel Buildings* (AISC, 2005b), referred to herein as *The Provisions*, for steel plate shear walls (SPSWs) that are designed such that their web plates buckle in shear and develop diagonal tension field action when resisting lateral loads. Energy dissipation and ductility during seismic events is principally achieved through yielding of the web plates along the diagonal tension field. Consistent with capacity design principles, *The Provisions* require that the vertical and horizontal boundary elements (VBEs and HBEs) of SPSWs, as shown in Figure 1, be designed to remain essentially elastic with the exception of plastic hinging at the ends of horizontal boundary elements. The commentary of *The Provisions* provides some guidance on how to achieve this requirement. However, the methods described in the commentary, as shown in this paper, do not necessarily lead to VBEs that meet the requirement of essentially elastic behavior under the forces generated by fully yielded web plates.

This paper reviews the current approaches provided in *The Provisions* commentary for determination of capacity design loads for the VBEs of SPSWs and also describes how the capacity design objective may be achieved using nonlinear static analysis. Then, a new procedure is proposed that uses a fundamental plastic collapse mechanism and linear beam analysis to approximate the design actions for VBEs of SPSWs for given web plates and horizontal boundary member sizes. The proposed procedure does not involve nonlinear analysis, making it practical for use in design. VBE design loads are estimated using both the current and proposed procedures for two example SPSW configurations. The resulting design loads are then compared with the VBE design loads as determined by nonlinear pushover analysis.

Jeffrey W. Berman is assistant professor, department of civil and environmental engineering, University of Washington, Seattle, WA.

Michel Bruneau is director, MCEER, professor, department of CSEE, University at Buffalo, Buffalo, NY.

CURRENT VBE DESIGN PROCEDURES

Three methods for ensuring capacity design of VBEs and HBEs for SPSWs are described in the commentary of *The Provisions*, two of the methods are linear and one is nonlinear. These are: the combined linear elastic computer programs and capacity design concept (LE+CD); the

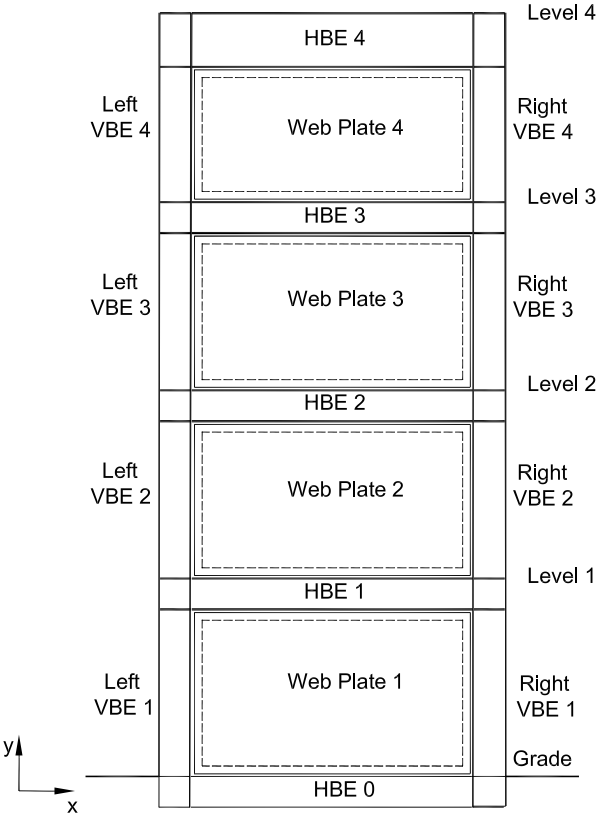

Fig. 1. General SPSW Configuration.

indirect capacity design approach (ICD); and nonlinear static analysis (pushover analysis). Each is reviewed briefly below and the steps in the two linear procedures that result in significant inaccuracies are identified. Note that nonlinear static analysis of SPSWs with web plates modeled as a series of strips oriented at α from the vertical, the angle of inclination of the tension field as calculated per *The Provisions*, has been shown to adequately represent the behavior of SPSW (Driver, Kulak, Kennedy and Elwi, 1998; Berman and Bruneau, 2004; and Berman and Bruneau, 2005; among others). That strip model is also used in elastic analyses of SPSW in the two linear procedures described below.

Combined Linear Elastic Computer Program and Capacity Design Concept (LE+CD)

The combined linear elastic computer program and capacity design concept as described in Commentary Section C17.4a of *The Provisions* consists of four steps (note that R_y is the ratio of mean to nominal yield stress of the web plate, A_s is the area of a strip in the strip model representation of a SPSW, and F_{yp} is the web plate yield stress):

1. Lateral forces: Use combined model, boundary elements and web elements, to come up with the demands in the web and boundary elements for the code required base shear. The web elements shall not be considered as vertical-load carrying elements.

2. Gravity load (dead load and live load): Apply gravity loads to a model with only gravity frames. The web elements shall not be considered as vertical-load carrying elements.

3. Without any overstrength factors, design the boundary elements using demands based on combination of the forces from the above steps 1 and 2.

4. Boundary element capacity design check: Check the boundary element for the maximum capacity of the web elements in combination with the maximum possible axial load due to overturning moment. Use the axial force obtained from step 1 above and multiply by the overstrength factor, Ω_o. Apply load from the web elements ($R_yF_{yp}A_s$) in the direction of α. For this capacity design check use a material strength reduction factor of 1.0. For the determination of the required strength of boundary elements and their connection to the web, neither the resistance factor (LRFD), nor the safety factor (ASD), are applied to the strength of the web.

While this procedure may, in some cases, result in proper capacity design of boundary elements, there is an inconsistency with respect to equilibrium. In step 4 the procedure requires that forces equal to the expected yield strength of the web panel be applied to the surrounding framing members in the direction of α. However, without simultaneous application of the lateral loads that caused the web plates to yield, the frame member moment diagrams resulting from the application of just the web plate forces will be incorrect because equilibrium with the applied loads is not satisfied and the deformed shape of the system is incorrect for those loads. To illustrate this, consider Figure 2, which shows a SPSW with the web plate represented by strip elements subjected to lateral loads (Figure 2a), and the model implied by step 4 of the LE+CD procedure where the strips have been replaced with plate yield forces, but no corresponding lateral loads have been applied. It is clear that the moment diagrams for the columns from these two cases will have different shapes regardless of the dimensions, geometry, or configuration of the SPSW. Unfortunately, calculation of those lateral loads and displacements is complex and since the procedure is meant to provide a simple linear method for capacity design of framing elements it is not useful to recommend the addition of such calculations. However, the concept that the forces from the yielding web plates may be applied to an otherwise elastic model in lieu of using full nonlinear analysis is promising and is the motivation for the proposed capacity design procedure below.

Indirect Capacity Design Approach (ICD)

The indirect capacity design approach presented in Commentary Section C17.4a of *The Provisions* is from the Canadian Standards Association steel design standard CAN/CSA-S16-01 (CSA, 2001) and proposes that the loads in the

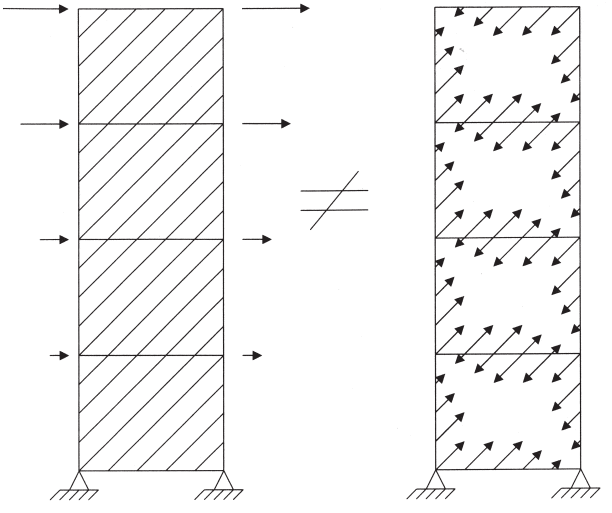

Fig. 2. Conceptual difference between: (a) SPSW subject to lateral load and (b) SPSW boundary frame subject to only infill plate yield forces.

VBEs of a SPSW may be found from gravity loads combined with seismic loads amplified by:

$$B = V_e / V_u \quad (1)$$

where

V_e = expected shear strength, at the base of the wall, determined for the web thickness supplied
= $0.5R_yF_{yp}t_wL\sin 2\alpha$, where L is the width of the wall

V_u = factored lateral seismic force at the base of the wall

In determining the loads in VBEs, the amplification factor, B, need not be taken larger than the seismic force reduction factor, R.

The VBE design axial forces shall be determined from overturning moments defined as follows:

1. The moment at the base of the wall is BM_u, where M_u is the factored seismic overturning moment at the base of the wall corresponding to the force V_u;

2. The moment, BM_u, extends for a height H but not less than two stories from the base, and;

3. The moment decreases linearly above a height H to B times the factored seismic overturning moment at one story below the top of the wall, but need not exceed R times the factored seismic overturning moment at any story under consideration corresponding to the force V_u.

The local bending moments in the VBE due to tension field action in the web shall be multiplied by the amplification factor, B.

This procedure relies on elastic analysis of a strip model (or equivalent) for the design seismic loads, followed by amplification of the resulting VBE moments by the factor B. Therefore, it produces moment diagrams and SPSW deformations that are similar in shape to what one would obtain from a pushover analysis. Similarly, the determination of VBE axial forces from overturning calculations based on the design lateral loads amplified by B results in axial force diagrams that are of the proper shape. However, the amplification factor used in both instances is found only for the first story and does not include the possibly significant strength of the surrounding frame. This leads to estimates of VBE demands that are less than those required to develop full web yielding on all stories prior to development of hinges in VBEs. For example, it is conceivable that the ratio of web thickness provided to web thickness needed for the design seismic loads is larger on the upper stories than on the lower stories. In these situations, the indirect capacity design approach would significantly underestimate the VBE design loads for the upper stories and capacity design would not be achieved. Additionally, frame members for SPSW may be large and the portion of the base shear carried by the surrounding moment frame could be substantial. For example, a recent SPSW implementation detailed in Monnier and Harasimowicz (2007) had VBEs at the bottom stories that were W14×730, the second largest W14 shape available. Neglecting the strength of the surrounding moment resisting frame in the ICD procedure when that frame has such substantial sections will certainly result in an underestimation of the expected SPSW shear strength, V_e, and VBE design loads that are underestimated for true capacity design.

Nonlinear Static (Push-Over) Analysis

Nonlinear static analysis of VBE strip models has been shown to give reasonable results for HBE and VBE moments and axial forces. Capacity design may be achieved by accounting for the actual thickness of the web plates and the ratio of mean to nominal web plate yield stress. However, as a design tool, nonlinear static analysis is time consuming as several iterations may be necessary to ensure capacity design of VBEs. Additional complexity results from having to properly account for possible formation of flexural-axial plastic hinges in the HBEs. Despite these issues, nonlinear static analysis of SPSW strip models generally gives accurate results for VBE demands and will be used to compare the adequacy of the proposed procedure below for two example SPSWs.

PROPOSED VBE DESIGN PROCEDURE

Objective

As discussed above there are two rather simple linear procedures for capacity design of SPSW VBEs given in the commentary of *The Provisions*. However, those methods, for different reasons, do not necessarily achieve the goal of VBE capacity design. Furthermore, the nonlinear static analysis procedure, which results in a more accurate estimation of the capacity design demands for VBEs, is tedious for broad use in design. Therefore, a need exists to develop a reasonably accurate and relatively efficient method for estimating the demands in VBEs when full yielding occurs in web plates for SPSW. This method should preferably involve only linear computer analyses without development of the complete strip model, and should account for the strength of surrounding framing (in other words, include the strength demands associated with hinging at the HBE ends).

The procedure proposed below to estimate VBE design loads to ensure capacity design of SPSWs combines a linear elastic beam model and plastic analysis. A model of the VBE on elastic supports is used to determine the axial forces in the HBEs and a plastic collapse mechanism is assumed to estimate the lateral seismic loads that cause full web plate yielding and plastic hinging of HBEs at their ends. A simple VBE free body diagram is then used to determine the design VBE axial forces

and moments. For use in design, iteration may be necessary as certain parameters are assumed at the beginning of the process that may need revision as the design progresses.

Plastic Collapse Mechanism

Plastic collapse mechanisms for SPSWs subject to lateral loads have been proposed by Berman and Bruneau (2003) and have been shown to agree well with experimental results for ultimate capacity of single and multistory SPSWs. They examined two types of plastic mechanisms for multistory SPSW, namely, a uniform collapse mechanism and a soft-story collapse mechanism which are shown schematically in Figures 3a and 3b respectively. For the purpose of capacity design of VBEs, it is conservative to use the uniform plastic collapse mechanism as it will result in larger base shear forces and larger VBE demands. Furthermore, if a soft-story mechanism is found to be likely, it is recommended that the SPSW be redesigned to develop more uniform yielding of the web plates over the height. This can be achieved, even for web plates of equal thickness over the height, by adjusting the sizes and moments of inertia of the surrounding HBEs and VBEs. Therefore, the uniform collapse mechanism shown in Figure 3a will be used in the proposed procedure for determination of capacity design loads for SPSW VBEs.

Proposed VBE Design Procedure

Free Body Diagrams of VBEs

Assuming that the web plates and HBEs of a SPSW have been designed according to *The Provisions* to resist the factored loads (or, for the case of HBE design the maximum of the factored loads or web plate yielding), the required capacity of VBEs may be found from VBE free body diagrams such as those shown in Figure 4 for a generic four-story SPSW. Those free body diagrams include distributed loads representing the web plate yielding at story i, ω_{xci} and ω_{yci}; moments from plastic hinging of HBEs, M_{prli} and M_{prri}; axial forces from HBEs, P_{bli} and P_{bri}; applied lateral seismic loads, found from consideration of the plastic collapse mechanism, F_i; and base reactions for those lateral seismic loads, R_{yL}, R_{xL}, R_{yR}, and R_{xR}. The following describes how the components of the VBE free body diagrams are determined. Note that for the purpose of this discussion lateral forces are assumed to be acting from left to right on the SPSW of Figure 4.

Forces from Plate Yielding

The distributed loads to be applied to the VBEs (ω_{yci} and ω_{xci}) and HBEs (ω_{ybi} and ω_{xbi}) from plate yielding on each story i may be determined as:

$$\omega_{yci} = \tfrac{1}{2} F_{yp} t_{wi} \sin 2\alpha \qquad \omega_{xci} = F_{yp} t_{wi} \left(\sin\alpha\right)^2 \qquad (2)$$

$$\omega_{ybi} = F_{yp} t_{wi} \left(\cos\alpha\right)^2 \qquad \omega_{xbi} = \tfrac{1}{2} F_{yp} t_{wi} \sin 2\alpha \qquad (3)$$

These are found from resolving the plate yielding force, occurring at an angle α from the vertical, into horizontal and vertical components acting along the VBEs and HBEs as demonstrated for a VBE in Figure 5. In that figure, *ds* is an incremental plate width perpendicular to the tension field,

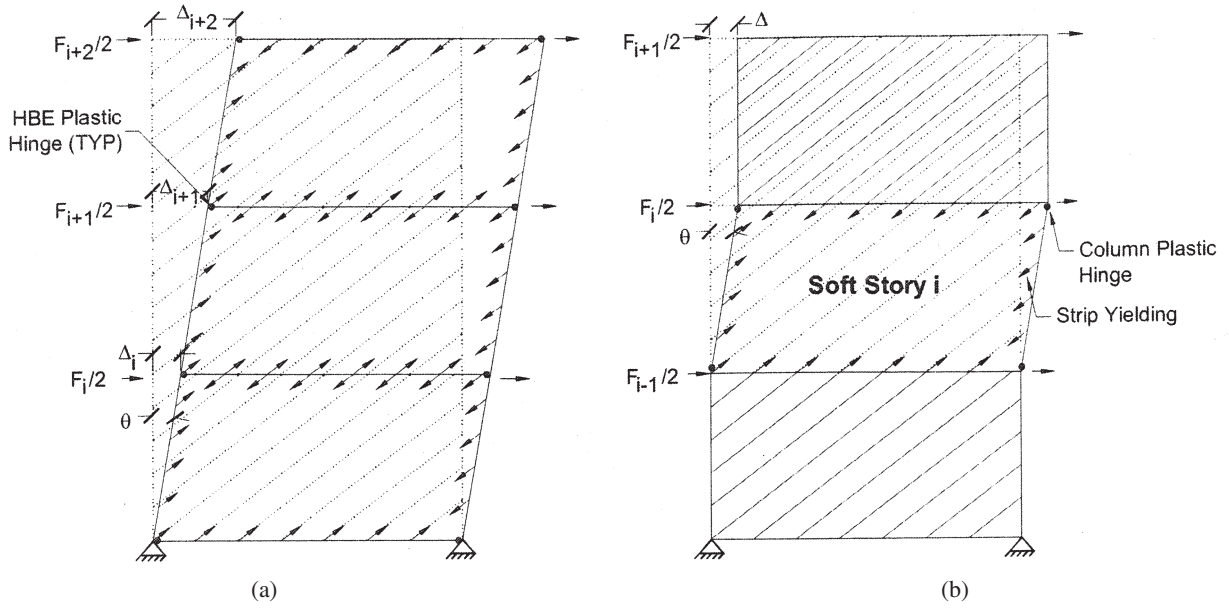

Fig. 3. SPSW Collapse Mechanisms: (a) Uniform Yielding Mechanism and (b) Soft-Story Mechanism.

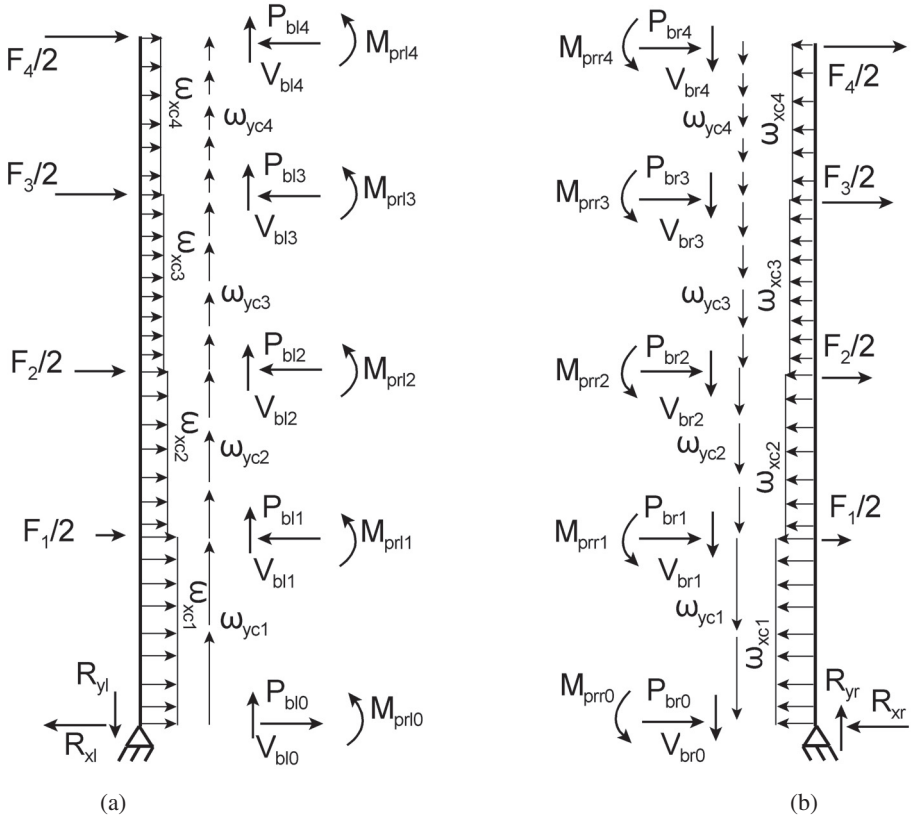

Fig. 4. VBE free body diagrams.

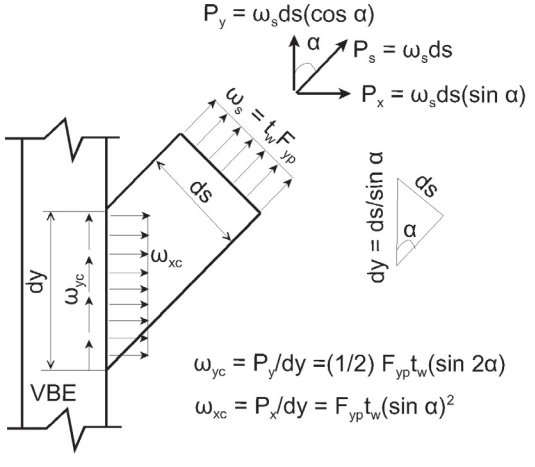

Fig. 5. Resolution of plate forces applied to a VBE.

dy is an incremental VBE height corresponding to *ds*, and P_s, P_x and P_y, are forces from plate yielding summed over *ds* in the tension field, horizontal and vertical directions, respectively. Note that the inclination angle, as determined per *The Provisions*, depends on the VBE cross-sectional area and moment of inertia and will have to be assumed at the beginning of a design procedure and then revised once VBEs have been selected. An initial assumption of 45° is suggested.

HBE Axial Forces

As part of estimating the axial load in the HBEs, an elastic model of the VBE is developed as shown in Figure 6. The model consists of a continuous beam element representing the VBE which is pin-supported at the base and supported by elastic springs at the intermediate and top HBE locations. HBE spring stiffnesses at each story *i*, k_{bi}, can be taken as the axial stiffness of the HBEs considering one-half the bay width (or HBE length for considerably deep VBEs), in other words:

$$k_{bi} = \frac{A_{bi}E}{L/2} \tag{4}$$

where

A_{bi} = HBE cross-sectional area
L = bay width
E = modulus of elasticity

This VBE model is then loaded with the horizontal component of the forces from the web plates yielding over each story, namely, ω_{xci}. An initial VBE size will have to be assumed for use in this model and some iteration may be required once that VBE size is revised. Additionally, it is reasonable to neglect the rotational restraint provided by the HBEs. This assumption has been observed to have a negligible impact on the resulting spring forces, P_{si}. Note that it is also reasonable, although less accurate, to estimate the HBE axial forces from the horizontal component of web plate yielding on the VBEs, P_{si}, considering VBE lengths tributary to each HBE, in other words:

$$P_{si} = \omega_{xci}\frac{h_i}{2} + \omega_{xci+1}\frac{h_{i+1}}{2} \tag{5}$$

Regardless of the method used, the spring forces are used below to determine the HBE axial forces. Note that these spring forces correspond to compression forces in the HBE, and can be of significant magnitude. Physically, one can envision the SPSW VBEs as being pulled toward each other by the uniformly distributed forces applied by the yielding webs, and the HBEs acting as regularly spaced "shoring" to keep the VBEs apart.

The axial force component in the intermediate and top HBEs resulting from the horizontal component of the plate yield forces on the HBEs, ω_{xbi}, is assumed to be distributed as shown in Figure 7. Note that for the bottom HBE, this distribution is the reverse of that in the top beam. These axial force components are then combined with the spring forces from the linear VBE model, resulting in the following equations for the axial force at the left and right sides of the intermediate and top HBEs (P_{bli} and P_{bri} respectively):

$$P_{bli} = -\left(\omega_{xbi} - \omega_{xbi+1}\right)\frac{L}{2} + P_{si} \tag{6}$$

$$P_{bri} = \left(\omega_{xbi} - \omega_{xbi+1}\right)\frac{L}{2} + P_{si} \tag{7}$$

where the spring forces should be negative indicating that they are adding to the compression in HBEs. As mentioned above, the axial forces from ω_{xbi} and ω_{xbi+1} in the bottom HBE may be taken as the mirror image of those shown in Figure 7, where ω_{xbi} is zero in that case as there is no web below the bottom HBE. Furthermore, there are no spring forces to consider at the bottom HBE location as the horizontal component

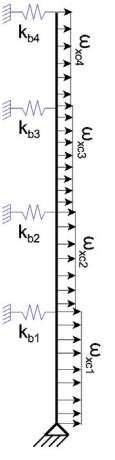

Fig. 6. Elastic VBE model with HBE springs.

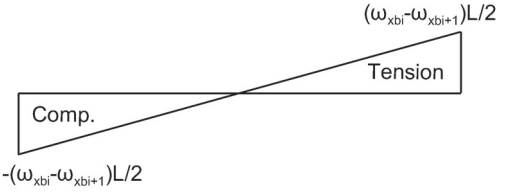

Fig. 7. Assumed HBE axial force distribution due to horizontal component of plate yield forces on the HBE.

of force from web plate yielding on the lower portion of the bottom VBE is added to the base reaction determined as part of the plastic collapse mechanism analysis, as described below. Therefore, the bottom HBE axial forces on the right and left hand sides, P_{br0} and P_{bl0} are:

$$P_{br0} = -\omega_{xb1}\frac{L}{2} \quad \text{and} \quad P_{bl0} = \omega_{xb1}\frac{L}{2} \tag{8}$$

HBE Reduced Plastic Moments and Corresponding Shear Forces

Once the HBE axial forces have been estimated it is possible to determine the plastic moment that will develop at the HBE ends for the assumed collapse mechanism, reduced for the presence of axial load. Note that it is conservative to assume that this reduction is negligible; however, since substantial axial loads may develop in the HBEs, resulting in significantly reduced plastic moment capacities, it can be advantageous to account for the reduced plastic moments at the left and right HBE ends, M_{prl} and M_{prr}, respectively.

The intermediate and top HBEs will have free body diagrams similar to that shown in Figure 8, except that there will be no plate forces acting above the top HBE. For the bottom HBE, the axial forces at the HBE ends will be in the opposite direction to those shown in Figure 8 and there will be no plate forces acting below the HBE. The reduced plastic moment capacity at the HBE ends, given here for the left end, can be approximated by (Bruneau, Whittaker and Uang, 1998):

$$1.18\left(1-\frac{|P_{bli}|}{F_{yb}A_{bi}}\right)Z_{xbi}F_{yb} \quad \text{if} \quad 1.18\left(1-\frac{|P_{bli}|}{F_{yb}A_{bi}}\right)\le 1.0$$
$$Z_{xbi}F_{yb} \quad \text{if} \quad 1.18\left(1-\frac{|P_{bli}|}{F_{yb}A_{bi}}\right) > 1.0 \tag{9}$$

where

F_{yb} = HBE yield strength
A_{bi} = HBE cross-sectional area for story i
Z_{xbi} = HBE plastic modulus for story i.

Using the reduced plastic moment capacities and the HBE free body diagram shown in Figure 8, the shear forces at the left and right ends of all HBEs, V_{bl} and V_{br} can be found from:

$$V_{bri} = \frac{M_{prri} + M_{prli}}{L} + \left(\omega_{ybi} - \omega_{ybi+1}\right)\frac{L}{2} \tag{10}$$

$$V_{bli} = V_{bri} - \left(\omega_{ybi} - \omega_{ybi+1}\right)L \tag{11}$$

Applied Lateral Loads

The final forces necessary to complete the free body diagram of the VBE are the applied lateral loads corresponding to the assumed collapse mechanism for the SPSW (Figure 3a). Following the derivation in Berman and Bruneau (2003) the governing equation for that collapse mechanism is:

$$\sum_{i=1}^{n_s} F_i H_i = \sum_{i=0}^{n_s} M_{prli} + \sum_{i=0}^{n_s} M_{prri} + \sum_{i=1}^{n_s} \frac{1}{2}\left(t_{wi} - t_{wi+1}\right)F_{yp}LH_i \sin\left(2\alpha_i\right) \tag{12}$$

where

F_i = applied lateral load at each story to cause the mechanism
H_i = height from the base to each story

and other terms are as previously defined. Note that the indices for the HBE plastic moment summations begin at zero so that the bottom HBE (denoted HBE_0) is included.

To employ Equation 12 in calculating the applied lateral loads that cause this mechanism to form, it is necessary to assume some distribution of those loads over the height of the structure; in other words, a relationship between F_1, F_2, etc. For this purpose, a pattern equal to that of the design lateral seismic loads from the appropriate building code may be used. This is an approximation that is simple and that has been observed to provide reasonable results for SPSW. It would also be appropriate to use the deformation pattern of the first mode of vibration of the structure for this purpose (obtained from a modal analysis), but this more sophisticated approach is unnecessary given that the code specified distribution of lateral seismic forces vertically on a lateral force resisting system is meant to simulate first mode characteristics. Once a load pattern is assumed and a relationship between the applied collapse loads at each story is determined, Equation 12 may be used to solve for those collapse loads.

The base shear force, V, for the collapse loading is found by summing the applied lateral loads. Horizontal reactions at the column bases, R_{xL} and R_{xR}, are then determined by dividing the collapse base shear by 2 and adding the pin-support reaction from the VBE model, R_{bs}, to the reaction under the left VBE and subtracting it off the reaction under the right

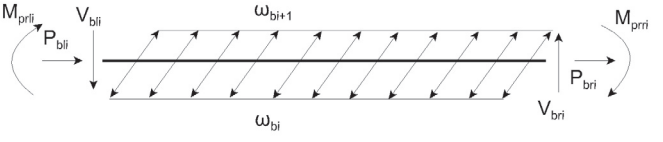

Fig. 8. HBE free body diagram.

VBE. Vertical base reactions can be estimated from overturning calculations using the collapse loads as:

$$R_{yl} = \frac{\sum_{i=1}^{n_s} F_i H_i}{L} \qquad \text{and} \qquad R_{yr} = -R_{yl} \qquad (13)$$

Determination of VBE Design Loads

The moment, axial, and shear force diagrams for the VBEs are established once all the components of the VBE free body diagrams are estimated. The diagrams give minimum design actions for those VBEs such that they can resist full web plate yielding and HBE hinging.

Additional Considerations

Though not explicitly considered in the above formulations, use of the ratio of the expected yield stress to the specified minimum yield stress, R_y, may be incorporated into the procedure when determining the distributed loads from plate yielding and when determining HBE plastic moment capacity. Additionally, when deep VBEs are used, the length between VBE flanges, L_{cf}, may be substituted for the column centerline bay width, L, when applying the plate yielding loads to the HBEs. Furthermore, using the schematic structure shown in Figure 3 for which structural members have no width, the HBE plastic hinges are assumed to form at the VBE centerlines, which is not the actual case. HBE hinges will typically form $d_b/2$ from the column face, where d_b is the HBE depth. This can be accounted for by either including in the VBE free body diagrams the distance from the column centerlines to the HBE hinge locations or by calculating the projected column centerline moment as is done for moment frames. This calculation is not included here for simplicity and because the increase in moment applied to the VBE is generally small relative to the magnitude of the moments generated by web plate yielding and HBE hinging. Gravity loads are another consideration that has not been included; however, they can easily be added to the vertical components of the web plate yield forces that are applied to the HBEs in Figure 8. They will then be accounted for in the resulting HBE shear forces and VBE axial forces. Finally, this procedure will provide reasonable VBE design forces for SPSWs that can be expected to yield over their entire height—typically shorter SPSWs. This procedure will likely be overly conservative for tall SPSWs where nonlinear time history analysis indicates that simultaneous yielding of the web plates over the entire SPSW height is unlikely. In those situations it may be acceptable to reduce the VBE axial forces obtained from this proposed procedure (following a procedure similar to that proposed by Redwood and Channagiri, 1991) to account for some web plates remaining partially elastic while others yield. However, at each story the VBEs should be designed to resist the moments generated by yielding of the web plates at that level and the corresponding frame moments.

EXAMPLE ESTIMATION OF VBE DESIGN LOADS

Two examples of the proposed procedure for estimating VBE design loads for their capacity design are described below. Since the primary inelastic elements in SPSWs are the web plates and the web plate strength is a function of thickness, the two examples explore the cases of variable and constant web plate thickness over the height of a four-story SPSW. In the SPSW with variable web plate thickness, a different thickness is used at each story and not limited to those available for common plate stock. For the case of constant web plate thickness over the height of the SPSW, the web plates were designed for the required story shear at the first story and that thickness is used over all four stories. Furthermore, that thickness was constrained to be available from common plate stock.

Structure Description and SPSW Design

The MCEER (Multidisciplinary Center for Earthquake Engineering Research) demonstration hospital was used as the prototype structure (Yang and Whittaker, 2002) for which the SPSWs were designed. For simplicity, four SPSWs were assumed to carry equal portions of the seismic load resulting from the active seismic weight of the structure of 9,800 kips (2,613 kips, 2,542 kips, 2,542 kips, and 2,103 kips at the 1st story, 2nd story, 3rd story and roof HBEs, respectively). The geometries of the two SPSWs are shown in Figure 9 and the structure is assumed to be located on Class D soil. Design seismic loads were calculated using FEMA 450 (FEMA, 2003) and the associated spectral acceleration maps. Design short and 1-second spectral ordinates, S_{DS} and S_{D1}, were calculated to be 1.17g and 0.44g respectively. The period of the structure was estimated using the FEMA procedures as 0.38 sec and using a response modification coefficient, R, of 7 and importance factor, I, of 1.5, the base shear for the structure was found to be 2,450 kips, or 612.5 kips for each SPSW. Distribution of the base shear up the height of the structure resulted in lateral loads of 215 kips, 195 kips, 132 kips and 71 kips, at each story from the roof down to the level of HBE_1 for each SPSW.

Figure 9 shows the web plate thicknesses selected for the two SPSWs designed for the above loading in accordance with *The Provisions*, and it also shows the selected HBE and VBE sizes. As mentioned above, cases of variable and constant web plate thickness, denoted SPSW-V and SPSW-C, respectively, have been considered. SPSW-V uses plate thicknesses that may not be available but correspond to the minimum required for the design story shear forces and SPSW-C uses the assumed minimum available plate thickness

of 0.1875 in. Note that ASTM A36 steel has been assumed for the web plates and ASTM A992 for the HBEs and VBEs. VBE selection was done after a first iteration of the proposed procedure for evaluation of design loads with an assumed tension field inclination angle of 45°. Described below are the calculations for a second iteration of the proposed procedure. Additionally, for simplicity and to provide a direct comparison between design loads resulting from the current and proposed procedures, the effects of gravity loads and vertical ground motion were neglected (in other words, only VBE design loads resulting from the horizontal seismic loading will be calculated).

Calculation of VBE Design Loads

The proposed procedure for evaluating VBE design loads was employed for the SPSWs shown in Figure 9. Calculation results for the tension field inclination angle and distributed loads from web plate yielding given by Equations 2 and 3, are shown for both SPSW-C and SPSW-V in Table 1. Note that the inclination angle, as given by *The Provisions*, depends mostly on the aspect ratio, h/L, of the bays and therefore, does not show substantial difference between SPSW-C and SPSW-V.

Table 2 shows the HBE spring stiffnesses, k_b, used in the linear VBE models for each wall and the resulting spring loads, P_s, where the entry for the bottom HBE is the horizontal reaction at the pin base of the VBE. The HBE axial forces, P_{bl} and P_{br}, reduced plastic moments, M_{prl} and M_{prr}, and shear forces, V_{bl} and V_{br}, at each HBE end are then calculated per Equations 6 through 11. Results for all HBEs in both example walls are given in Table 2. For comparison purposes, the HBE spring forces were also estimated by considering the horizontal component of web plate yielding forces applied to the VBE tributary to each HBE, as given by Equation 5. The results given in Table 2 show some deviation relative to the spring forces from the VBE model, although for preliminary design of VBEs the difference may be insignificant.

Next, the applied seismic lateral loads at each story were found for the assumed collapse mechanism, similar to that shown in Figure 3a, using Equation 12. Note that it was assumed that those applied loads to cause collapse were in the

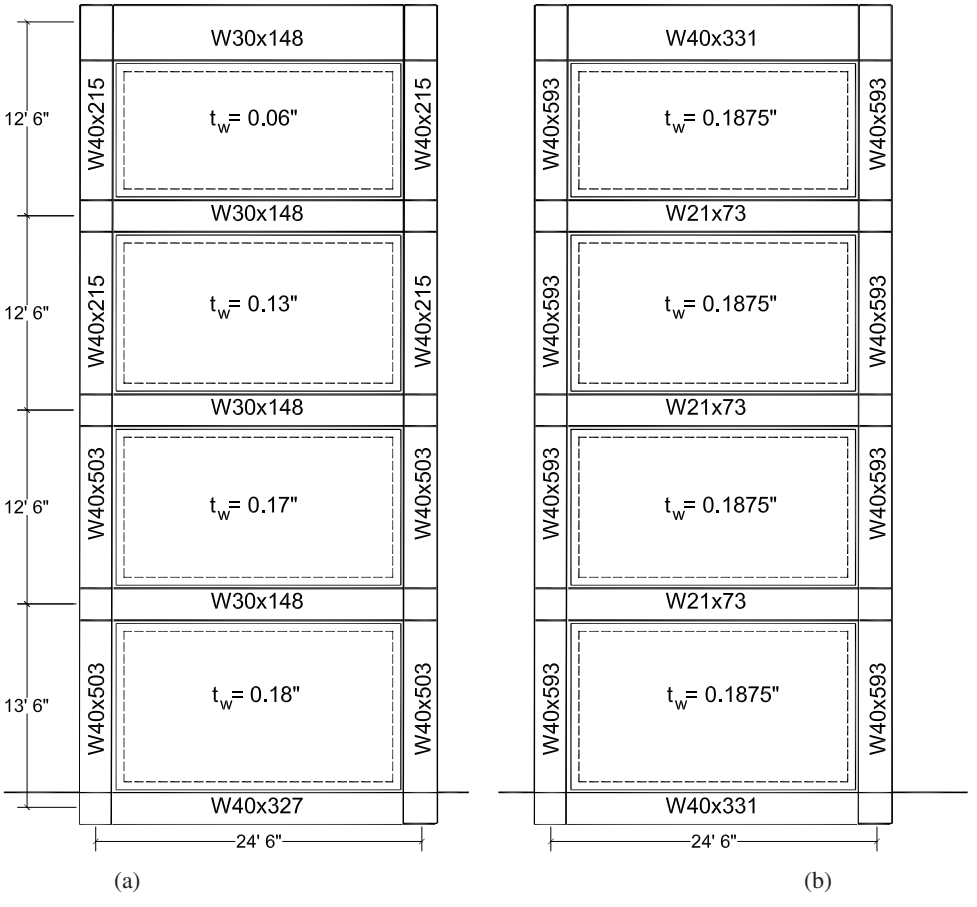

Fig. 9. Example SPSWs: (a) SPSW-V and (b) SPSW-C.

Table 1. Distributed Loads from Yielding Web Plates						
Wall	Story	α (deg)	ω_{yc} (kip/in.)	ω_{xc} (kip/in.)	ω_{yb} (kip/in.)	ω_{xb} (kip/in.)
SPSW-C	1	46	3.37	3.49	3.26	3.37
	2	48	3.35	3.75	3.00	3.35
	3	48	3.35	3.75	3.00	3.35
	4	48	3.35	3.75	3.00	3.35
SPSW-V	1	46	3.24	3.36	3.13	3.24
	2	48	3.06	3.42	2.74	3.06
	3	48	2.23	2.49	1.99	2.23
	4	48	1.13	1.26	1.01	1.13

Table 2. Linear VBE Model Parameters, Results and Corresponding HBE End Actions										
Wall	HBE	k_b (kip/in.)	P_s [b] (kips)	P_s [c] (kips)	P_{bl} (kips)	P_{br} (kips)	M_{prl} (kip-in.)	M_{prr} (kip-in.)	V_{bl} (kips)	V_{br} (kips)
SPSW-C	0	(a)	-277	-283	496	-496	71500	71500	965	8
	1	4242	-540	-564	-543	-537	4811	4862	-5	71
	2	4242	-622	-563	-622	-622	4095	4095	28	28
	3	4242	-537	-563	-537	-537	4864	4864	33	33
	4	19235	-277	-281	-770	216	68030	71500	915	34
SPSW-V	0	(a)	-250	-272	477	-477	70500	70500	940	19
	1	8582	-542	-529	-569	-515	20860	21560	86	202
	2	8582	-463	-443	-585	-341	20650	23820	42	261
	3	8582	-295	-281	-456	-134	22320	25000	17	305
	4	8582	-71	-95	-237	95	25000	25000	22	319

[a] Not applicable, in the linear VBE models there are pin supports at the bottom HBE locations.
[b] Values at the bottom HBE locations are the horizontal reactions at the pin supports.
[c] Spring forces approximated by Equation 5.

same pattern of distribution as the design lateral loads given above. Resulting lateral loads, F, are given in Table 3 and Table 4 gives the corresponding base shear, V, and base reactions, R_{xl}, R_{yl}, R_{xr}, and R_{yr}, for each of the example walls.

Axial, moment and shear force diagrams for the VBEs of the two SPSWs are shown for the left VBE of SPSW-C in Figures 10a, 10b and 10c, respectively. The resulting forces at the bases of the columns, where they are a maximum, are given in Table 5 for both SPSWs. Assuming lateral bracing of the columns at each story, the moment-axial capacity interaction equation values, given by Equation H1-1 of the AISC *Specification for Structural Steel Buildings* (AISC, 2005a), were 0.96 and 1.0 for the VBE sizes for SPSW-C and SPSW-V respectively, considering the VBE sections shown in Figure 9. Note that SPSW strength and VBE demand are proportional to the bay width, L, and in the case considered here the bay width is large. Lower SPSW overstrength and VBE demands may be achieved by reducing the bay width, however, the aspect ratio of the bay, L/h, must be greater than 0.8 and less than or equal to 2.5, as specified in *The Provisions* Section 17.2b.

Comparison with Current Procedures

To judge the adequacy of both the current and proposed approximate procedures for determining VBE design loads, nonlinear static analysis of strip models of SPSW-C and SPSW-V are used. The strip models had tension only strip

Table 3. Seismic Loading for Assumed Collapse Mechanism		
Wall	**Story**	***F*** **(kips)**
SPSW-C	1	236
	2	440
	3	649
	4	716
SPSW-V	1	197
	2	367
	3	541
	4	597

Table 4. Base Shear and Reactions for Assumed Collapse Mechanism					
Wall	***V*** **(kips)**	R_{xl} [(a)] **(kips)**	R_{yl} [(a)] **(kips)**	R_{xr} [(a)] **(kips)**	R_{yr} [(a)] **(kips)**
SPSW-C	2041	-1298	-3107	-744	3100
SPSW-V	1702	-1101	-2591	-601	2600
[(a)] Positive *x* and *y* directions are right and up, respectively.					

Table 5. Actions at Column Bases from Proposed Procedure				
Wall	**Column Side**	**Axial (kips)**	**Moment (kip-in.)**	**Shear (kips)**
SPSW-C	Left	2142	71500	802
	Right	-3115	71500	248
SPSW-V	Left	1651	70500	624
	Right	-2610	70500	164
[(a)] Positive *x* and *y* directions are right and up, respectively.				

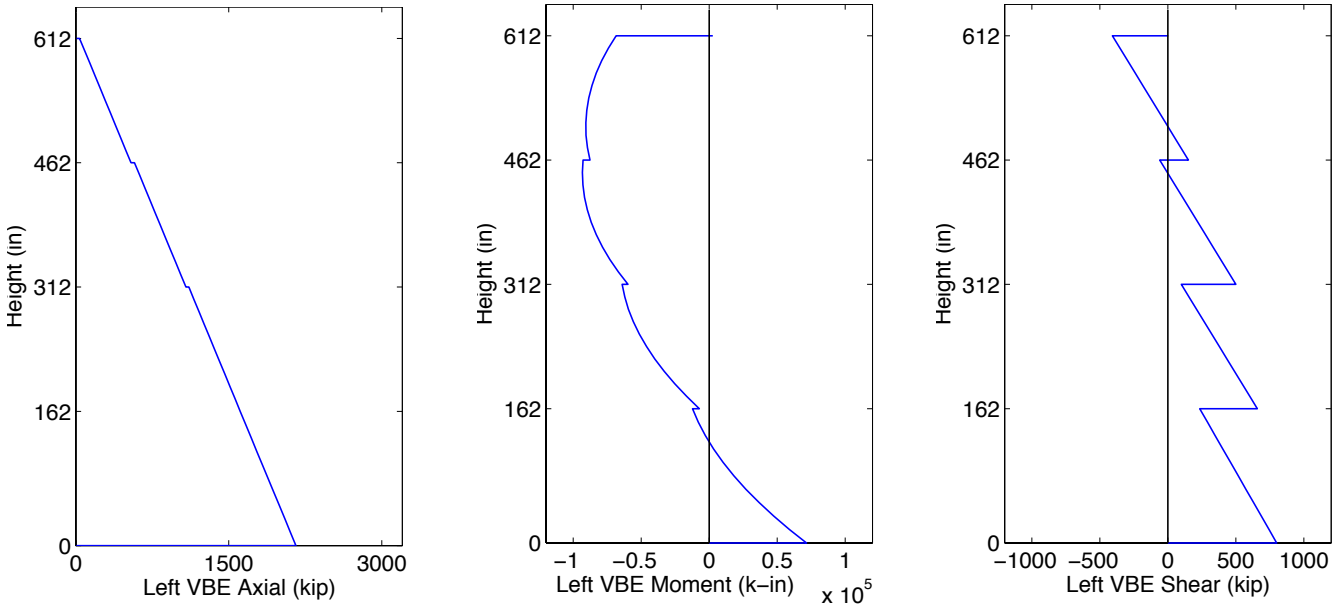

Fig. 10. Force diagrams for the VBE of SPSW-C: (a) axial, (b) moment, and (c) shear.

elements with elastic-perfectly-plastic behavior. Flexural-axial hinges were also added at all possible HBE and VBE locations. The HBE and VBE hinges were defined to have moment-axial interaction per FEMA 356 (FEMA, 2000) and a low strain hardening level (in other words, 0.5%) introduced to ensure numerical stability but close to zero because none of the design procedures that will be compared consider strain hardening. Resulting pushover curves for the two SPSWs are shown in Figure 11. The analyses showed that all web elements yielded and many HBEs formed hinges prior to yielding of any VBEs. Note that linear analyses of the strip models for the design seismic loads were also performed for use in the LE+CD and ICD approaches as described below.

VBE design loads were calculated again using the LE+CD procedure as per the commentary of *The Provisions*. The distributed loads from web plate yielding given in Table 1 were applied to linear models of the surrounding moment resisting frames for each SPSW and resulting VBE moments were recorded. VBE axial loads were then found by multiplying the axial loads from the linear strip model analysis factored by the 2.5 overstrength factor.

The indirect capacity design approach (ICD) was also used to estimate the VBE design loads for each SPSW. Moments from the linear strip models were factored by B, which was 2.10 and 2.03 for SPSW-C and SPSW-V, respectively. Axial loads were found from B times the overturning moment as described in the commentary of *The Provisions*.

Figures 12 through 15 compare axial loads and moments from the three procedures for approximating VBE design loads (in other words, LE+CD, ICD, and the proposed procedure) with those from pushover analysis for both SPSW-C and SPSW-V. As shown, the proposed procedure agrees well with pushover results in terms of both VBE axial force and moment. Furthermore, the proposed procedure is able to capture the important aspects of SPSW behavior that effect the VBE force diagrams, such as moment-axial interaction in HBEs, and proper distribution of HBE axial load to the right and left VBEs.

The LE+CD procedure agrees well with pushover analysis for VBE axial force as shown in Figures 12 and 14. However, because the procedure neglects the application of the lateral loads to cause web plate yielding when evaluating the VBE moments, the moment diagrams in Figures 13 and 15 are not in agreement. Neglecting the applied loads to cause infill yielding (recall Figure 2), results in moment diagrams that do not include the significant contributions of frame action under those loads, which in these cases are actually large enough to not only change the magnitude but also the sign of the VBE moments. Although it appears the VBE moment diagrams from the LE+CD for the VBEs from SPSW-V may simply be reversed, that is not the case, and those for SPSW-C would not agree even if they were converted into their mirror image.

Finally, the ICD approach reasonably estimates the VBE axial forces; however, because the overstrength is very large for these SPSWs, it is not able to adequately estimate the VBE moments. As shown in Figure 13 and 15, the ICD results in VBE moment diagrams that have similar shape to those from pushover analyses but significantly underestimates the values. Therefore, the proposed procedure is the only one of the three methods available for estimating design loads for VBEs that ensures web plate yielding is able to fully develop prior to hinging in VBEs.

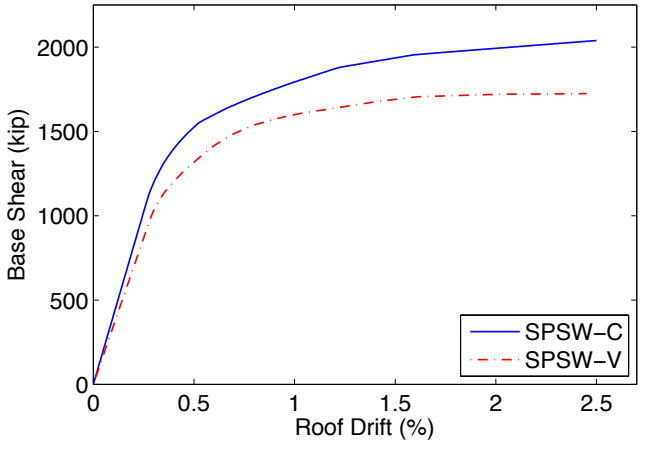

Fig. 11. Pushover Curves for Example SPSW.

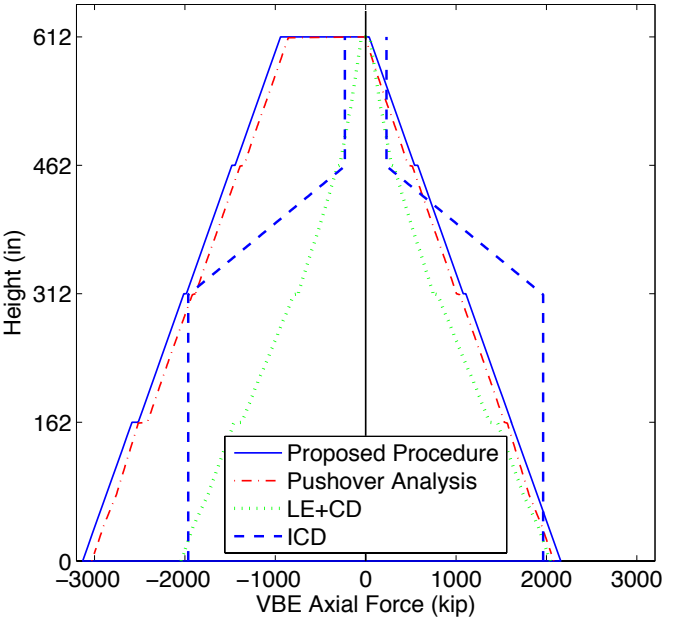

Fig. 12. Comparison of VBE Axial Forces from Various Methods for SPSW-C.

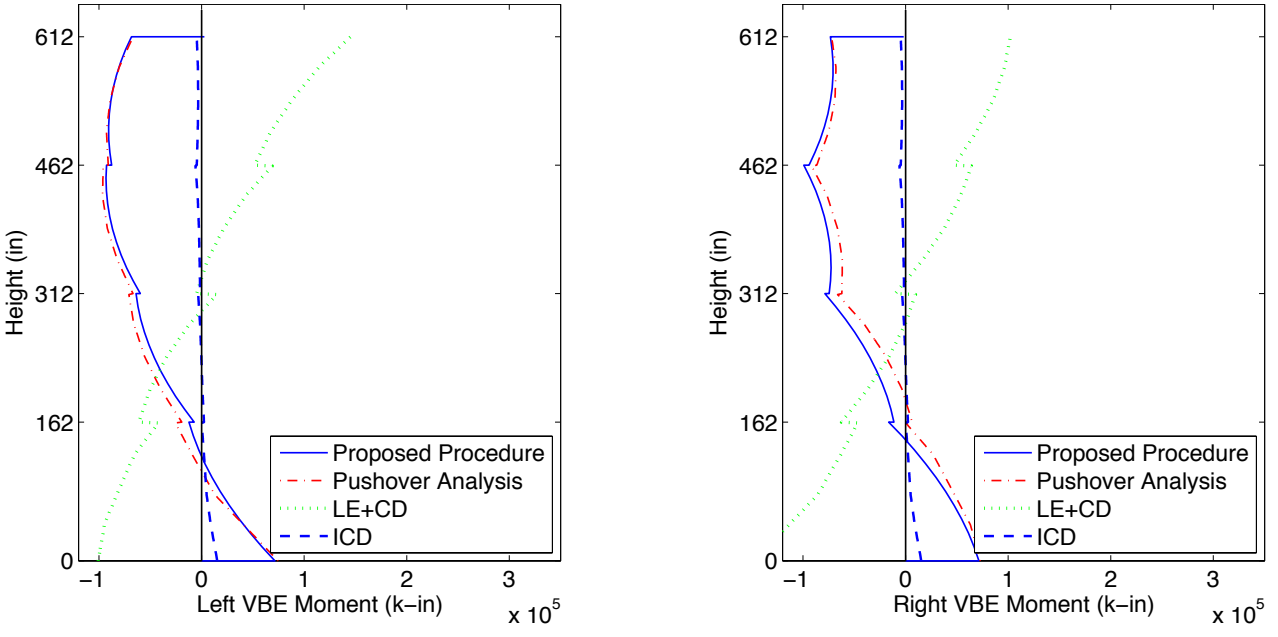

(a) (b)

Fig. 13. Comparison of VBE moments from various methods for SPSW-C.

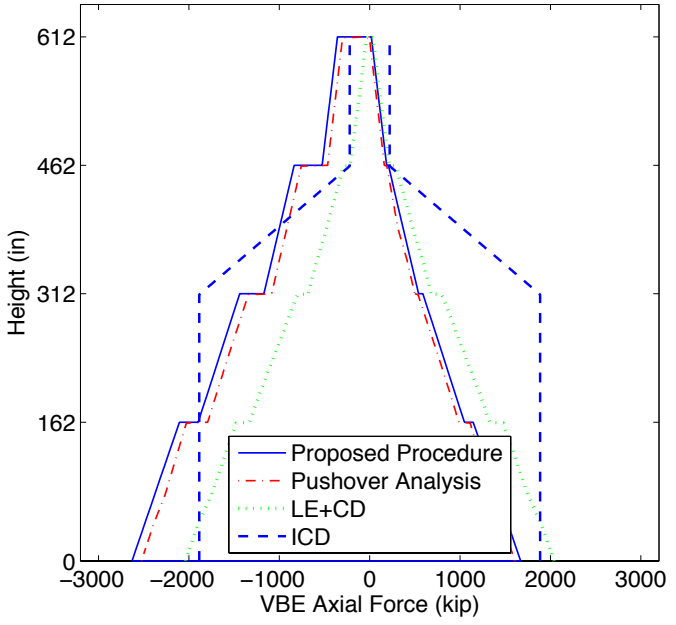

Fig. 14. Comparison of VBE axial forces from various methods for SPSW-V.

CONCLUSIONS

A procedure for estimating the design loads for VBEs of SPSWs has been proposed. The procedure does not involve nonlinear analysis and is based on an assumed plastic collapse mechanism and linear model of one of the vertical boundary elements. Moment and axial force diagrams from the proposed procedure were shown to agree well with results from pushover analyses of two example steel plate shear walls. Furthermore, deficiencies in the two approximate methods for capacity design of VBEs in the commentary of the *The Provisions* were identified and they were found to result in moment diagrams that differed significantly from those observed in pushover analyses.

ACKNOWLEDGMENTS

This work was supported in part by the Earthquake Engineering Research Centers Program of the National Science Foundation under Award Number ECC-9701471 to the Multidisciplinary Center for Earthquake Engineering Research. However, any opinions, findings, conclusions and recommendations presented in this paper are those of the authors and do not necessarily reflect the views of the sponsors.

REFERENCES

AISC (2005a), *Specification for Structural Steel Buildings*, ANSI/AISC 360-05, American Institute of Steel Construction, Chicago, IL.

AISC (2005b), *Seismic Provisions for Structural Steel Buildings*, ANSI/AISC 341-05, American Institute of Steel Construction, Chicago, IL.

Berman, J.W. and Bruneau, M. (2003), "Plastic Analysis and Design of Steel Plate Shear Walls," *Journal of Structural Engineering*, ASCE, Vol. 129, No. 11, pp. 1448–1456.

Berman, J.W. and Bruneau, M. (2004), "Steel Plate Shear Walls Are Not Plate Girders," *Engineering Journal*, AISC, Vol. 41, No.3, 3rd Quarter, pp. 95–106.

Berman, J.W. and Bruneau, M. (2005), "Experimental Investigation of Light-Gauge Steel Plate Shear Walls," *Journal of Structural Engineering*, ASCE, Vol. 131, No. 2, pp. 259–267.

Bruneau, M., Whittaker, A.S. and Uang, C.M. (1998), *Ductile Design of Steel Structures*, McGraw-Hill, New York, NY.

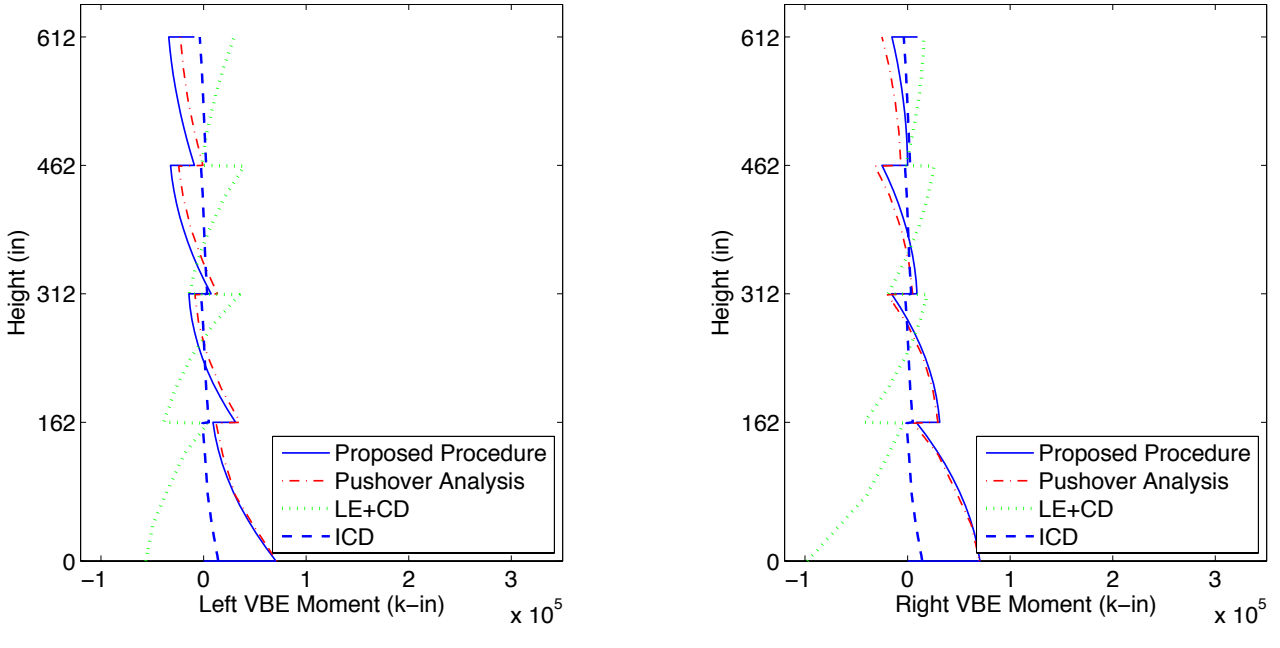

(a) (b)

Fig. 15. Comparison of VBE Moments from Various Methods for SPSW-V.

CSA (2001), *Limit States Design of Steel Structures*, CAN/CSA-S16-01, Canadian Standards Association, Willowdale, Ontario, Canada.

Driver, R.G., Kulak, G.L., Kennedy, D.J.L. and Elwi, A.E. (1998), "Cyclic Test of Four-Story Steel Plate Shear Wall," *Journal of Structural Engineering*, ASCE, Vol. 124, No. 2, Feb., pp. 112–130.

Federal Emergency Management Agency (2000), "Prestandard and Commentary for the Seismic Rehabilitation of Buildings," FEMA 356, Washington, DC.

Federal Emergency Management Agency (2003), "NEHRP Recommended Provisions for Seismic Regulations for New Buildings and Other Structures: Part 1-Provisions," FEMA 450, Washington, DC.

Monnier, A.B. and Harasimowicz, A.P. (2007), "Shear Strength," *Modern Steel Construction*, AISC, January, pp. 22–25.

Redwood, R.G. and Channagiri, V.S. (1991), "Earthquake-Resistant Design of Concentrically Braced Steel Frames," *Canadian Journal of Civil Engineering*, Vol.18, No. 5, pp. 839–850.

Yang, Y.T. and Whittaker, A.S. (2002), "MCEER Demonstration Hospitals, Mathematical Models and Preliminary Analysis Results," *Technical Report*, Multidisciplinary Center for Earthquake Engineering Research, Buffalo, NY.

Effects of Nonverticality on Steel Framing Systems—Implications for Design

ANDREA E. SUROVEK and JUSTIN JOHNSON

The *Specification for Structural Steel Buildings* (AISC, 2005a), hereafter referred to as the *Specification*, allows the engineer a great deal of freedom in selecting the type of analysis to be used when assessing the strength and stability of a structure or framing system. Chapter C states:

> "Any method that considers the influence of second order effects (including *P*-Δ and *P*-δ effects), flexural, shear and axial deformations, geometric imperfections, and member stiffness reduction due to residual stress on the stability of the structure and its elements is permitted."

By individually identifying each of the phenomena that affect member and system strength in a framing system, the *Specification* is highlighting for the engineer the importance of each of these phenomena. Consequently, an understanding of each of these effects is beneficial in applying the new stability provisions of the *Specification*. This paper focuses on the effects of geometric imperfections, with an emphasis on frame nonverticality, or out-of-plumbness. The objectives of this paper are to:

- Illustrate how initial imperfections affect the strength of members and framing systems.
- Discuss how imperfections affect the magnitude and distribution of internal member forces and moments.
- Demonstrate the sensitivity of different types of unbraced frames to imperfections.
- Outline how imperfections are included in the AISC Specification approaches for assessment of frame stability.
- Discuss implications of the current limits on when imperfection effects may be neglected in the presence of lateral loads in the direct analysis approach of Appendix 7.

Andrea E. Surovek is assistant professor, civil and environmental engineering, South Dakota School of Mines and Technology, Rapid City, SD.

Justin Johnson is project engineer, Phelps Dodge Corporation, Tempe, AZ.

The first section of the paper describes the types of initial imperfections typically considered in planar frame analysis and their effect on members and framing systems. This is followed by a discussion of how the effects of imperfections are treated in the AISC *Specification* (AISC, 2005a).

A parametric study is presented in which the sensitivity of framing systems to imperfection effects is investigated with respect to a number of parameters, including slenderness ratios, leaning load levels, gravity-to-lateral load ratios, and lateral frame stiffness, as measured by a second-order to first-order drift ratio. Understanding the types of frames that show sensitivity to imperfections provides a basis for determining when imperfections can have an influence on their inclusion in a design approach and decisions on when they might be neglected in the analysis.

In addition to the sensitivity study, a number of columns and simple frames are analyzed with and without imperfections using the direct analysis approach for assessing frame stability outlined in Appendix 7 of the AISC *Specification* (AISC, 2005a). The differences in the interaction checks for simple columns and frames are used to discuss the current limits on when imperfection effects may be neglected in the *Specification* in the presence of a higher lateral load.

INITIAL IMPERFECTIONS

In planar frame analysis, two types of imperfections affect strength and stability due to the amplification of the in-plane moments:

- Frame out-of-plumbness (or nonverticality) that may occur during erection, designated by Δ_0 in Figure 1.
- Member out-of-straightness which is a sweep of the member between the member ends that occurs during fabrication (one possible pattern is shown by δ_0 in Figure 1). It is typically considered as a single curvature sweep with the maximum imperfection at the midpoint of the member.

The AISC *Code of Standard Practice for Steel Buildings and Bridges* (AISC, 2005b) specifies the following tolerances for these two imperfections:

- Maximum member out of straightness, δ_0, of $L/1000$.
- For buildings less than 20 stories, out-of-plumbness, Δ_0, of $H/500$ in any shipping piece with a maximum lean of 1 in. towards the exterior or 2 in. towards the interior over the building height. Additional restrictions based on building height are imposed as shown in Figure 2.

Imperfections are considered in design because they amplify the moments in members when second-order effects are considered. The principal effect of an initial out-of-straightness on an individual member is the additional of an internal moment when the axial load, P, acts through the initial out-of-straightness, δ_0, as shown in Figure 1. This moment reduces the maximum axial capacity of a column. P-δ_0 moments can also impact adjoining members if their effect is to amplify the end moments. In many practical cases, this effect on end moments (when present) is minimal.

The initial out-of-plumbness (or nonverticality) also affects member strength, with the additional moment caused by the axial load, P, acting through the nonverticality, Δ_0. The P-Δ_0 moment also impacts the forces and moments in connecting elements, including connections, beams, base plates, slabs, etc. Figure 3 shows a column in which P-Δ_0 moments are transferred from the column to the adjoining beam (and, of course, the connection between them.)

INCLUSION OF INITIAL IMPERFECTIONS IN AISC SPECIFICATION BASED DESIGN APPROACHES

In the most recent version of the AISC *Specification* (2005a), significant changes were made to the way in which stability may be assessed in steel framing systems. In Chapter C, the *Specification* states that the required strengths for member design may be checked with member forces and moments obtained from one of the following analysis methods:

- Second-order analysis using nominal frame stiffness and a minimum lateral load of $0.002Y_i$, where Y_i is the gravity load applied at level i.
- Direct analysis, as outlined in Appendix 7 of the AISC *Specification*.
- First-order analysis, provided limitations on axial load levels are met, with an additional notional load, N_i, equal to

$$N_i = 2.1\left(\frac{\Delta}{L}\right)Y_i \qquad (1)$$

where

Δ = first-order drift
L = story height

Fig. 1. Column flexure due to the axial load, P*, acting through imperfections δ_0 (out-of-straightness) and Δ_0 (out-of-plumbness).*

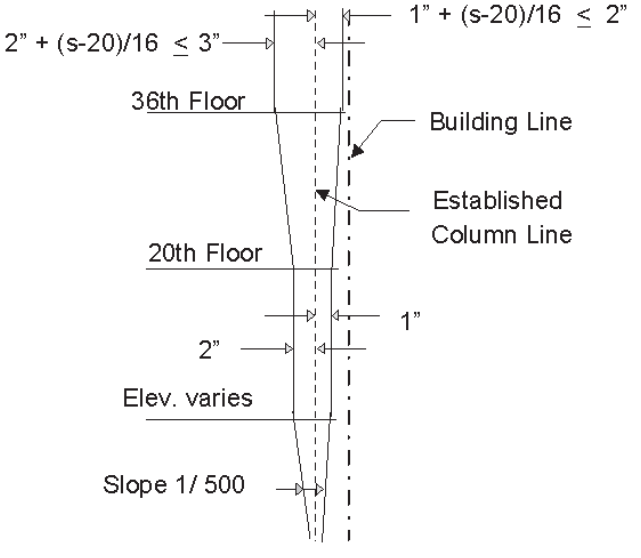

Fig. 2. AISC specified allowable erection tolerances for building frames.

In all cases, the initial out-of-plumbness is included, in some fashion, directly on the analysis side of the design process. A minimum lateral load of $0.002Y_i$, required in both the second-order and direct analysis approaches, provides amplified moments and forces equivalent to those obtained when an $L/500$ out-of-plumbness is modeled directly. In the first order approach, the effect of the initial imperfection is one factor included in the total notional load, N_i. The first-order approach is similar to notional load approaches used internationally, where a single horizontal load is used to account for multiple phenomena.

While out-of-straightness can have an important influence on the maximum strength of members in which the strength limit involves a nonsway failure mode, the modeling of member out-of-straightness within an analysis of the overall structural system is more cumbersome than the modeling of a uniform frame nonverticality. In lieu of direct modeling, the effect of out-of-straightness on the strength is accounted for in the axial strength term of the interaction equation given by Equations E3-2 through E3-4 in the AISC *Specification* (AISC, 2005a). This is the case in all of the approaches listed above.

The direct analysis approach of Appendix 7 meets all of the criteria listed in Chapter C. In the development of the direct analysis approach (Maleck, 2001; Surovek-Maleck and White, 2004), an emphasis was placed on including in the analysis, in as transparent a fashion as possible, both the effects of geometric imperfections and the stiffness reduction due to inelasticity and residual stresses.

The direct analysis approach includes the effects of the two planar initial geometric imperfections as follows:

- Out-of-straightness is explicitly accounted for by either altering the frame geometry or adding a notional load of $N_i = 0.002Y_i$ at each level, where Y_i is the total factored gravity load acting on level i. The notional load is equivalent to a uniform nominal out-of-plumbness of $L/500$.

- Out-of-straightness is implicitly accounted for by calculating the compressive strength of the column using the column curve provided in Chapter E of the specification. The development of this curve includes the reduction in strength due to out-of-straightness.

By modeling the out-of-plumbness directly in the analysis, the increase in second-order moments due to the imperfections is incorporated in the analysis results. In contrast, the out-of-straightness is not measured directly as an increase in second-order moment, but is accounted for as a decrease in member strength.

FRAME SENSITIVITY TO INITIAL OUT-OF-PLUMBNESS

Structural engineers can intuitively understand that for some frames, such as highly redundant, laterally stiff frames, the initial imperfections will have a negligible effect on the overall frame strength. This naturally leads to the questions:

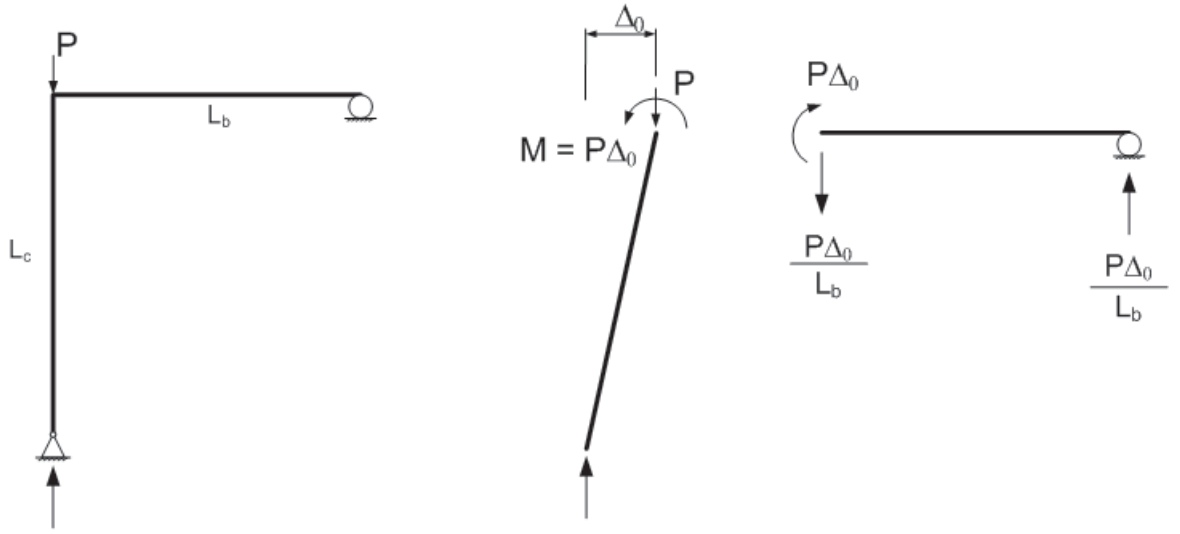

Frame forces without consideration of imperfection. Note lack of load on the beam.

Frame forces including effects of out-of-plumb, Δ_0. Despite the lack of transverse loading, there are forces and moments transferred to the beam.

Fig. 3. Transfer of forces and moments due solely to initial nonverticality (out-of-plumbness).

"How sensitive are frames to initial imperfections?" and, "When can these effects be neglected?"

In order to address these questions, a parametric study was designed to determine:

- The sensitivity of different frame configurations to initial out-of-straightness.
- Which parameters most affect the significance of the out-of-plumbness on the strength of the frame.

Ultimate frame strength was determined using rigorous second-order, inelastic analyses (aka "plastic zone analyses"). The analysis included initial nonverticality, directly modeled in the frame geometry, as well as the effects of residual stresses on the inelastic response. This analysis approach is typically used to determine the "exact" strength of a frame. (Kanchanalai, 1977; White and Chen, 1993). Initial out-of-straightness was not modeled in order to isolate the effects of nonverticality on the frame response. Both P-Δ and P-δ effects were captured by the analysis. Frame parameters considered in the study included:

- Column slenderness ratios (L/r).
- Leaning load levels, that is, the axial load on pinned-pinned columns that do not provide stiffness to the lateral resistance of the frame.
- Gravity-load to lateral-load ratios.
- Lateral frame stiffness (as measured by the B_2 factor in the AISC *Specification*).

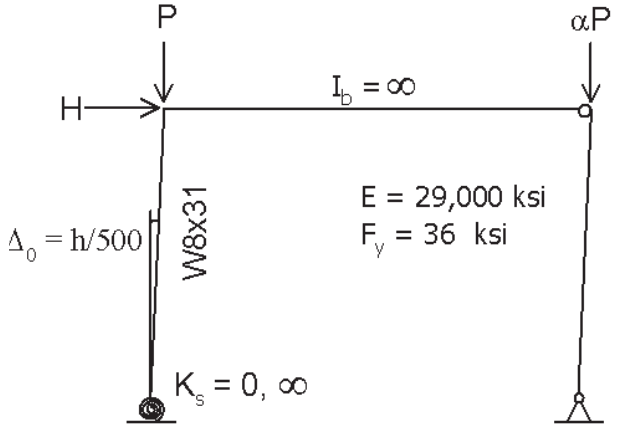

Fig. 4. Imperfection study portal frame example.

The frames studied were divided in two groups: axially loaded portal frames, shown in Figure 4, and multi-bay frames with distributed member loading. The behavior of portal frames with concentrated axial forces was examined with respect to the sensitivity of the ultimate frame strength to the inclusion of nonverticality in the model. In these studies, the beams were considered to be rigid and to remain elastic; thus, the load capacity of the portal frames was entirely dependent on the failure of the beam-column.

Previous studies that have been performed to assess the effects of imperfections (Wald, 1991; DeLuca, Faella and Mele, 1993; Clarke and Bridge, 1997) have considered frames that are loaded only with concentrated nodal loads. The effects of relative beam-to-column stiffness, inelastic behavior of beams, and particularly, moment transferred to the columns from the adjoining members due to transverse beam loading were not considered. Consequently, the studies are limited in that, in all cases, the load capacity of the frame was dependent only on the column strength. In addition to the portal frames, the frames considered in this study included 14 single-story, multi-bay frames as well as 11 multi-story, multi-bay frames with distributed beam loads. All of the frames (other than those originally studied by others) were designed per AISC strength criteria as well as to meet serviceability limits. The frames were designed considering a reasonable set of parameters with regard to frame stiffness and gravity-load to horizontal-load ratios, although a few very flexible frames were considered. Both strong-column, weak-beam and strong-beam, weak-column frames were considered to assess the impact of the failure mode of the frame on the imperfection sensitivity.

Portal Frame Studies

A number of small, stability critical portal frames in strong-axis bending were analyzed by second-order, inelastic analyses to assess the effects of nonverticality on sensitive benchmark frames. These types of frames are often studied to consider limiting cases with respect to beam-column and frame stability (Kanchanalai, 1977). The portal frame studied, which is oriented in strong-axis bending, is shown in Figure 4. Parameters considered in the study included gravity-load to horizontal-load ratios ($\Sigma P/\Sigma H$), as well as base fixity, column slenderness (L/r), and amount of leaning load (α). The pinned columns in frames UP and UR in Figure 9 represent leaning columns. The beam was modeled as rigid and of sufficient length so that overturning moments did not impact results. Values of the parameters considered included:

$\Sigma P/\Sigma H$ = 10, 20, 33, 50, 100, 200

L/r = 20, 30, 40, 50, 60, 70, 80, 90, 100

α = 0, 1, 2, 4

Figure 5 illustrates the impact of horizontal-to-gravity load ratios on imperfection sensitivity, measured as

$$\text{imperfection sensitivity} = [(\lambda_0 - \lambda_i)/\lambda_0](100\%) \qquad (2)$$

where

λ_0 = ultimate load parameter for the perfect structure
λ_i = the corresponding parameter with the inclusion of an H/500 imperfection

In strong axis bending with a single leaning load, only those frames with $\Sigma P/\Sigma H > 50$ showed greater than 5% imperfection sensitivity. In Figure 6, the impact of leaning loads on imperfection sensitivity is highlighted. For frames with larger leaning loads ($2P$ to $4P$), the imperfection sensitivity is as high as 11%, but only when combined with very high gravity to horizontal load ratios. Column slenderness was not a significant parameter for lower values of $\Sigma P/\Sigma H$ but increased in significance for higher load ratios where the behavior is dominated by axial effects. As shown in Figure 6, the effects of leaning loads increases for higher $\Sigma P/\Sigma H$ again due to axial effects; however, this effect of higher leaning load diminishes as slenderness ratios increased. It is interesting to note that the slenderness ratio has little to no impact on the sensitivity of frames with low $\Sigma P/\Sigma H$ ratios.

Generalized Frame Studies

To extrapolate the results of the above portal frame studies to less idealized framing systems, 25 frames in strong axis bending were analyzed with and without imperfections to determine their sensitivity to the inclusion of imperfections in the geometry. The frames were subjected to distributed gravity loading. Fifteen frames were designed per AISC specifications, two were modifications of the first fifteen to illustrate a particular behavior, and eight were taken from previous research studies. The details on all of the studied frames are provided in Appendix A.

Single Story Frames

Twelve of the LRFD-designed frames were single-story frames ranging from one to eight bays. All of the frames, except one, were designed for a low 10 psf nominal wind load (to accentuate stability effects due to gravity load) and to meet a maximum drift criterion of H/500 [using a service load combination of $1.0D + 0.5L + 0.7W$ per Ellingwood (1996)]. The heavy gravity load was defined as 100 psf dead and 150 psf live, while light load was defined as 50 psf dead and 50 psf live. The results for the 12 single-story frames are presented in Table 1.

Only four of the frames considered had greater than 5% imperfection sensitivity. Of these, three were designed as weak-column/strong-beam frames in order to limit yielding in the beams at failure. In particular, two of these frames were designed with overstrength beams to limit or eliminate yielding in the beams at the failure load levels. All of these sensitive frames exhibited extensive spread of plasticity in the columns with no significant beam plasticity present at failure. The fourth frame exhibiting imperfection sensitivity was a two-bay, pinned-base frame that was allowed to exceed drift limits by 40% and had a second order amplification factor, B_2, of 1.9.

All of the frames that showed greater than 5% sensitivity to imperfections have B_2 values greater than 1.3. While Figure 7 shows a general trend in greater sensitivity with respect to higher B_2 values for the symmetric frames which meet drift criteria, it indicates that there is not a direct correlation between lateral frame stiffness, as measured by the B_2

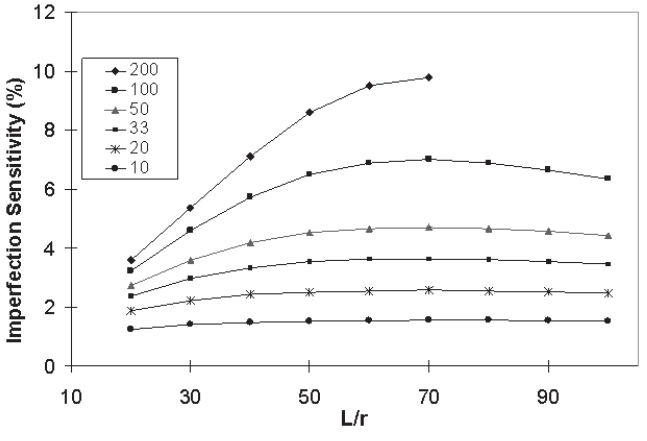

Fig. 5. Imperfection sensitivity versus $\Sigma P/\Sigma H$, strong-axis bending, $\alpha = 1$, $K_s = 0$.

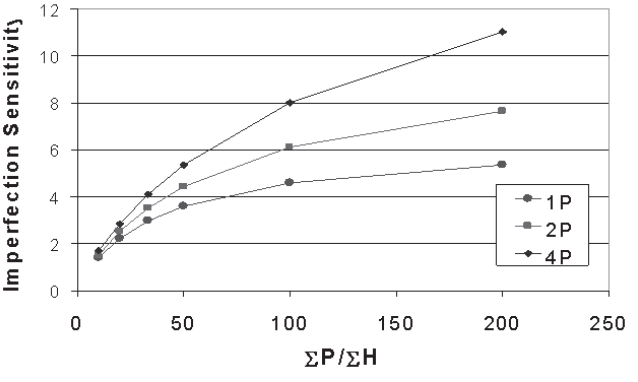

Fig. 6. Imperfection sensitivity due to leaning loads, L/r = 20, $K_s = 0$.

factor, and the effect of the initial imperfection on the ultimate strength of the frame.

The frames with higher B_2 values all exhibited limited yielding in the beams and failure largely associated with plasticity and eventually instability in the columns. In addition to the symmetric frames studied, two-bay, single-story unsymmetrical frames with differing base fixity were analyzed. Due to the tendency of these frames to drift under gravity load, the P-Δ_0 moments due to the imperfections were not significant when compared to the P–Δ moments due to the drift under gravity load, and neither exhibited a sensitivity greater than 1%, despite having B_2 values of 1.5 to 2.4.

Multi-Story Frames

Eleven multi-story frames were studied. Eight of these were two story frames previously studied by Ziemian (1990) with variation in the following parameters: symmetry, base fixity and load level. Of these frames, none exhibited greater than 2.25% imperfection sensitivity. Two six-story, two-bay fixed base frames were designed under heavy and light gravity loading. Design of the heavily loaded frame was controlled by the maximum live load combination, while design of the members in the lightly loaded frame was controlled by both wind and gravity load combinations. In both cases, imperfection sensitivity was less than 3%.

In general, only those frames that were "stability critical", that is those frames where the failure was dependent on instability of the columns rather than yielding of the beams, were likely to be sensitive to the initial imperfection. Leaning load levels and $\Sigma P/\Sigma H$ ratios have a direct impact on frame sensitivity, all other parameters remaining constant. While lateral stiffness has some impact on overall sensitivity of a frame to imperfections, there was no direct correlation.

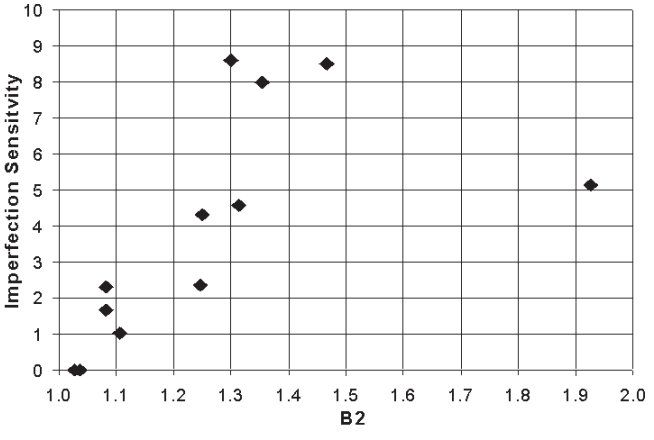

Fig. 7. Imperfection sensitivity for symmetric frames.

NEGLECTING THE IMPERFECTION EFFECT IN THE PRESENCE OF A LATERAL LOAD PER AISC APPENDIX 7

Appendix 7 of the AISC *Specification*, which outlines the direct analysis approach, allows for the notional load representing initial imperfections to be treated as a "minimum horizontal load" in frames where the ratio of second-order drift to first-order drift, Δ_2/Δ_1, (approximated by the B_2 factor) is less than 1.5. In other words, the notional load representing the imperfection may be neglected if a larger lateral load is applied to the structure. While not explicitly stated in the specification, it is presumed this limit must be checked and met at each story level.

Logic would suggest that since the notional loads represent physical imperfections, and since these physical imperfections would be present regardless of the load condition, the notional loads should be additive to other lateral loads. However, the verification studies used to validate the direct analysis method (Maleck and White, 2003) suggest that for stability critical frames that meet the B_2 limit, the unconservative error associated with disregarding the impact of the imperfection in the presence of a higher lateral load is typically less than 6%.

In order to verify the maximum unconservative error associated with neglecting the imperfection in the presence of a larger lateral load, a small verification study was run that focused specifically on this effect. The studies were designed to correspond with those used to verify the direct analysis method and included:

- individual column cases in which parameters considered fixity and gravity-load to horizontal-load ratios
- portal frames considered in the original verification studies for the direct analysis method that exhibited the highest unconservative error

In these studies, interaction diagrams were created based on results from rigorous second-order plastic zone analyses and compared to those developed from direct analysis results. The second-order analysis results for the direct analysis approach were performed using a closed form second-order analysis solution developed by LeMesurier (1977). LeMesurier's method accounts for both $P\Delta$ and $P\delta$ effects and is, for all practical purposes, exact for the sidesway problems studied in this work.

Both first-order (P versus M_1) and second-order (P versus M_2) interaction curves were developed, where M_1 is the maximum primary bending moment in the member due to the applied loading, and M_2 is the maximum internal second-order bending moment, located at the member ends in all the problems considered.

The P versus M_2 curves represent the strength of the member and, for the direct analysis approach, are the familiar interaction equations provided in Chapter H of the AISC *Specification*. The moments M_2 are the moments that must be transferred to the adjacent framing (in other words, to the beams and their connections at the beam-column joints) for satisfaction of equilibrium at the beam-column joints. The P versus M_1 interaction curves represent the maximum loadings that can be applied to the column or frames. The first order curves are of particular interest in design.

The error in the design interaction curves relative to the rigorous plastic zone solutions was measured for the columns and frames with and without imperfections. This error is defined as

$$e = \frac{r_{PZ} - r}{r_{PZ}} \tag{3}$$

where

r_{pz} = radial measure to the interaction curve developed using plastic zone analysis

r = radial measure to the interaction curve developed using the direct analysis approach

The radial error represents a measure of the error in the interaction check, or an overall error in the strength as measured. The horizontal error is a measure of the error in the first order column moment. The maximum moment in the cases studied occurred at the end of the column, so this represents the error in the moment being transferred to adjoining members and connections as well as the maximum moment in the column.

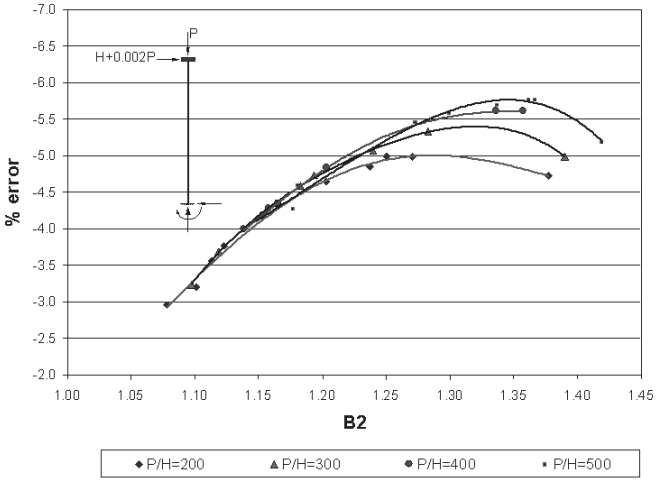

Fig. 8. Sensitivity of fixed-guided columns to exclusion of imperfection in addition to horizontal load, H.

Column Studies

As anticipated, the maximum strengths (as indicated by the interaction check) of columns with higher ratios of gravity to horizontal loads ($\Sigma P/H$) were more sensitive to the exclusion of the imperfection. For the fixed-guided case shown in Figure 8, the difference in strength between the columns with both the imperfection notional load and the lateral load and those that excluded the notional load was below 6% in all cases. It is interesting to note that the general trend does not continue to increase as lateral stiffness decreases. Similar error levels were observed for pinned-fixed columns and cantilever columns, and in no case did the unconservative error exceed 6%.

However, when considering the error in the moment calculated in the columns, the error was entirely dependent on the gravity-load to horizontal-load ratio. The error associated with the resulting first order column moment was as high as 50% for a $\Sigma P/\Sigma H$ ratio of 500. Because the error is associated with a high axial-load to horizontal-load ratio, the effect on the column interaction check is nominal (<6%), since the interaction check is dominated by the axial term.

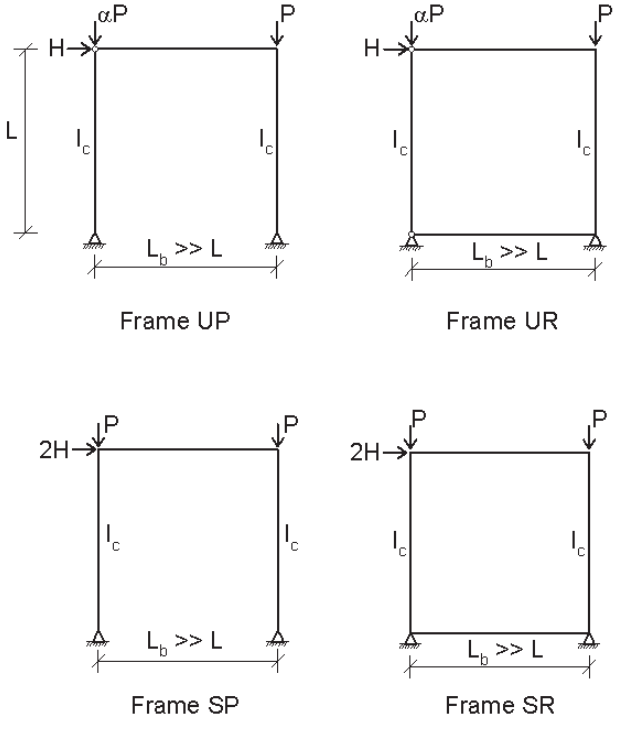

Fig. 9. Portal frames used in the verification of the direct analysis approach.

Portal Frame Studies

In this study, the most unconservative of the verification studies for the direct analysis approach (Maleck and White, 2003) were replicated with and without imperfections. Only cases where $B_2 < 1.5$ were considered. Both second-order analyses including *P*-δ effects and those including only *P*-Δ effects were performed. The verification frames are shown in Figure 9; they are similar in parameters to those shown in Figure 4 with the exception that the beam stiffness was also considered, as measured by the *G* factor found in the Commentary to Chapter C of the Specification, given by:

$$G = \frac{\Sigma \frac{I_C}{L_C}}{\Sigma \frac{I_G}{L_G}} \quad (4)$$

where

I_C = moment of inertia of the column
I_G = moment of inertia of the girder
L_C = unsupported length of the column
L_G = unsupported length of the girder

The frame designations indicate whether they are symmetric or unsymmetric (S, U), pinned or restrained at the base (P, R), oriented in weak or strong axis bending (W, S), have infinitely rigid (G0) or flexible beams (G1 or G3), and the level of leaning column load (α). Only the most critical frame studies were recreated (For complete results of the original study, the reader is directed to Maleck and White, 2003). The only variation from the initial study is that error was only measured for interaction values where $B_2 < 1.5$. The highest unconservative error was reported in the UP_W40_G1_α1 and SP_W60_G0 frames; both frames were laterally supported by columns in weak axis bending. None of the strong axis frames exhibited more than 6% error when a rigorous second-order analysis (that is, one considering both *P*-Δ and *P*-δ effects) was used. Figure 10 shows the first order interaction curves for the UP_W40_G1_α1 frame using a rigorous analysis, and Figure 11 shows the results for the *P*-Δ analysis. The complete results of the most sensitive cases are shown in Table 2.

The verification studies were based on the error in the column moment, only. For most practical adjoining members, if a distributed load is present, the moment being transferred by the column (particularly the moment due to an imperfection) will not be a significant portion of the maximum moment on the beam or connection. However, in the rare cases where the beam is not transversely loaded, such as the frame configuration shown in Figure 3, omission of the imperfection effect may lead to a rather unconservative design of the beam or connection. In cases where the design of connecting elements may be negatively affected by omission of this moment, such as in the case listed above, the notional load representing the imperfection should not be neglected regardless of the B_2 factor.

CONCLUSIONS AND RECOMMENDATIONS

For the engineer engaged in design of steel frames, a basic understanding of how initial imperfections affect frame strength and behavior is beneficial, particularly when interpreting the stability design provisions of the AISC Specification. The discussed studies of columns and framing systems considering the effects of nonverticality and a careful assessment of the current AISC provisions suggest the following:

1. The ultimate strength of most practical building frames will not be sensitive to initial nonverticality.

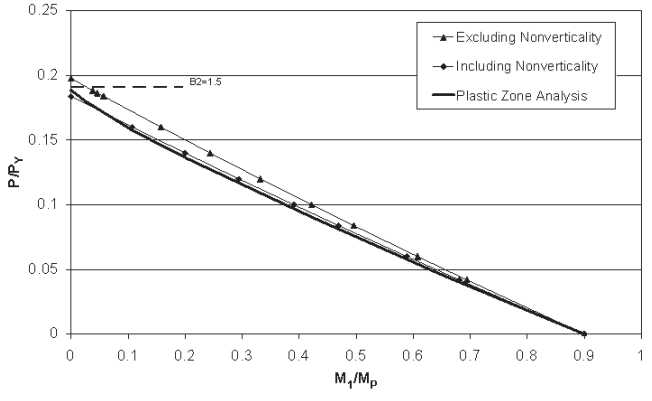

Fig. 10. First-order normalized interaction curves for UP_W40_G1_α1 frame P-δ *(rigorous) analysis.*

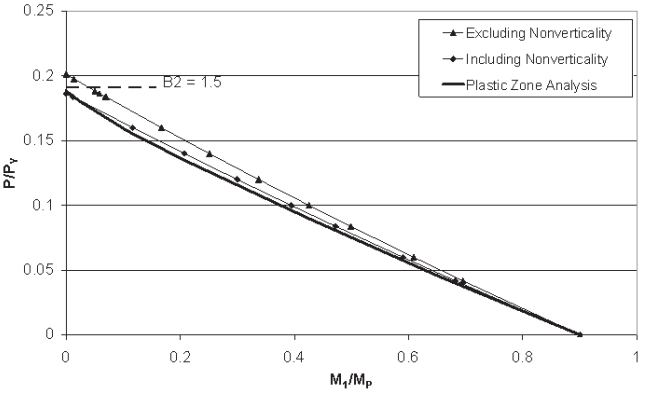

Fig. 11. First-order normalized interaction curves for UP_W40_G1_α1 frame, P-Δ *analysis.*

Table 1. Imperfection Sensitivity of Single-Story Symmetric Frames			
Imperfection Sensitivity	Number of frames	B_2	$\Sigma P/\Sigma H$
< 2%	4	1.03–1.1	60–280
2–5%	4	1.07–1.31	140–710
> 5%	4	1.3–1.93	280–1100

Table 2. Radial Error Measured in Interaction Checks for Verification Frames for $B_2 < 1.5$				
	Error with Imperfection		Error without Imperfection	
Frame Designation	P-Δ	P-δ	P-Δ	P-δ
SP S40 G0	-4%	-3%	-7%	-6%
SP S60 G0	-4%	-2%	-8%	-6%
SP S20 G0	-2%	-2%	-6%	-5%
UP W40 G1 α2	-1%	0%	-8%	-6%
SP W60 G0	-6%	-5%	-10%	-8%
SP W80 G3	-2%	-1%	-2%	-2%

2. The parameters that have the greatest effect on imperfection sensitivity include gravity-load to horizontal-load ratios, frame symmetry, and amount of leaning load. However, the primary cause of initial imperfection sensitivity in frames is the mode of failure and whether that failure is initiated by instability of a column rather than yielding in a beam.

3. Frames for which imperfection effects are negligible are not easily identified quantitatively, as no single parameter controls the sensitivity.

4. The provision of AISC *Specification* Appendix 7, in which the effects of imperfections may be neglected in lieu of higher lateral loads when $B_2 < 1.5$, is shown to produce a maximum unconservative error of 8%. This error occurred in a highly stability-critical portal frame laterally supported by a weak axis column only. When a less rigorous P-Δ analysis is used, the maximum unconservative error was 10%. For practical frames, this maximum unconservative error will be significantly smaller. Most practical frames will not be governed by the behavior of a weak-axis, unbraced, laterally resisting column.

5. If neglecting imperfections in the presence of a larger lateral load per Appendix 7, the engineer should be careful to consider the "special" cases where the beam design may be significantly impacted by the moment amplification due to the imperfection.

One point to consider is: When using the direct analysis approach in Appendix 7, is it easier to modify the geometry or calculate notional loads than to perform the calculations necessary to determine whether the imperfection effects can be neglected? Consider that if a direct second order analysis algorithm is used (that is, if B_1 and B_2 factors are not being separately calculated), a separate first-order analysis is still required to determine if the imperfection can be ignored. If the imperfection effect is small enough to neglect, inclusion of the notional load will have a negligible effect on the final design. In short, if the impact of including imperfections is negligible, economy will not be lost by including these effects, and this requires less effort than determining whether they can be neglected. It is also more rational, since the notional load represents a potential physical phenomenon that is independent of the load case.

Currently the maximum permissible imperfection is incorporated into the design provisions. There is a lack of data on measured nonverticality in constructed facilities to warrant a reduction of this imperfection. There are very few published studies that include surveyed measurements of a constructed building (Bridge, 1998; Beaulieu and Adams, 1978). Bridge concluded that many individual columns exceeded construction tolerances; however, story and global imperfection tolerances were met by compensating imperfections.

More data on erected structures would be useful if modifications to these provisions in the form of reduced requirements for imperfections were to be considered in future editions of the *Specification*.

REFERENCES

AISC (2005a), *Specification for Structural Steel Buildings*, American Institute of Steel Construction, Inc., Chicago, IL.

AISC (2005b), *Code of Standard Practice for Steel Buildings and Bridges*, American Institute of Steel Construction, Inc., Chicago, IL.

Beaulieu, D. and Adams, P. (1978), "Results of a Survey on Structural Out-of-Plumbs," *Canadian Journal of Civil Engineering*, Vol. 5, No. 4, Dec, 1978, pp. 462–470.

Bridge, R.Q. (1998), "The Inclusion of Imperfections in Probability-Based Limit States Design," *Proceedings, 1998 Structural Engineering World Congress*, San Francisco, California, July.

Clarke, M.J. and Bridge, R.Q. (1997), "Notional Load Approach for the Assessment of Frame Stability," Chapter 4, *Effective Length and Notional Load Approaches for Assessing Frame Stability: Implications for American Steel Design*, American Society of Civil Engineers, pp. 181–278.

DeLuca, A., Faella, C., and Mele, E. (1993), "Advanced Analysis: Numerical Results and Design Guidelines for Rigid and Semi-Rigid Sway Frames," in *Plastic Hinge Based Methods for Advanced Analysis and Design of Steel Frames – an Assessment of the State of the Art*, Structural Stability research Council, Bethlehem, PA, pp. 41–64.

Ellingwood, Bruce (1996), "Structural Serviceability: Review and Standard Implementation," *Building an International Committee of Structural Engineers, Proceedings of Structures Congress XIV*, American Society of Civil Engineers, pp. 436–442.

Kanchanalai, T. (1977), "The Design and Behavior of Beam-Columns in Unbraced Steel Frames," AISI Project No. 189, Report No. 2, Civil Engineering/Structures Research Lab., University of Texas, Austin, TX, 300 pp.

LeMessurier, W. J. (1977), "A Practical Method of Second Order Analysis. Part 2: Rigid Frames," *Engineering Journal*, AISC, Vol. 14, No. 2, pp. 49–67.

Maleck, Andrea E. (2001), "Second-Order Inelastic and Modified Elastic Analysis and Design Evaluation of Planar Steel Frames," Ph.D. Dissertation, Georgia Institute of Technology, 579 pp.

Maleck (Surovek), A.E. and White, D.W. (2003), "Direct Analysis Approach for the Assessment of Frame Stability: Verification Studies," *Proceedings of the 2003 SSRC Annual Technical Sessions and Meeting*, Baltimore, April, pp. 423–441.

Surovek-Maleck A.E. and White, D.W. (2004), "Alternative Approaches for Elastic Analysis and Design of Steel Frames. I: Overview," *Journal of Structural Engineering*, ASCE, Vol. 130, No. 8, pp. 1186–1196.

Wald, F. (1991), "Sensitivity of Semi-Rigid Frames to Initial Imperfections," *Journal of Constructional Steel research*, Vol. 18, pp. 309–316.

White, D.W. and Chen, W.F., eds. (1993), *Plastic Hinge Based Methods for Advanced Analysis and design of Steel Frames – An Assessment of the State of the Art*, Structural Stability Research Council, Bethlehem, PA, 299 pp.

Ziemian, R.D. (1990), "Advanced Methods of Inelastic Analysis for in the Limit States Design of Steel Structures," Ph.D. Thesis, Cornell University, Ithaca, NY.

APPENDIX A

Parametric Study Frames

Beam and column designations used in the single and multi-story frames are presented below. The frame designations are shown in Figure A.1. Steel designations used in the single and two-bay symmetric test frames are given in Tables A.1 and A.2, respectively. The remaining frame designs are given in Figures A.2–A.11. Table A.3 presents the B_2 factors, analysis results, and imperfection sensitivities for each of the test frames. The imperfection sensitivity was calculated with

$$\text{imperfection sensitivity} = [(\lambda_0 - \lambda_i)/\lambda_0](100\%)$$

where

λ_0 = ultimate load parameter for the perfect structure

λ_i = the corresponding parameter with the inclusion of an H/500 imperfection

Details of the frames with designations beginning with U or S may be found in Ziemian (1990).

For the symmetric frames:
story height = 12 ft
bay width = 25 ft
frame spacing = 25 ft

For the unsymmetric frames:
story height = 12 ft
bay widths = 20 ft and 30 ft
frame spacing = 25 ft

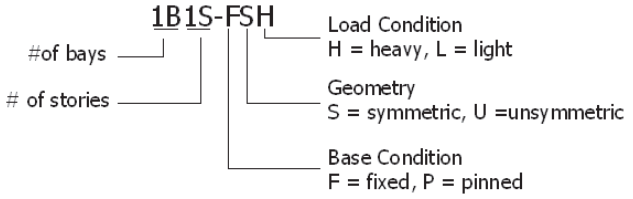

Fig. A.1. Key to frame designation.

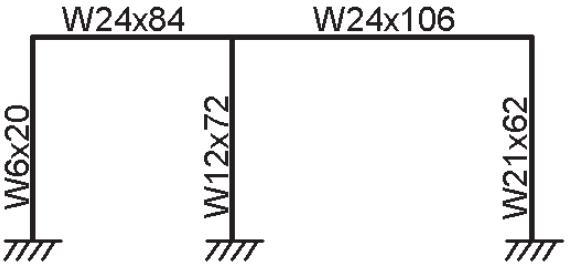

Fig. A.2. 2B1S-FUH.

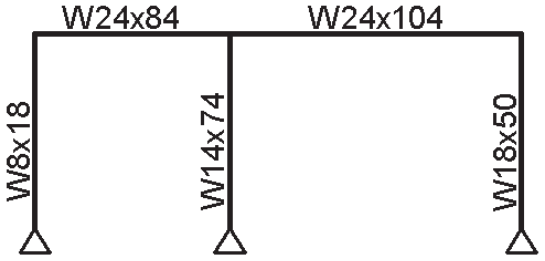

Fig. A.3. 2B1S-PUH.

Fig. A.4. Frame 4B1S-PSH1.

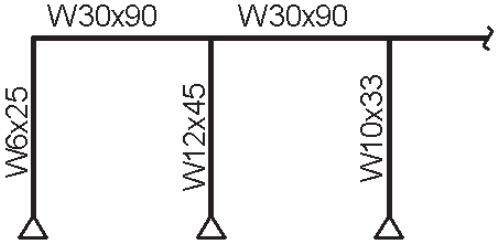

Fig. A.5. Frame 4B1S-PSH2 (oversized beams).

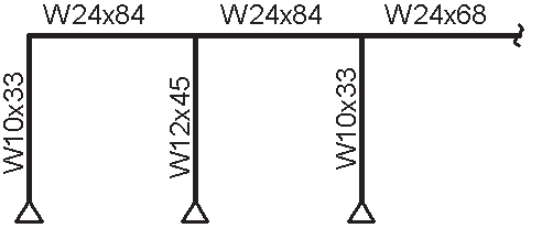

Fig. A.6. Frame 5B1S-PSH1.

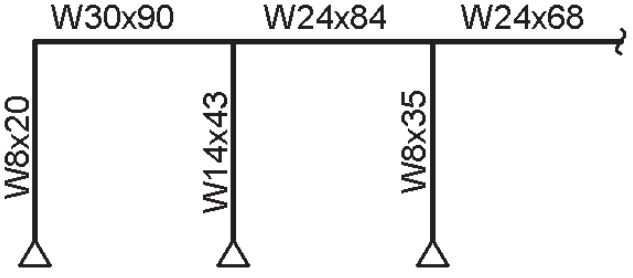

Fig. A.7. Frame 5B1S-PSH2 (oversized beams).

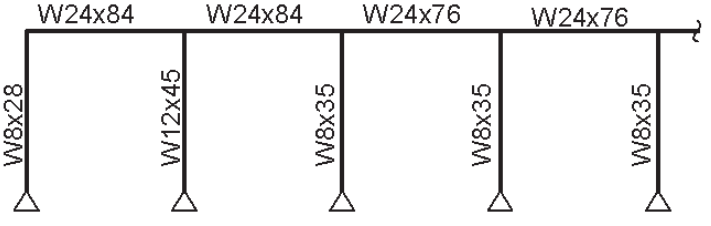

Fig. A.8. Frame 8B1S-PSH.

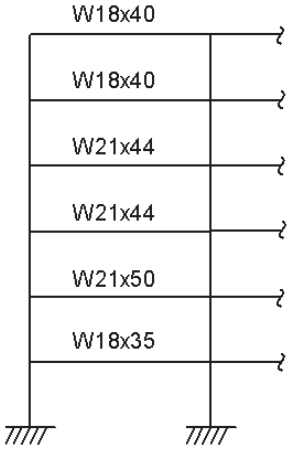

Story	Ext. Col	Int. Col
1	W14x99	W14x159
2	W14x99	W14x132
3	W14x82	W 12x96
4	W14x68	W12x72
5	W14x61	W12x45
6	W 8x28	W 6x15

Fig. A.9. Frame 2B6S-FSL.

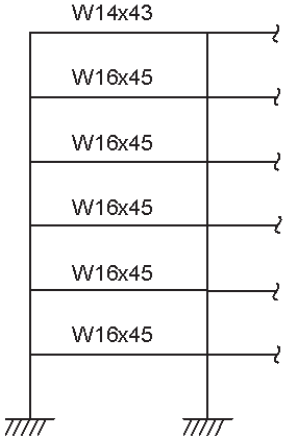

Story	Ext. Col	Int. Col
1	W14x48	W14x74
2	W14x48	W12x58
3	W12x40	W 8x48
4	W10x39	W 8x35
5	W10x33	W 8x28
6	W 8x24	W 6x15

Fig. A.10. Frame 2B6S-FSL.

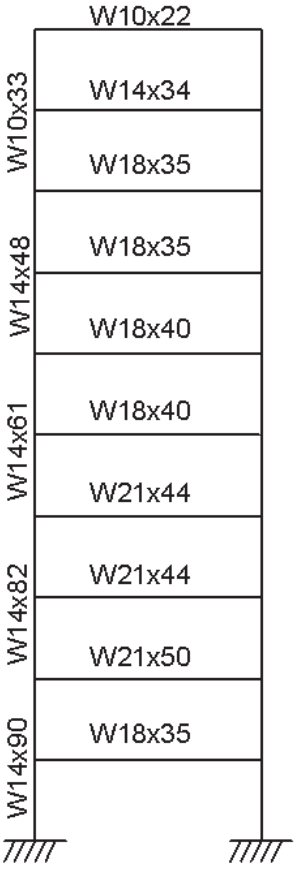

Fig. A.11. Frame 1B10S-FSL.

Table A.1. Single Bay Steel Sizes		
Designation	Beam	Column
1B1S-FSH	W30x90	W12x53
1B1S-PSH1	W30x99	W14x43
1B1S-PSH2	W24x104	W8x40
1B1S-FSL	W12x58	W8x31
1B1S-PSL	W12x58	W10x39

Table A.2. Two-Bay Symmetric Steel Sizes			
Designation	Beam	Exterior Column	Interior Column
2B1S-FSH	W27x84	W10x33	W8x40
2B1S-PSH	W24x94	W8x25	W8x40

Table A.3. Results of Planar Frame Analyses				
Frame Designation	B_2	λ_i	λ_o	Sensitivity (%)
1B1S-FSH	1.028	1.478	1.478	0
1B1S-PSH1	1.082	1.517	1.522	2.31
1B1S-PSH2	1.247	1.322	1.354	2.36
1B1S-FSL	1.037	1.165	1.165	0
1B1S-PSL	1.082	1.449	1.425	1.67
2B1S-FSH	1.106	1.606	1.623	1.11
2B1S-PSH	1.926	1.324	1.392	5.13
2B1S-FUH	1.546	1.485	1.486	0.02
2B1S-PUH	2.42	1.359	1.37	0.75
4B1S-PSH1	1.25	1.441	1.503	4.32
4B1S-PSH2	1.354	1.496	1.616	8
5B1S-PSH1	1.314	1.427	1.492	4.57
5B1S-PSH2	1.3	1.495	1.624	8.61
8B1S-PSH	1.47	1.351	1.466	7.84
2B6S-FSH	–	1.299	1.3	0.34
2B6S-FSL	–	1.413	1.418	0.37
1B10S-FSL	–	1.38	1.434	3.54
U-P36L	–	1.144	1.145	0.07
U-P36H	–	1.073	1.088	1.46
U-F36L	–	1.163	1.164	0.2
U-F36H	–	1.161	1.162	0.1
S-P36L	–	1.226	1.227	0.03
S-P36H	–	1.218	1.246	2.23
S-F36L	–	1.242	1.264	1.8
S-F66H	–	1.184	1.189	0.4

Current Steel Structures Research

REIDAR BJORHOVDE

Standardization is essential to activities in all walks of life, but probably nowhere as important as it is for all aspects of the construction industry. The approaches vary somewhat from country to country and region to region, but it is a fact that quality in all respects depends on a body of practically oriented standards. The complexity of the subject cannot be overestimated, since there are so many materials and components and methods of fabrication and erection that govern the quality of the final product. The various steel construction institutes play key roles in all of these efforts, primarily because that is where the technical expertise resides. However, the interaction between any institute and its constituency is critical as well, and the model of cooperation that is used in North American standardization work is an excellent vehicle to bring all interested parties to the table, so to speak. The AISC Committee on Specifications, for example, is made up of approximately 45 individuals, with one third from consultants, one third from academia and one third from industry. The arrangement works extremely well, producing a steel design standard that is second to none in terms of state-of-the-art approaches and practical usefulness.

On the other hand, design manuals are the final element of the research and development and standardization work. Whether the manuals appear in the form of "hard" printed copies or as electronic tools is immaterial: the point is that they are critical to the users of the standards that have been developed. The AISC *Manual of Steel Construction* is currently in its 13th edition, and is accompanied by numerous other manuals and design guides that together aim to make the work of steel construction professionals easier. This approach is pursued just about everywhere in the world, most recently in Europe, where the European Convention for Constructional Steelwork (ECCS) has embarked on an aggressive program of design manual development. The ECCS program aims at having a full complement of manuals that will ease the acceptance and adoption and use of Eurocodes 3 (steel structures) and 4 (composite construction) by professionals throughout Europe. This is a major effort, for certain, but it is critical for industry and indeed the economies of the various countries.

Reidar Bjorhovde is the Research Editor of the AISC *Engineering Journal*.

The projects that are presented in this paper reflect a broad range of state-of-the-art work. A recent project in Spain has provided a broad assessment of the methods that are used to determine the moment capacity of laterally unsupported beams. One German study focuses on residual stresses in high strength steel shapes, using a new measurement technique, and another German project looks at the influence of the Bauschinger Effect on the deflections of cambered beams. Projects addressing seismic effects continue to be very prominent in the US and many other locales, and a novel structural system utilizing repairable "fuses" is examined in a major, multi-university and design firm US project. Full-scale testing forms part of several investigations, including a four-story building that has been tested to collapse in Japan. Finally, numerous researchers continue to develop software that may eventually be used in practice, and one such recent product from Belgium deals with analysis and design of plated structures.

References are provided throughout the paper, whenever such are available in the public domain. However, much of the work is still in progress, and reports or publications have not yet been prepared for public dissemination.

EFFECTS OF MATERIAL CHARACTERISTICS ON MEMBER BEHAVIOR

Residual Stresses in Hot-Rolled Shapes of S460 Steel: This project is conducted at the Technical University of Darmstadt in Darmstadt, Germany, with Professor Jörg Lange as the director.

The S460 steel grade is a high strength low alloy material with a specified minimum yield stress of 460 MPa (65 ksi). There is significant interest in the use of this and similar high strength grades for construction, but a drawback to their application continues to be that knowledge of the residual stress magnitudes in high strength steel shapes is very limited. Although the value of the modulus of elasticity is the same for all grades of steel and the levels of residual stress therefore should not vary much between identical shapes in different grades, there are still applications where the actual stress levels are needed. This is especially the case for stability issues such as column buckling, and also for girders where fatigue and fracture may play a role.

Traditional residual stress measurements are commonly made via destructive test methods, such as sectioning and hole drilling, to mention the two most common methods (Tebedge, Alpsten and Tall, 1971; Galambos, 1998). These approaches are very accurate but extremely costly and time-

consuming. The Darmstadt project focuses on the use of a magnetic effect ("Barkhausenrauschen") and the fact that the spatial structure of magnetic fields changes during demagnetization. Further, stresses in the ferromagnetic material change the magnetic fields significantly, and this change can be quantified. With appropriate calibration tests, the values of the residual stresses can be determined.

This testing method offers major potential for the determination of uniaxial and biaxial residual stress distributions. The work continues to improve calibration techniques and hence the accuracy of the stress magnitudes that are determined. It is expected that the residual stress data base for such high strength steel members will be significantly enlarged. The benefits for bridge construction in particular may be very useful.

Influence of the Bauschinger Effect on Deflections of Cambered Beams: This is another study that has been conducted at the Technical University of Darmstadt, also with Professor Jörg Lange as the director.

The Bauschinger Effect is a phenomenon that affects the response characteristics of steels that undergo strain hardening. It is also referred to as the directionality of strain hardening (Dieter, 1986). For example, a specimen that has been loaded in tension past the yield level and into strain hardening will unload elastically. Upon reloading in the same direction as the original load, the material will appear to have a level of yield stress that is the same as the level of stress at which the original test was stopped. Reversing the sense of the loading to zero and then into compression, the point at which yielding commences in compression is significantly lower than the original compressive yield stress. This is the Bauschinger Effect. It is completely reversible, to the effect that if the original loading were in compression, the higher yield stress would occur under this state of stress and the lower value would be found for tension. The Bauschinger Effect is important for high-deformation operations such as plate bending or other functions where the material is alternately subjected to high strains in tension and compression.

The study at the Technical University of Darmstadt started out as an investigation of the strength and behavior of steel and composite beams under service conditions, and specifically aimed at determining the deflections of such members (Grages, 2007; Grages, Lange and Sauerborn, 2007). One of the original issues was that the calculated deflections often understated the measured values. The measurements were made at various stages of various structures, and one of the interesting findings was that cambered beams deflected more than straight members. It was initially thought that this was caused by the residual stresses in the members, although it should have been clear that such could not be the case. The magnitudes of the service loads and the accompanying deflections and rotations are very small and the response of the beams is elastic for all practical purposes. Any local yielding due to the combination of service load stresses and residual stresses would almost certainly not take place, and the local yielding that was developed during the cambering operation would also be very limited. Of course, the latter would depend on the amount of cambering or curving, but it will be very small for the usual fraction of the dead load camber, as is common in American practice.

Short beam segments in S355 steel (50 ksi yield stress) were loaded to varying levels of strain beyond yield, and then loaded in the opposite direction. These tests imposed various degrees of prestrain, as high as 2%, and demonstrated that the Bauschinger Effect was clearly reflected in the cyclic stress-strain relationships. Using 18 m (60 feet) long beams that were curved to varying degrees, tests and additional analyses showed significant differences between the measured and computed deflections, as illustrated in Figure 1. The agreement between tests and theory is generally very good. A non-cambered beam was included for reference.

It is certainly possible to take this type of behavior into account in the analysis of a structure, but it is a question whether it is strictly necessary. The study demonstrates and explains the behavior that can be anticipated. On the other hand, the structural displacements will stabilize once the loads have been applied, and no further deflection increases should be expected. Finally, the amount of cambering that is needed can take these kinds of increases into account, if it is deemed necessary for the service performance of the members and the structure.

STRUCTURAL MEMBER RESPONSE MODELING

Equivalent Moment Distribution Factors for Lateral-Torsional Buckling: This research project has been conducted at the University of Navarra in Pamplona, Spain, with Professor Miguel Serna and Dr. Aitziber Lopez as the directors.

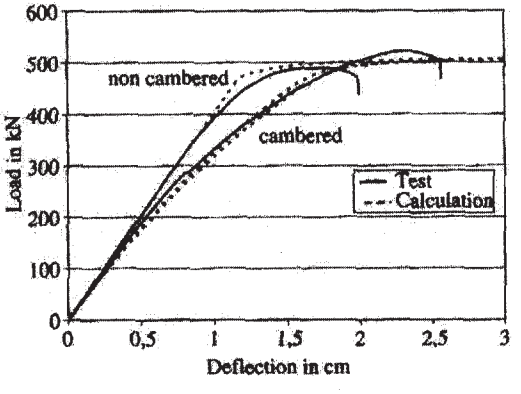

Fig. 1. Deflections of cambered and non-cambered beams (courtesy of Hauke Grages).

The equivalent moment factor, C_b, has been used for many years and by many design codes worldwide in the design of laterally unsupported beams that may fail in lateral-torsional buckling. It is a convenient conversion factor that translates the actual moment distribution into an equivalent uniform distribution, for which the theoretical elastic buckling solution is well known. Some of the early research studies on the subject were conducted in the 1960s and 70s by W.J. Austin, J.W. Clark and others (Galambos, 1998). Very significant work has been done for the past 25 years or so by Galambos, Trahair, Nethercot and other researchers. The C_b equation that has been used in the AISC *Specification* (AISC, 2005) for several editions is attributed to Kirby and Nethercot (1979), and it offers the convenience of applicability to all types of moment distributions.

The investigation by Serna and Lopez focused on the fact that the current C_b equation does not take into account any lateral bending or warping restraint at the supports or support points for the beam. Examining a wide range of beam support and moment distribution cases, using finite element as well as finite difference solutions, the study incorporated the following restraint conditions:

(i) no restraint to lateral bending and warping

(ii) full restraint to lateral bending and warping

(iii) restraint to lateral bending only

(iv) restraint to warping only

As an example, Figure 2 shows a typical symmetric moment distribution that was used for the analysis of an 8 m (26 ft 8 in.) long IPE 500 beam. This is a 20-in.-deep hot-rolled shape with no closely comparable American counterpart; the flange width of the IPE 500 is 8 in., the flange thickness is ⅝ in. and the web thickness is ⅜ in. Figure 3 shows the resulting equivalent moment factor values, as determined by the finite difference solution, by the solution of the researchers, and by the AISC C_b expression from the 1994 *LRFD Specification for Structural Steel Buildings* (which is the same as in the 2005 *Specification for Structural Steel Buildings*).

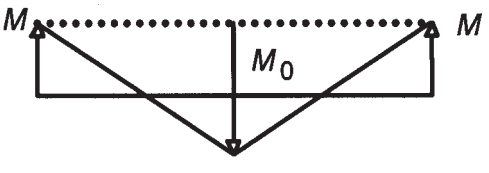

Fig. 2. Linear moment distribution used in computational example (courtesy of M. Serna).

The values of the end moment ratio M/M_0 are shown in the horizontal axis; the values of the equivalent moment factor are shown on the vertical axis. Albeit much more complex than the expression used in the current codes, the researchers observe that including the warping restraint leads to significantly higher C_b-values than what is predicted by the expressions of the 1994 AISC LRFD *Specification* and the 2000 British code BS 5950; further, including the effect of the bending restraint leads to lower C_b-values. These findings are demonstrated by the data shown in Figure 3. The study included a broad range of comparisons with the two code documents, and the researchers note that the lower C_b-values for the end-restraint case indicate that the codes may be unconservative for such cases. The higher values for the warping-included cases obviously indicate conservative code criteria.

SEISMIC RESPONSE OF STEEL STRUCTURES

Controlled Rocking of Steel-Framed Buildings with Replaceable Energy Dissipating Fuses: This is a very substantial investigation of the performance of a novel type of structural system, currently underway as a joint project of the University of Illinois, Stanford University, Hokkaido University in Japan, and the California consulting firms Tipping & Mar Associates and GPLA. The directors are Professors Gregory G. Deierlein of Stanford University and Jerome F. Hajjar of the University of Illinois. It is supported by funding from the NEES program of the National Science Foundation.

The principal aim of the project is to arrive at performance and design criteria that will eliminate residual drift and also concentrate the structural damage in the replaceable fuses of the braced frame. Residual drift is the permanent sway that

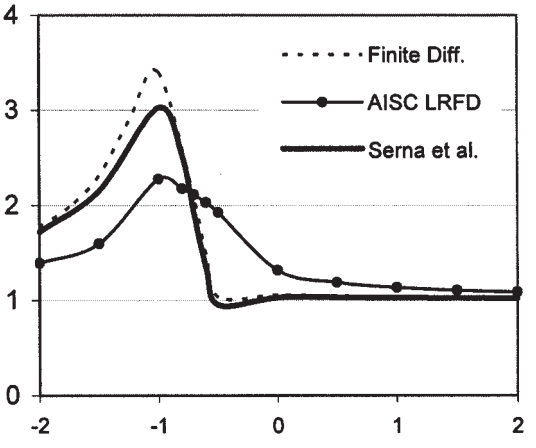

Fig. 3. Values of C_b for the IPE 500 example beam (courtesy of M. Serna).

remains in the building following an earthquake. The revolutionary concept of this system is that the seismic damage will be focused primarily, if not entirely, in the replaceable shear fuses that are incorporated in the frame, along with the self-centering post-tension bars that form an integral part of the system. That is, rather than focusing totally on limiting or preventing the local or overall failure of the frame, the rocking concept and shear fuses aims specifically at providing for economical repair of a damaged structure. Figure 4 illustrates the basic elements and the key behavioral aspects.

The project is further enhanced by the collaboration with researchers for a project of Hokkaido University in Japan. A full-scale test of a frame with square built-up tubular columns and wide-flange beams was recently (September 27, 2007) tested at the three-dimensional E-Defense facility in Japan. Figure 5 shows this frame after the completion of the test. Evaluations of the results are forthcoming.

COMPUTER SOFTWARE DEVELOPMENT

Software for Design of Plate Structures against Plate Buckling: This is a major software development that has been undertaken by the research group at the University of Liège in Liège, Belgium. The project director has been Professor René Maquoi. Funded by the COMBRI project of the European Union, the software is intended for use in the analysis and design of steel-plated structures for bridges.

The design criteria that have been used in this software development are those of the plate buckling requirements of Eurocode 3, Section 1-5 (CEN, 2005). The focus is on the following criteria:

(i) Accurate determination of elastic plate buckling stresses for rectangular stiffened plates, covering a much wider range of design parameters than what is currently available

(ii) Accounting for the stabilizing effects of the torsional stiffness of stiffeners and the rotational stiffness of the edges of the plates

(iii) Providing an effective graphical interface to improve the interpretation of the analytical results

(iv) Offering an efficient substitute for much more complex finite element analysis

Named EBPlate, the program is available for downloading at no cost at the websites www.cticm.com and www.steelbizfrance.com . It is noted that CTICM is the French steel construction institute.

REFERENCES

AISC (2005), *Specification for Structural Steel Buildings*, ANSI/AISC 360-05, Chicago, IL.

CEN (2005), *Eurocode 3: Design of Steel Structures – EN 1993*, Comité Européen de Normalisation, Brussels, Belgium.

Dieter, George E. (1986), *Mechanical Metallurgy*, 3rd Edition, McGraw-Hill, Inc., New York, NY.

Galambos, T.V. (1998), *Guide to Stability Design Criteria for Metal* Structures, Editor, 5th Edition, Wiley-Interscience, New York, NY.

Grages, Hauke (2007), *Beitrag zur Verformungsanalyse von Verbundträgern*, Ph.D. Dissertation, Technical University of Darmstadt, Darmstadt, Germany.

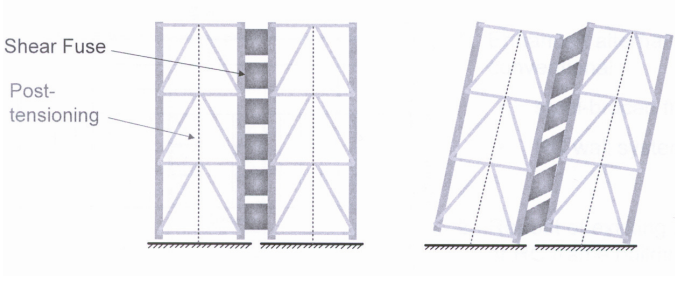

Fig. 4. Self-centering frame with replaceable shear fuses (courtesy of J.F. Hajjar).

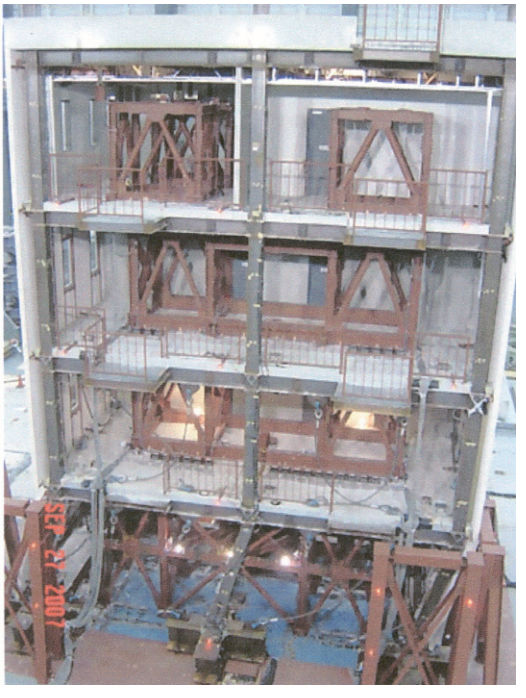

Fig. 5. Full-scale frame test at the E-defense facility near Kobe, Japan.

Grages, Hauke, Lange, Jörg, and Sauerborn, Norbert (2007), "Influence of the Bauschinger Effect on the Deflection Behaviour of Cambered Steel and Steel-Concrete Composite Beams," in *Steel and Composite Structures*, Y. C. Wang and C. K. Choi (Eds.), Taylor and Francis, London, England, pp. 133–138.

Kirby, P.A. and Nethercot, D.A. (1979), *Design for Structural Stability*, Wiley-Interscience, New York, NY.

Serna, M.A., Lopez, A., Puente, I. and Yong, D.J. (2006), "Equivalent Uniform Moment Factors for Lateral-Torsional Buckling of Steel Members," *Journal of Constructional Steel Research*, Vol. 62, No. 6, pp. 566–580.

Tebedge, N., Alpsten, G.A. and Tall, L. (1971), "Measurement of Residual Stresses: A Comparative Study of Methods," Fritz Engineering Laboratory Report No. 337.8, Lehigh University, Bethlehem, PA.

ACKNOWLEDGMENTS

Special thanks are due the following members of the International Structural Steel Research Advisors (ISSRA) who provided input to this paper:

Eduardo Bayo, University of Navarra, Pamplona, Spain
Ulrike Kuhlmann, University of Stuttgart, Stuttgart, Germany
René Maquoi, University of Liège, Liège, Belgium
Luis da Silva, ECCS and University of Coimbra, Coimbra, Portugal

Additional assistance has been provided by Jörg Lange, Technical University of Darmstadt, Darmstadt, Germany; Dieter Ungermann, University of Dortmund, Dortmund, Germany; Jerome F. Hajjar, University of Illinois, and Judy Liu, Purdue University.

Suggested Reading from Other Publishers

The following abstracts summarize papers published by others on the subject of steel design and construction that may be of interest to *Engineering Journal*.

Reidar Bjorhovde, Research Editor of the AISC *Engineering Journal*, prepared the following abstracts from the *Journal of Constructional Steel Research*.

From Volume 63, Number 8, 2007 of the *Journal of Constructional Steel Research* (JCSR) published by Elsevier, Ltd.:

Strength Design Criteria for Steel Members at Elevated Temperatures
Jiro Takagi and Gregory G. Deierlein

Design equations for steel members at fire-level temperatures are evaluated by comparisons with nonlinear finite element simulations. The AISC and Eurocode 3 equations for laterally unsupported W-shape columns, beams and beam-columns are evaluated for temperatures between ambient and 800 ºC (1,472 ºF). It is shown that the Eurocode provisions are accurate to within 10 to 20% of the finite element results. The AISC equations predict capacities that are as much as 100 percent unconservative (i.e. the design capacities are twice as large as the finite element solutions). The differences are particularly large for members with intermediate slenderness and for temperatures above 300 ºC (572 ºF). Modifications are proposed for the AISC equations that improve the accuracy to within 20 to 30% of the nonlinear finite element findings. The paper also discusses the limitations of member-based design criteria and examines research and development needs for structural fire engineering.

From Volume 63, Number 9, 2007 of the Journal of Constructional Steel Research (JCSR) published by Elsevier, Ltd:

Capacities of Headed Stud Shear Connectors in Composite Steel Beams with Precast Hollow-Core Slabs
Dennis Lam

The author observes that almost all shear connector tests have been performed with either solid slabs or with slabs on steel deck. However, hollow-core slabs have become very common in composite construction. A push-out test for use with hollow-core slabs is developed, and a very large number of tests have been conducted. A number of tests have also been performed with solid slabs, to verify the proposed push-out procedure. Design equations for studs in hollow-core slabs are also presented.

Effect of Shear Force on the Initial Stiffness of Top and Seat Angle Connections with Double Web Angles
F. Danesh, A. Pirmoz and A.S. Daryan

Extensive 3D numerical modeling of a variety of connections has been performed, using realistic material properties and member and connection details. Effects such as connection slip, bolt pretension and friction forces have been incorporated in the models. A large number of connection tests have also been conducted, in good agreement with the analytical results. The effect of the shear force is examined for several levels of load, and it is shown that the shear force reduces the initial stiffness. An equation is developed that reflects the influence of the shear force on the stiffness.

Experimental Behavior of High Strength Steel End-Plate Connections
Ana M. Girão Coelho and Frans S. K. Bijlaard

Addressing issues such as high steel strength, limited ductility and connection rotation capacity, a large number of tests and analyses of end-plate connections has been conducted. The columns and beams in the test specimens were of the steel grade S355 (355 MPa = 50 ksi specified minimum yield stress); the steel grade S690 (690 MPa = 100 ksi yield stress) was used for the end plates. The major contributions of the study are: (i) the characterization of the nonlinear behavior, (ii) the validation of the use of Eurocode 3 criteria for such connections, and (iii) the ductility analysis of such high strength steel connections. The connections that were tested satisfy current design provisions for stiffness and strength, and they exhibit reasonable rotation capacity. [It is noted (*Bjorhovde comment*) that Eurocode 3 currently does not have provisions for steel with yield strength larger than 460 MPa (65 ksi)].

The Semi-Rigid Behavior of Three-Dimensional Steel Beam-to-Column Joints Subjected to Proportional Loading
Part I: Experimental Evaluation
Part II: Theoretical Model and Validation
J. M. Cabrero and Eduardo Bayo

A number of three-dimensional extended end-plate connections have been tested for static proportional loads, with bending about both major axes. It is shown that the rotational stiffness increases with this type of loading. Further, as expected, increasing the end-plate thickness increases the flexural stiffness and strength, but reduces the rotation capacity.

In the analytical companion part of the project, the component method that is used in Eurocode 3 was expanded to take into account the 3D response characteristics. A new component that is used for bending of laterally supported plates is introduced, along with complete elastic models for major and minor axis bending of the connections. The expanded method of analysis offers significant improvement for three-dimensional analysis.

From the July 2007 issue of *Stahlbau*, published by Ernst & Sohn:

Orthotropic Decks—Past Developments and Future Outlook
Roman Wolchuk

Bridges with steel orthotropic decks, first introduced in the 1950s in Germany, have been subsequently built in other countries, with several thousand of such structures now in service throughout the world. The performance record of orthotropic decks has been satisfactory, excepting occasional fatigue cracking which had occurred on some decks built in the 1960s and 1970s, mainly caused by inappropriate details and fabrication defects. Specific causes of such failures are discussed, including locked-in tensile stresses at welds made in constrained conditions, excessive fabrication tolerances, faulty welds, local stress concentrations at structural discontinuities. Surfacing failures have been due to the initial use of thin 10 to 12 mm deck plates with excessive local deck flexibility causing stresses in the surfacing acting compositely with the deck plate.

Development of design methods for orthotropic decks is discussed. For basic design simplified approaches, such as the Pelikan-Esslinger method, are generally used. For assessment of the local stresses in the plating finite elements analysis may be useful, however, this method is not applicable in the vicinity of the welds where the material is generally plasticized because of the residual stresses due to the weld shrinkage, actual magnitudes and distribution of which are unknowable to the designer. The classical (Wöhler's) fatigue theory is valid only within the elastic limits of the material. Because of these analytical difficulties and impracticality of refined numerical investigations in the deck design , current design specifications permit empirical fatigue safety assessment by conformance with approved geometric standards.

Due to their light weight, durability and load carrying capacity, orthotropic decks have a promising future being indispensable in the super-long span bridges. Because of their capability for being structurally integrated with the main members of the existing steel bridges, orthotropic decks are also excellently suited for replacing the deteriorating concrete decks. In the U.S. nearly 40% of highway bridges are now considered "structurally deficient" or "functionally obsolete", with failed concrete decks accounting for about two-thirds of the deficiency cases. Several major U.S. bridges have recently received new orthotropic decks. Special problems encountered with redecking are discussed.

The use of orthotropic decks may be substantially increased by further optimization of their structural properties and by their cost reduction. Nearly 75% of the cost of an orthotropic deck is due to the cost of fabrication and erection labor. Optimization and cost reduction measures are suggested, such as using longer deck spans and minimizing the number of expensive intersections of the deck ribs with the cross beams and simplification of these details. Fatigue-safe and economical standard designs and details could be established by further research and testing and incorporated in future design codes, which should also include stringent fabrication and welding rules for orthotropic decks. International cooperation in these efforts would be welcome.

From 6 November 2007 issue of *The Structural Engineer*, published by The Institution of Structural Engineers, United Kingdom:

Hot v. Cold Formed Hollow Sections
(Corus Tubes)

The quality and type of hollow sections is vitally important for the overall performance of a structure. When considering the differences in the quality and performance of both hot finished and cold formed hollow sections, there are five main considerations that have to be taken into account: manufacture, properties, performance, certification and cost. This article addresses these considerations for the two types of hollow sections.

A New Design for Steel Bridge Decks Using Laser Fabrication
S.R. Bright and J.W. Smith

Steel orthotropic decks provide a lightweight form of construction, essential for weight-critical structures. However, their cost and poor record of fatigue durability has discouraged their use for mainstream construction. As a result, steel decks are generally considered an option of last resort, only used where the minimization of self-weight is essential, such as long-span and moveable bridges. An innovation is proposed to overcome these problems and transform the design of steel decks. The innovation is based upon the use of laser welding to produce an enclosed "sandwich panel" profile. The sandwich profile overcomes many of the constraints to structural performance associated with the use of conventional orthotropic steel decks.

From the December 2007 issue of *Journal of Protective Coatings and Linings*, pp. 12–14:

Intumescents: Swell Coatings for Fire Protection

This article contains a brief survey of recent literature on the subject of intumescent coatings.

ERRATA

Geometric Formulas for Gusset Plate Design

Paper by JANICE J. CHAMBERS and TONY C. BARTLEY
(3rd Quarter, 2007)

Revise the author affiliation for Tony C. Bartley on page 255 as follows:

Tony C. Bartley is a graduate student, department of civil & environmental engineering, University of Utah, Salt Lake City, UT.

Revise Equation 26 on page 261 as follows:

$$L_3 = \frac{a - g\sin\theta_B}{\cos\theta_B} + \frac{\sin\theta_{cc}}{\cos\left(\theta_B - \theta_{cc}\right)}\left(H - k\right) - L_{Le} \qquad (26)$$

Revise the equation in the lowest box of Fig. 9 (cont'd) on page 262 as follows:

$$L_3 = \frac{a - g\sin\theta_B}{\cos\theta_B} + \frac{\sin\theta_{cc}}{\cos\left(\theta_B - \theta_{cc}\right)}\left(H - k\right) - L_{Le}$$

Revise footnote a in Table 2 on pages 264 through 267, replacing "radians" with "degrees," as follows:

[a] All units are in inches (in.) and degrees; 1 in. = 25.4 mm.

In the "Input" column of Ex. 4 in Table 2 on page 265, replace "$\theta_{cc} = -9.0$" with "$\theta_{cc} = 9.0$".

In the "Input" column of Ex. 12 in Table 2 on page 267, replace "$a = 14.5$" with "$a = 19.5$".

Limit State Response of Composite Columns andBeam-Columns Part 1: Formulation of Design Provisions for the 2005 AISC Specification

Paper by ROBERTO T. LEON, DONG KEON KIM and JEROME F. HAJJAR
(4th Quarter, 2007)

Revise Equation (AISC 2005 I2-5) on page 346 as follows:

$$P_e = \pi^2 (EI_{eff})/(KL)^2 \qquad \text{(AISC 2005-I2-5)}$$

GUIDE FOR AUTHORS

SCOPE: The ENGINEERING JOURNAL is dedicated to the improvement and advancement of steel construction. Its pages are open to all who wish to report on new developments or techniques in steel design, research, the design and/or construction of new projects, steel fabrication methods, or new products of significance to the uses of steel in construction. Only original papers should be submitted.

GENERAL: Papers intended for publication must be submitted by mail to the Editor, Cynthia J. Duncan, ENGINEERING JOURNAL, AMERICAN INSTITUTE OF STEEL CONSTRUCTION, One East Wacker Drive, Suite 700, Chicago, IL, 60601-1802.

The articles published in the *Engineering Journal* undergo peer review before publication for (1) originality of contribution; (2) technical value to the steel construction community; (3) proper credit to others working in the same area; (4) prior publication of the material; and (5) justification of the conclusion based on the report.

All papers within the scope outlined above will be reviewed by engineers selected from among AISC, industry, design firms, and universities. The standard review process includes outside review by an average of three reviewers, who are experts in their respective technical area, and volunteers in the program. The maximum number of papers sent to a single reviewer is three per year, with a frequency of not more than one per quarter. Papers not accepted will be returned to the author. Published papers become the property of the American Institute of Steel Construction, Inc. and are protected by appropriate copyrights. No proofs will be sent to authors. Each author receives three copies of the issue in which his contribution appears.

MANUSCRIPT PREPARATION: Manuscripts must be provided on PC-formatted media, such as a CD-ROM, in Microsoft Word format. A laser-quality proof must accompany your submittal. Fonts and spacing must be suitable for easy reading and reproduction (for the peer-review process). Do not embed photographs, diagrams, illustrations, charts or graphs within the electronic manuscript files. Only equations may be embedded within the flow of the text. Specific requirements for electronic graphics are outlined below. *Engineering Journal* reserves the right not to publish a submittal if suitable graphics cannot be provided by the author.

Title and By-Line: Exact name, title and affiliation of the author or authors are required to appear on the first page of the manuscript.

Body Text: Please restrict font usage to Times, Helvetica, Times New Roman, Arial, and Symbol (for Greek and mathematical characters.)

Headings: All headings should be typed flush left, using upper and lower case, with two line spaces above.

Tables: Each table should appear on its own page. Footnotes to tables should appear below the table, identified by superscripted lower case letters (a, b, c, etc.).

Equations: Whenever possible, equations should be set using Microsoft Equation Editor or MathType (www.mathtype.com). Please set equations using Times New Roman, Times, and/or Symbol fonts.

Captions: Captions should be typed, double-spaced, and located at the end of the electronic manuscript. All photos and graphics must be clearly marked to indicate their corresponding caption.

References: Should be noted clearly in the text and listed, double-spaced, on a separate page in the following sample format.

In text: (Doe, 1992)

In Reference List:

Doe, J.H. (1992), "Structural Steel," *Engineering Journal*, AISC, Vol. 100, No. 1, 1st Quarter, pp. 2–10.

Footnotes: Footnotes should be noted clearly in the text with a superscript asterisk, and should appear at the bottom of the text page, in the following style:

*For a detailed discussion, see...

Graphics (other than photographs): Provide a clear $8\frac{1}{2}$ in. × 11 in. laser-quality proof of each graphic element. Graphics should reproduce cleanly in black-and-white format. Graphics may be submitted and reproduced in color at the Editor's discretion. Please restrict font usage to Helvetica, Arial or Symbol, in sizes suitable for at least 50% reduction (12 pt. minimum). Line weights must be suitable for 50% reduction. When possible, provide each graphic element in a separate electronic file. TIF or EPS file formats are preferred, with a minimum resolution of 300 dots per inch.

Photographs: Provide either original photographs or high-quality electronic files and laser-quality proofs. Electronic photographs may be submitted as grayscale TIF or JPG images, one photograph per file. Photographs may be submitted and reproduced in color at the Editor's discretion. Minimum image resolution is 300 dots per inch. Photographs should be a minimum of 4 in. wide, so the minimum image width is 1200 pixels. Detailed photographs may require resolutions up to 1200 dots per inch. Photos embedded in word-processing documents are not acceptable.